67-61

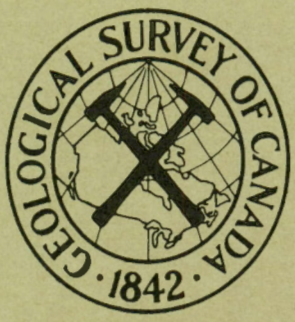

GEOLOGICAL SURVEY OF CANADA

DEPARTMENT OF ENERGY, MINES AND RESOURCES

PAPER 67-61

PETROLOGY OF ADAMANT PLUTON, BRITISH COLUMBIA

(Report and 42 figures)

P. E. Fox

Price, $2.00

1969

GEOLOGICAL SURVEY
OF CANADA

PAPER 67-61

PETROLOGY OF ADAMANT PLUTON, BRITISH COLUMBIA

P. E. Fox

DEPARTMENT OF ENERGY, MINES AND RESOURCES

Available by mail from the Queen's Printer, Ottawa,

from Geological Survey of Canada,
601 Booth St., Ottawa,

and at the following Canadian Government bookshops:

HALIFAX
1735 Barrington Street

MONTREAL
Æterna-Vie Building, 1182 St. Catherine Street West

OTTAWA
Daly Building, Corner Mackenzie and Rideau

TORONTO
221 Yonge Street

WINNIPEG
Mall Center Building, 499 Portage Avenue

VANCOUVER
657 Granville Street

or through your bookseller

Price: $2.00 Catalogue No. M44-67-61

Price subject to change without notice

The Queen's Printer
Ottawa, Canada
1969

CONTENTS

	Page
Abstract	vii
Introduction	1
Physical features	1
Method of study	2
Field study	2
Laboratory work	2
(i) Microscopic methods	2
(ii) Chemical methods	3
(iii) X-ray methods	3
(iv) Mineral separations	3
Acknowledgments	4
General geology	4
Structural relations	5
External structure	5
Internal structure	8
Geological boundaries	8
Foliation	9
Lineation	12
Shear zones and folds	12
Joints	15
Xenoliths	15
Summary and discussion	15
Lithology and petrography	17
Country rocks	17
Plutonic rocks	18
Monzonite	21
(i) Megascopic description	21
(ii) Microscopic description	23
Transition zone	24
(i) Megascopic description	24
(ii) Microscopic description	24
Hornblende quartz monzonite and granodiorite	26
(i) Megascopic description	26
(ii) Microscopic description	28
Biotite-hornblende granodiorite and quartz diorite	32
(i) Megascopic description	32
(ii) Microscopic description	32
Pegmatite and aplite	34
Quartz veins	36
Compositional variations in the main rock units	36
(i) Modal variations	36
(ii) Plagioclase composition	36
Rock chemistry	38

Page

Summary and discussion 38
Mineralogy 41
Alkali feldspar 41
Optical properties 41
Structural state 45
Composition 48
Coexisting plagioclase 53
Pyroxenes 53
Hornblende and biotite 56
Oxide minerals 61
Interpretation and significance 63
Alkali feldspar 63
Pyroxenes 64
Hornblende and biotite 64
Oxidation ratio 65
Bulk composition 69
(i) SiO_2 71
(ii) MgO 72
Ratio of biotite:hornblende 72
Petrogenesis and emplacement history 74
Origin of the monzonite 74
Origin of the peripheral rocks 76
Composition and origin of the vapour phase 76
Discussion 77
Emplacement history 79
References 80
Appendix A – Modal and chemical analyses 86
B – Field and map numbers 98
C – Optic angles of alkali feldspar 99
D – Albite in solid solution 100

Table 1. Average modal compositions 21
2. Average chemical compositions 41
3. X-ray and optical data for alkali feldspar 46
4. Chemical composition of alkali feldspar 48
5. Albite content of K-phase 49
6. Chemical composition and optical properties of augite 54
7. Chemical composition and optical properties of hypersthene 55
8. Estimated temperature of formation of pyroxenes 56
9. Chemical composition and optical properties of hornblende 58

Page

Table 10. Chemical composition and optical properties of biotite 59
11. Analyses of G-1, W-1, and biotite 10 96

Illustrations

Frontispiece
View westward from Sentinel Peak viii

Figure 1. Geological map of Adamant pluton, British Columbia ..... in pocket
2. Regional geological map ..... in pocket
3. Sample locality map ..... in pocket
4. East contact of Adamant pluton 6
5. Vertical contact near Granite Glacier 7
6. Ovoidal inclusions in hornblende quartz monzonite ... 9
7. Migmatitic zone in biotite-hornblende granodiorite .. 10
8. Migmatitic zone in hornblende quartz monzonite 11
9. Planar structure in hypersthene monzonite 13
10. Linear structure in pluton and country rock 13
11. Fold with pegmatite and aplite veins 14
12. Modal classification diagram 19
13. Modal variation in different rock units 20
14. Hand specimen of hypersthene-augite monzonite 22
15. Photomicrograph of monzonite 22
16, a, b. Photomicrographs of transition zone 25
17. Textural relations among mafic minerals 27
18. Alkali feldspar and quartz contents plotted against the ratio of hornblende + biotite 29
19. Hand specimen of hornblende quartz monzonite 30
20 a, b. Photomicrographs of hornblende quartz monzonite .. 31
21. Hand specimen of biotite-hornblende granodiorite ... 33
22. Hand specimen of strongly foliated granodiorite 33
23. Sharp-walled pegmatite dyke in quartz monzonite ... 35
24. Histograms of plagioclase determinations 37
25. Bulk chemistry 39
26. Optical character of alkali feldspars 43
27. Mean 2V histograms of alkali feldspars 44
28. Structural state of alkali feldspars 47
29. Albite in solid solution related to bulk albite and anorthite contents 50
30. Albite in solid solution related to 2V 52
31. Approximate phase relations 52
32. Comparison of Adamant pyroxenes 57

Page

Figure 33. Fe:Mg ratios of hornblende and biotite 57
34. Relationship between Mg:Fe^2 and Fe^3:Fe^2 of hornblende and biotite 60
35. FeO:MgO ratios of hornblende, biotite and rock plotted against oxidation ratio 62
36. Fe-Si-O system (a), and phlogopite-annite join (b) .. 66
37. Oxidation ratio plotted against distance from core ... 70
38. Oxidation ratio plotted on map of pluton 71
39. Generalized data showing effects of oxidation ratio and μH_2O on hornblende and biotite 73
40. Temperature – water vapour pressure diagram showing minimum melting curves of basalt, syenite, and granite 75
41. Scheme of chemical analyses 97
42. Determination curves for albite 101

ABSTRACT

Adamant pluton is an elongate, east-trending mass surrounded by amphibolite facies metamorphic rocks of the Proterozoic Horsethief Creek Group. The pluton is a composite body consisting of a hypersthene-augite monzonite core enclosed by hornblende quartz monzonite. The core grades into the peripheral rock through a transition zone in which the monzonite core is progressively recrystallized to hornblende quartz monzonite. Chemical analyses show that this transition is isochemical.

Internal structure is characterized by foliation and lineation patterns consistent with two fold systems found in the northern Selkirk Mountains, and a prominent marginal foliation locally associated with zones of migmatite. Plagioclase foliation and poorly developed lineation in the monzonite core are obliterated and locally truncated by a younger hornblende and biotite foliation in the recrystallized periphery of the body.

Analyses of augite and hypersthene show a constant Fe:Mg ratio for this mineral pair. Coexisting hornblende and biotite have variable Fe:Mg ratios which are correlated with changes in oxidation state due to a thermal gradient from the core to margin of the pluton. High μH_2O in rocks at the margin caused a decrease of the hornblende: biotite ratio. The internal structure, petrology, and mineralogy of the pluton indicate a metamorphic origin for the peripheral rock, and a magmatic one for the older monzonite core. It is concluded that the pluton was originally emplaced as a single igneous intrusion of pyroxene monzonite. Subsequently, this body underwent metamorphism and reintrusion during the late Mesozoic, the most recent episode of deformation and metamorphism in the northern Selkirk Mountains.

Frontispiece. View westward from Sentinel Peak, British Columbia.

PETROLOGY OF ADAMANT PLUTON, BRITISH COLUMBIA

INTRODUCTION

Adamant pluton occurs in the northern Selkirk Mountains about 50 miles north of Revelstoke, British Columbia, and five miles west of the junction of Bush and Columbia Rivers (Fig. 1). The pluton lies in parts of map areas 82 N/12, N/13, M/9 and M/16.

Mountainous topography and the Columbia River make access to the area difficult. The Columbia River isolates the area from the only nearby road, the Big Bend Highway, which follows the east bank of the Columbia River. The area may be reached from the road by crossing Columbia River at the mouth of Swan Creek and following Swan Creek to its headwaters at Granite Glacier (localities noted in Fig. 2). A cable-crossing at Surprise Rapids owned by the British Columbia Department of Lands and Forests provides a direct means of crossing the river. The map-area may be reached from this point by climbing to the 7,000-foot ridge that separates Columbia River from the headwaters of Tabernacle Creek. A steep gully immediately to the southwest of the cable-crossing provides access through thick underbrush below timberline.

There are no roads or trails within the map-area and travel is generally restricted to glacier-filled basins and valleys. Mountaineering techniques are essential to safe and efficient travel.

Prior to the present study no geological work had been done in the Adamant Range apart from the collection of a few samples by mountaineering parties. Adamant Range forms a small part of Rogers Pass map-area (Wheeler, 1963) and Big Bend map-area (Wheeler, 1965).

Field study of Adamant pluton was carried out in 1959, 1960, 1961. Two weeks were spent on the project in 1959 and 1960 while the writer was working with J.O. Wheeler of the Geological Survey of Canada. A more intensive study was done in a three month field season in 1961.

PHYSICAL FEATURES

Eroded remnants of Adamant pluton constitute the Adamant Range of the Selkirk Mountains. The Adamant Range has typical alpine topography (Frontispiece). The backbone of the Range consists of Mount Austerity (11,000 feet), Turret Peak (10,960 feet), Adamant Mountain (11,050 feet), and Pioneer Peak (10,750 feet). These impressive peaks lie near the centre

Revised manuscript received: July 14, 1966.

of the pluton and provide a vertical exposure of 2,000 feet between the peaks and glaciers below. Mount Sir Sanford (11,590 feet), the highest peak in the Selkirk Mountains, forms a prominent peak near the southern boundary of the area.

Glaciers cover much of the area above 7,000 feet, particularly on north-facing slopes. With few exceptions, the glaciers are broken by prominent ice-falls and large crevasse fields. Terminal zones consist of rubble-filled valleys or outwash plains although polished bedrock is commonly exposed between the glacier snouts and drift-covered valleys. Sharp-crested lateral moraines are common along glacier flanks and valley sides.

Below 7,000 feet valleys are steep-walled and heavily timbered. Valley streams are fast flowing: most have glacier meltwater as their source.

METHOD OF STUDY

Field Study

Early in the field study of Adamant pluton a 'working hypothesis' of magmatic emplacement was adopted. This view became untenable with further study and a complex structural and metamorphic history became apparent. The aim of this report is to study the origin and emplacement of the pluton with emphasis on its chemistry and mineralogy.

The pluton was mapped on a scale of one-half inch to one mile. A base map with a contour interval of 100 feet provided sufficient topographic detail to map geological features accurately. Field work was carried out from a number of small camps in the area. Provisions were cached by helicopter early in the field season, and other equipment and personal effects back-packed into the area, and from one camp to another. During the field work, specimens were cached at convenient sites and collected by helicopter at the end of the field season.

Laboratory Work

Localities for samples studied in the laboratory are noted on Figure 3 (in pocket).

(i) Microscopic Methods

Approximately 200 thin sections of selected rocks were studied by standard petrographic methods. Universal stage techniques were used for optic angle measurements and the determination of plagioclase composition

(Rittmann zone method). Conoscopic methods permitted optic angle measurements within one degree. Refractive index corrections were applied to measurements (Federow method, in Emmons, 1943).

Refractive indices were determined in sodium light, and oils checked by an Abbe refractometer. Index determinations are generally within ± 0.003.

A Swift point-counter was used for modal analyses; 1,000 to 1,500 points were counted per slide. Rocks poor in alkali feldspar were stained with sodium cobalti-nitrite. During the staining procedure, etching with hydrofluoric acid was timed to etch feldspar but not quartz. This technique allowed plagioclase to be distinguished from quartz without further staining of the slide with rhodozonic acid. In general, however, no identification problems were encountered.

(ii) Chemical Methods

Samples for chemical analyses were selected on the basis of best areal coverage consistent with exposure and lithologic complexity. Five to ten pounds of rock chips were collected from suitable outcrops, bagged, labelled, and cached with other specimens. Care was taken to select a hand specimen with each sample.

Rocks and minerals were analyzed at the Geological Survey of Canada and Carleton University. Rapid chemical methods were used at the Geological Survey for rock analyses, and conventional methods for mineral analyses. Spectrophotometric and titration methods were used at Carleton University for both rock and mineral analyses. A summary of the methods used in the Carleton laboratory, together with analyses of standard materials is given in Appendix A.

(iii) X-ray Methods

Powder cameras were used for routine identification of opaque and accessory minerals. Guinier camera and diffractometer techniques were used extensively for compositional and structural studies of alkali feldspar.

(iv) Mineral Separations

Hornblende, biotite, hypersthene, augite, alkali feldspar, and oxide minerals were separated from selected rocks for detailed study. Crushing, sizing, and rough separation were made by the Geological Survey of Canada, and purification of the separates made by the writer. Standard heavy liquid and magnetic methods were used. No difficulty was found in obtaining pure mineral separates.

ACKNOWLEDGMENTS

Field support and facilities were provided by the Geological Survey of Canada. Much of the routine analytical work incorporated in this study was done for the writer by the staff of various laboratories of the Geological Survey. A special note of appreciation is expressed to J.O. Wheeler for his suggestions and help during the field work. The field assistance of G.E. Antenbring, P.G. Williams, and W.A. Tupper is gratefully acknowledged. G. Pouliot of the Geological Survey of Canada, and T.L. Wright and D.B. Stewart of the United States Geological Survey kindly assisted in the X-ray study of alkali feldspar.

A.W. Hounslow took particular interest in the study and supervised much of the writer's analytical work.

The writer is indebted to J.E. Reesor, J.M. Moore, and G.Y. Chao for advice and guidance during this study.

The writer received financial support from Carleton University, the Geological Survey of Canada (grant 2-62 to J.M. Moore), and an Ontario Graduate Fellowship.

GENERAL GEOLOGY

Adamant pluton is a granitic body emplaced in medium grade metamorphic rocks of the northern Selkirk Mountains. The pluton is one of the northernmost granitic batholiths that has intruded Proterozoic and lower Palaeozoic rocks of the Selkirk and Purcell Mountains. Rocks enclosing the pluton are of late Precambrian age, belonging to the Horsethief Creek Group (Wheeler 1963, 1965).

Horsethief Creek Group consists of shales, slates, feldspathic grits, and minor limestones in the Dogtooth and Selkirk Mountains. In the northern Selkirks, these rocks pass into quartzite, garnet-mica schist, and interlayered marble. Metamorphic grade increases to the northwest along the central part of the Selkirk Mountains. Garnet, kyanite, and sillimanite zones are encountered in order and each widens to the northwest. Garnet zone rocks west of Adamant pluton pass abruptly into sillimanite rocks, thus the metamorphic zones are foreshortened here or eliminated by faults. The pluton occurs at the southern extremity of the sillimanite zone and extends eastward into the kyanite zone.

Regional fold axes and thrust faults trend north in the southern Selkirks and northwest in the northern Selkirk Mountains. Northeast-trending folds in the western ranges of the northern Selkirks have been described by Wheeler (pers. comm., 1964) as being older than the predominant northwest trend.

Regional structure in the northern Selkirk Mountains has a crude symmetry: structures in the Dogtooth and eastern Selkirk Mountains are overturned and overthrust to the northeast whereas rocks of the western Selkirk Mountains are thrust to the southwest. A vertical section through the Selkirk structure would show rock units in a symmetrical, fan-shaped arrangement. The axial trace of the fan forms a structural axis along the central part of the Selkirk Mountains (Fig. 2) from Battle batholith to Mount Sir Sanford where it swings sharply to the west. The axis occurs in the oldest rocks of the northern Selkirks and is an axis of symmetry to the metamorphic zones that wedge out southward. Farther south the structural axis swings west of the Horsethief Creek slates and lies within rocks of the Hamill Group (Cambrian). On a large scale, the fan-shaped structure of the Selkirk Mountains appears to plunge southward.

Adamant pluton occurs in the axial zone of the northern Selkirk Mountains and is oriented east-west, oblique to the predominant regional structural pattern. The long axis of the pluton conforms to axes of easterly trending folds that have been described in the region by Wheeler.

STRUCTURAL RELATIONS

EXTERNAL STRUCTURE

A zone of complexly folded rock forms a structural aureole in which northwest striking metasediments have been disrupted and forced into conformity with the contact of Adamant pluton (Fig. 1, in pocket). The aureole extends outward from the north and south flanks for about three-quarters of a mile, but east of the pluton the rocks are only slightly deflected from their regional trend. Structural relations at the east contact are illustrated in Figure 4. At the contact, plutonic rocks lie concordantly on thick, west dipping quartzite and marble beds. The west end of the pluton, although poorly exposed, is bounded by vertically dipping quartzite – mapped as Hamill Group by Wheeler (1965) – that forms the valley floor and west wall of Norman Wood Creek. Farther south this quartzite appears to be part of a belt of east dipping Hamill Group rocks that occur west of the Selkirk structural axis (Fig. 2). Hamill quartzite crosses the structural axis near the end of Adamant pluton and forms the west boundary of the mass. The west contact, like the east, appears to be determined by competent quartzite units in the country rock.

Much of the north contact is bounded by vertically dipping, and locally, complexly folded, marble. Figure 5 shows the dark, massive rocks of the pluton adjacent to upright metasediments. The contact between the two rocks is exposed almost continuously for a vertical distance of 1,000 feet.

Figure 4. East contact of Adamant pluton exposed along the north wall of Palmer Creek (looking north from a point near Mount Sir Sanford). Plutonic rocks lie on a dark weathering quartzite and marble that forms a prominent cliff below the contact and on Mount Stockmer (light coloured peak at right). A thin concordant plate of quartzite occurs above the contact.

Large scale folds in the structural aureole strike east, oblique to regional trends. East trending folds are marked by grey or buff marbles on Mount Enterprise, and by two belts of marble along the northern flank of the pluton between Austerity and Windy Creeks. Marble beds on Mount Enterprise form isoclinal folds that have little or no plunge, and axial planes that dip gently toward the pluton. In contrast, folds between Austerity and Windy Creeks are complex and steeply plunging.

Small scale folds and crenulations in the structural aureole have variable plunges but trend east-west parallel to the north and south contact. South of the pluton and its structural aureole, folds and crenulations conform to regional trends. Two such orientations are present in rocks on Mount Sir Sanford and Palisade Mountain: a predominant northwest trending set, and a northeast set of fold axes. The latter folds are associated with a conspicuous easterly plunging syncline that makes up the summit of Palisade Mountain. The relationship between the syncline and folded marble beds on Mount Sir

Figure 5. Vertical contact between quartz monzonite (left) and upright metasediments near Granite Glacier. Contact is exposed here almost continuously for 1,000 feet vertically. View looking west across Granite Glacier.

Sanford is not evident. Fold axes in pelitic rocks and quartzites immediately north of the syncline plunge northwest, thus Palisade Mountain syncline is beyond the structural aureole of Adamant pluton. The Mount Sir Sanford structures may have been reoriented into northeast plunging folds but it is more probable that the Palisade Mountain fold is one of the early northeasterly trending folds that have been recognized elsewhere in the region by Wheeler (1965).

East of the pluton, fold axes such as those on Mount Stockmer and east of Stockmer Glacier trend north subparallel to fold axes south of Adamant pluton. The absence of a distinct structural aureole such as that bounding the north and south contacts suggests that these folds are probably unrelated to emplacement of the pluton.

INTERNAL STRUCTURE

Adamant pluton is a club-shaped mass about 60 square miles in area. The pluton is oriented east-west, is about 16 miles long, and varies in width from 2 miles at Stitt Creek to 4 miles between Silvertip Glacier and Mount Enterprise. The north wall of the body is steep or vertical (see cross-sections, that accompany Fig. 1). The east contact dips 55° west, and the south flank near Silvertip and Adamant Glaciers dips 50° to 70° north. The southern flank of the pluton between Belvedere Glacier and Norman Wood Creek, and the west end appear to be vertical but are poorly exposed and generally covered by talus or drift.

The east part of the pluton consists of a series of rocks arranged in a roughly concentric manner around a core of hypersthene-augite monzonite (map-unit 3). Monzonite is everywhere separated from country rocks by hornblende quartz monzonite and granodiorite (map-unit 5). Biotite-hornblende granodiorite and quartz diorite (map-unit 6) occur along the east margin of the pluton. Monzonite grades into quartz monzonite and granodiorite through a zone one-quarter to one-half mile thick (map-unit 4). This zone is complex and not readily classified. In view of its position between monzonite and quartz-bearing rocks and its gradational character it will be referred to as the 'transition zone'.

Two isolated, elliptical pods in the west part of the pluton are lithologically similar to the transition zone. These rocks grade into and are surrounded by quartz monzonite.

Geological Boundaries

The pluton-country rock contact is well exposed in alpine regions but in valleys is covered by glaciers or rock debris. Where exposed the contact is sharp and straight or gently curving. There is no evidence of a chilled margin at the contact, nor are there small apophyses or veins of plutonic rock cutting the country rock. The contact conforms to bedding or locally truncates it at small angles. Different country rocks flank the pluton at different places but the same country rock unit frequently occurs along the contact for many thousands of feet. Quartzite and marble occur along the entire east contact of the pluton, and a single marble unit borders the north contact from Austerity Creek to Norman Wood Creek, a distance of eight miles.

Within the pluton, rocks change gradually from one type to another. Sharp contacts, cross-cutting features, or inclusion zones between rock units are absent. Only one occurrence was found in which blocks of the transition zone occur in hornblende quartz monzonite. These occur near Thor Peak and are illustrated in Figure 6. The blocks are identical to outcrops of the transition zone a few hundred feet to the west. Inclusions vary from 6 inches to 6 feet in length, and are either large single ovoidal inclusions or groups of

small ones. Many are well defined, but others are indistinct and appear to grade into the enclosing quartz monzonite. A hornblende-rich zone occurs along the margin of large inclusions, and forms a distinct ring around the small ones. Figure 6 also shows discontinuous dykes and patches of aplite locally concentrated between disjointed inclusions. The aplite bodies lack sharp walls, and grade into the surrounding quartz monzonite.

Foliation

Planar structure is the most prominent structural feature in the pluton, but rocks are foliated to varying degrees. Monzonite is faintly foliated, the planar structure being the result of aligned plagioclase laths. Planar arrangement of hornblende and biotite crystals produces foliation in quartz monzonite and granodiorite. These rocks are strongly foliated along the margin of the body, but elsewhere foliation is commonly indistinct.

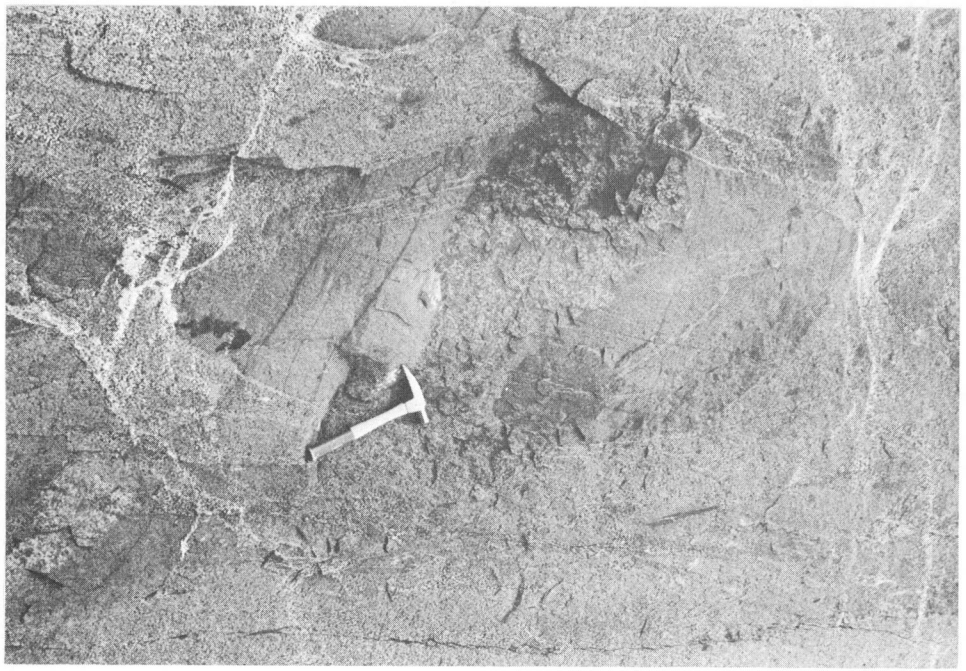

Figure 6. Ovoidal inclusions of transition zone in hornblende quartz monzonite (southwest face of Thor Peak). Small inclusions in upper left of photo have hornblende-rich rims; large inclusion in centre has a broad hornblende-rich margin. Diffuse aplite veins are concentrated between inclusions and grade into the enclosing quartz monzonite.

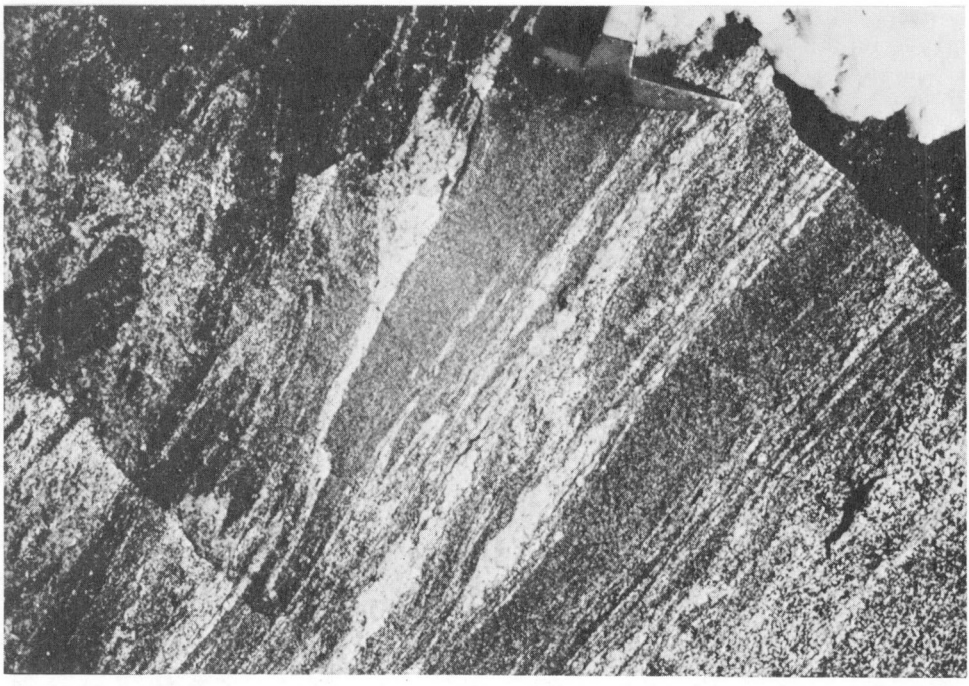

Figure 7. Migmatitic zone in biotite-hornblende granodiorite near east contact. Lenses and contorted veins of aplite occur mixed with mafic rocks. Typical biotite-hornblende granodiorite is shown in upper left corner, mafic blocks are mixed with aplite in lower right. (Cirque face south of Wotan Peak)

Foliated rocks along the margin locally grade into zones of migmatite that are concordant to the planar structure in the pluton. The migmatites consist of lenses, knots, and intricately folded veins of aplite mixed with hornblende-rich mafic rocks (Figs. 7 and 8). The host rock is more mafic than quartz monzonite or granodiorite, and, as illustrated in Figure 7, locally occurs as round to angular blocks of various sizes. In Figure 8, aplite veins are contorted and wrap around bodies of hornblende quartz monzonite. The foliation, intricate folds, and locally disjointed rock suggest plastic flow in the migmatite zones.

The foliation pattern is complex, but a number of relations are evident (see Fig. 1, in pocket). A consistent northwest-striking foliation is evident west of the monzonite core in the interior of the body. Foliation here, as elsewhere, is independent of the boundaries between the various rocks composing the pluton. Hornblende foliation can be traced from hornblende quartz monzonite into the two transition zone bodies without deviation, the overall trend of the foliation being parallel to the regional northwest structure.

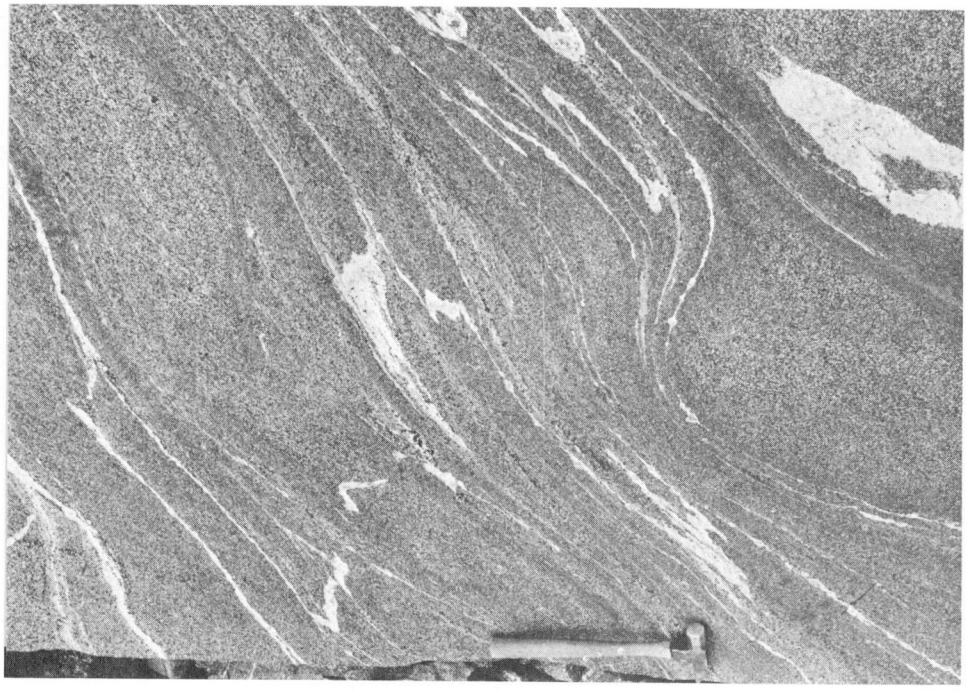

Figure 8. Migmatitic zone in hornblende quartz monzonite near Austerity Glacier. Contorted aplite veins are bounded by mafic selvages. Selvages are foliated, and more mafic than the pillow-shaped bodies of quartz monzonite (outcrop between Belvedere and Austerity Glaciers).

Foliation in the east part of the pluton is of two types: Hornblende and biotite foliation in the peripheral rock, and plagioclase foliation in the monzonite and transition zone core. Near Adamant Glacier and Mount Enterprise, foliation in hornblende quartz monzonite and biotite-hornblende granodiorite is steep or vertical and parallel to the walls of the pluton. Farther east, foliation planes conform to the general curvature of the eastern edge, and to the west dipping contact. The consistent northwest strikes noted west of the monzonite core are not evident in the east part. Evidently the planar structures here have been strongly influenced by the walls of the body, and particularly by the west dipping contact.

Foliation in monzonite is represented in Figure 9 in more detail than on the accompanying map. North and northwest trends are common, and these continue into the transition zone. Such trends are generally oblique to the outer boundary of the transition zone. Only at the east end of the mass is foliation concordant to the lithologic boundary between the transition zone and hornblende quartz monzonite. Although foliation at many localities is

continuous from monzonite to hornblende quartz monzonite, plagioclase foliation is always obliterated at the outer margin of the transition zone, and replaced by a foliation of aligned mafic minerals. Discordant relations between the two types were noted in rocks near the southwest terminus of Austerity Glacier. West-striking plagioclase foliation in monzonite and transition zone is truncated by the boundary between hornblende quartz monzonite and the transition zone. A few feet west of the boundary, on strike with the plagioclase foliation, a northwest-trending hornblende foliation parallel to the boundary is evident in hornblende quartz monzonite. The implication is clear that the mafic foliation in the quartz monzonite is a later structure than plagioclase foliation in the monzonite.

There are thus three foliation types in the pluton: a marginal structure that conforms to the steeply dipping walls and inward dipping east contact, a northwest striking foliation in the interior west of the monzonite core, and an early plagioclase foliation in the monzonite body.

Lineation

Hornblende prisms form faint linear structures in the pluton. Each such structure is steep or vertical along the walls of the mass, but plunges 40 to 60 degrees northwest in the interior of the quartz monzonite and granodiorite. Lineation in monzonite, however, plunges easterly (Fig. 9).

Lineation in the monzonite and transition zone was observed at three localities only. Linear structures here are formed by "trains" of hornblende crystals that have grown as mantles around pyroxene grains. The formation of mantles has apparently emphasized trains of pyroxene crystals that are pre-existing structures in the monzonite body. Where hornblende is absent, these linear features are not evident owing to the small size and equant shape of the pyroxene grains.

Lineation in the monzonite together with that in quartz monzonite and granodiorite, and regional fold axes in rocks south of Adamant pluton are represented in Figure 10. Linear structures in the quartz monzonite and granodiorite conform to northwest-trending regional fold axes, and lineation in monzonite and the transition zone conforms to those of the northeast-trending folds. Thus, regional structural patterns of both the northeast and northwest fold systems are found in the rocks of the pluton.

Shear Zones and Folds

Folds and small inward-dipping thrust faults are locally abundant near the margin of the pluton. Figure 11 shows a typical fold in hornblende quartz monzonite near the south contact. The fold is an open structure, and its axial plane dips 25 degrees north. Small mafic inclusions in quartz

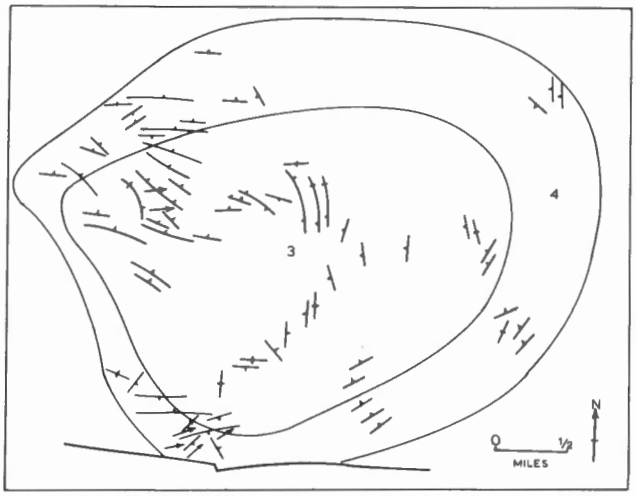

Figure 9. Planar structure in hypersthene monzonite and transition zone due to aligned plagioclase laths. Trains of mafic crystals form linear structures (arrows). Dips and plunges are moderate to steep (40° - 70°), dips rarely vertical. 3 = hypersthene monzonite, 4 = transition zone.

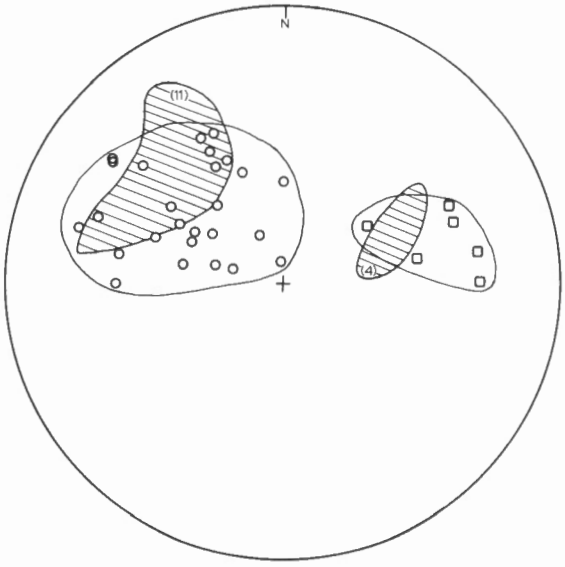

Figure 10. Linear structure in the pluton and in country rock south of the pluton. Shaded areas represent the two regional fold orientations (see text), circles and squares are lineations in the peripheral rock and monzonite core respectively. (Total number of points = 47, number of points in shaded area are shown in parentheses).

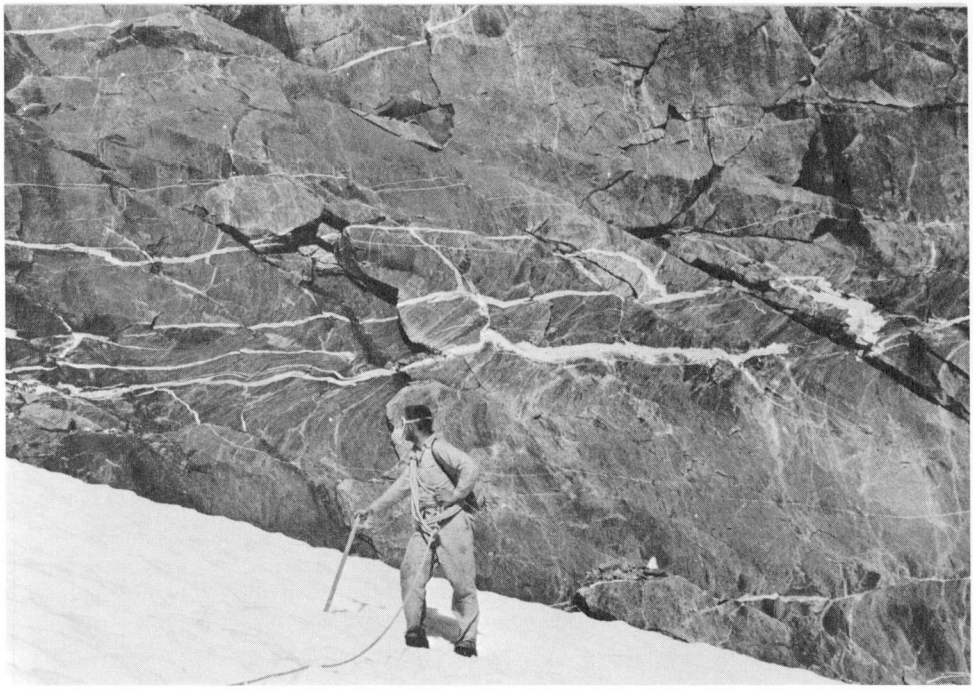

Figure 11. Fold with associated pegmatite and aplite veins in hornblende quartz monzonite. Fold is marked by deflected foliation planes and by ribbon-like mafic inclusions. Small shear zone is evident in lower right corner. (Looking north at outcrop near Silvertip Glacier.)

monzonite appear to have been deformed into long ribbons from their usual ovoidal shape. These deformed inclusions make shears and folds conspicuous features here and elsewhere. Reverse movement of the upper block southward over the lower is indicated by the shape of the structure. The same relative movement was determined for nearby inward dipping faults (or shear zones).

Aplite dykes parallel to the axial planes of folds, and locally filling shear zones, are common features. The dykes shown in Figure 11 are thickest along the zone of apparent maximum deformation. The dykes there are massive but other dykes near Thor Peak are partly or totally granulated, as though movement along shear zones continued after emplacement of the dyke material. Thus the formation of the aplite dykes, shear zones, and folds appear to be closely related in time.

Joints

Rocks of the pluton are well jointed. Although joints were not studied in detail, a single joint system appears to be common to all rocks. Joint surfaces are frequently coated with epidote and hematite. The most prominent joint set strikes northwest and dips steeply southwest or northeast. Serrated ridges, sharp cols, and rock towers are prominent topographic features controlled by these joints. Northwest joints also strike at a small angle to lineation in the pluton. A second set of joints strikes northeast, and dips 20 degrees southeast. A third set strikes parallel to these but dips 65 degrees northwest.

Xenoliths

Xenoliths of country rock are common along the margin of the body and range in size from a few inches to bedded quartzite blocks twenty to thirty feet thick. Large quartzite xenoliths near the east contact are shown in Figure 4. Bedding in the blocks is concordant to underlying quartzite in the country rock. Large inclusions also occur in hornblende quartz monzonite below the southwest terminus of Austerity Glacier. These xenoliths consist of interbedded marble and quartzite. The blocks are about twenty feet thick, vertical and strike parallel to the regional northwest trend.

SUMMARY AND DISCUSSION

(1) The pluton is bounded on its north and south sides by a structural aureole in which regional structures are disrupted and reoriented into conformity with the edge of the pluton. Disruption of these structures appears to be the result of forceful emplacement. There has been no disruption on the east or west ends of the pluton where emplacement appears to have been controlled by competent beds of quartzite in the country rock.

(2) Foliated rocks occur everywhere in the pluton but planar structure is best developed along the margin where it is occasionally associated with migmatite zones. The presence of both mafic rock and aplite veins in the migmatite suggests, but does not prove, that the veins represent consolidated low melting liquids, and that the mafic rocks and selvages bordering some of the veins are refractory ferro-magnesian residues. The origin of migmatite by partial melting is a popular concept, and will not be discussed further here. The contorted appearance and foliated character of the migmatite zones further suggests that they were zones of intense movement or flow.

(3) Foliation attitude is independent of lithologic boundaries.

(4) Plagioclase foliation in monzonite appears to be an early structure in the pluton. It strikes obliquely to the outer boundary of the transition zone, and at one place, is truncated by foliation in hornblende quartz monzonite. Thus the two foliation types are different in age.

(5) A regional structural imprint is evident in rocks of the pluton. A consistent northwest foliation and lineation in the interior conforms to the predominant regional structure. However, easterly trending lineation in monzonite, although poorly developed, conforms to the early, easterly trending folds in the region (Fig. 10).

(6) The long axis of the pluton is also parallel to these early folds.

A number of conclusions may be drawn from the above. First, monzonite is structurally the oldest rock in the pluton, and its internal structure may reflect an early period of deformation in the region. Secondly, the pluton was involved in deformation that produced the prominent northwest folds. Thirdly, forceful emplacement of the body into its present location is indicated by the structural aureole and marginal foliation.

This analysis suggests that the three isolated bodies of pyroxene-bearing rock in the interior of the pluton are remnants of an early body that formed in accordance with regional northeasterly trending structures. The elongate shape of the pluton in this view is thus a feature inherited from an old structural position in the fold belt.

Structures in the interior of quartz monzonite and granodiorite correspond to northwest regional trends, and appear to reflect a regional imprint on the rocks during their formation. A syntectonic relationship is suggested, but the discordant trend of the pluton and disruption of northwest structures cannot be reconciled by syntectonic emplacement. However, if the discordant trend is a feature inherited from an early history, as suggested above, subsequent metamorphism of the pluton during emplacement and development of the northwest trending regional structures would account for the observed structural and lithologic relationship. It is implicit in this view that the pluton moved from its initial position during regional deformation and metamorphism and intruded as a crystalline diapir. The early lithology of the body should then have adjusted to new chemical and physical conditions accompanying its mobilization and emplacement into higher crustal levels. The rocks bounding the monzonite body must be the result of metamorphism of the monzonite mass during the latest and most pronounced period of deformation and metamorphism in the northern Selkirks. It will be shown below that the texture, chemistry, and mineralogy of these rocks reflect this proposed metamorphic history.

LITHOLOGY AND PETROGRAPHY

COUNTRY ROCKS

Country rocks consist of interbedded mica schist, impure quartzite, grey and buff marble beds, and a few garnet amphibolite bodies that occur interlayered with pelitic rocks near the east margin of the area. All were mapped as a single unit (map-unit 1) except for distinctive marble horizons which were mapped separately (map-unit 2).

Schist is coarse grained and usually contains thin quartz-rich beds. Foliation is invariably crumpled and many schists have a corrugated appearance. The schist close to the pluton is more strongly foliated than elsewhere in the region. Mica folia wrap around knots of garnet and quartzo-feldspathic material, and ptygmatic structures and straight-walled dykes of aplite are common. Quartzite occurs as disrupted and fractured beds, boudins, and isolated blocks. Dilatant zones between segments of disrupted beds are filled with pegmatitic material that gradually diminishes in grain size away from the fractures.

Garnet-muscovite-biotite-quartz schist is predominant. Quartz is invariably anhedral and forms lenticular aggregates or knots. Muscovite and reddish brown biotite are generally intergrown and wrap around garnet porphyroblasts. The latter are equant and generally crowded with inclusions of quartz, mica, opaque material, and sillimanite. These inclusions locally form helicitic fabric within the garnet. Sillimanite occurs in schists that contain discrete veins, dykes, and irregular lenses of quartzo-feldspathic material. Felty seams and coarse bundles of sillimanite are intergrown with micas. Plagioclase (about An_{25}) is the characteristic feldspar. It does not occur in all of the schist but where present makes up 5 to 10 per cent of the rock. Microcline was observed in rocks from north of Swan Creek. Apatite, zircon, tourmaline, and iron oxides are accessory minerals. Accessory chlorite associated with biotite and garnet, and dusty sericite inclusions in plagioclase are the only minerals that can be attributed to retrograde metamorphism or hydrothermal alteration.

Quartzite forms prominent cliffs on Mount Palmer and along the east margin of the pluton. It is generally grey or green with buff-coloured feldspar evident on the weathered surface. It consists of a granular mosaic of anhedral quartz and plagioclase intergrown with subparallel plates of deep red biotite, and somewhat coarser grained flakes of muscovite. A few red garnets are locally present. Quartz and plagioclase (An_{15}) make up 90 per cent of the rock. Biotite and garnet are partly altered to chlorite, and plagioclase to sericite. Zircon and apatite are accessory minerals.

Grey and buff weathering marble forms marker horizons within an almost featureless country rock. Beds are highly contorted, particularly on

Mount Sir Sanford, Mount Enterprise, and along the north edge of the pluton near Windy Creek, but bands of marble trace out large structures. On Mount Sir Sanford the marble consists of granoblastic carbonate with minor graphite; a similar rock occurs along the northern flank of the pluton near the headwaters of Windy and Stitt Creeks. Folded marble beds on Mount Enterprise contain coarse blades of tremolite and phlogopite.

Amphibolite is not common in the country rock but is exposed in a syncline east of Stockmer Glacier, in polished outcrops below Granite and Silvertip Glaciers, and in outcrops north of Swan Creek and Granite Glacier. It consists of plagioclase (An_{35}) and green hornblende with minor amounts of garnet, biotite, and quartz. Garnet and biotite are slightly altered to chlorite. Sphene occurs in all samples and zircon, apatite, and scapolite are present in some.

Pegmatite and aplite dykes make up a small portion of the country rock. Although grain size varies from one exposure to another, the dykes are usually medium to coarse grained. They typically consist of 50 per cent quartz, 5 to 10 per cent muscovite, and 40 to 45 per cent feldspar. The proportion of plagioclase (An_{25}) to microcline varies considerably from one specimen to another. Muscovite is everywhere present, and biotite and garnet occur in some dykes. Biotite is frequently altered to chlorite.

Migmatitic rock forms a thin and frequently discontinuous selvage around the pluton. The zone is usually a few hundred feet wide, and is well exposed along the south flank of the pluton between Belvedere Glacier and Mount Stockmer, at the tip of Granite Glacier, and along the north flank near Austerity Creek. It is absent along the east contact. The migmatite consists of a strongly foliated mixture of sillimanite-bearing mica schist and discontinuous aplite veins both parallel to the foliation and in the form of ptygmatic structures. The occurrence of this zone as mantle around the body suggests that it is related to the emplacement of the pluton; and apart from structural disruption, appears to represent the only feature in the country rock that can be attributed to emplacement of the pluton.

PLUTONIC ROCKS

Modal compositions of representative rocks composing the pluton are given in Appendix A, and classified in Figure 12 (sample localities are shown in Fig. 3). Average modal compositions are shown in Table 1. The approximate composition and general modal variation within the various rock units is shown in Figure 13. A progressive mineralogical change from the hypersthene-augite monzonite core to the quartz-rich peripheral rock is evident in the diagram.

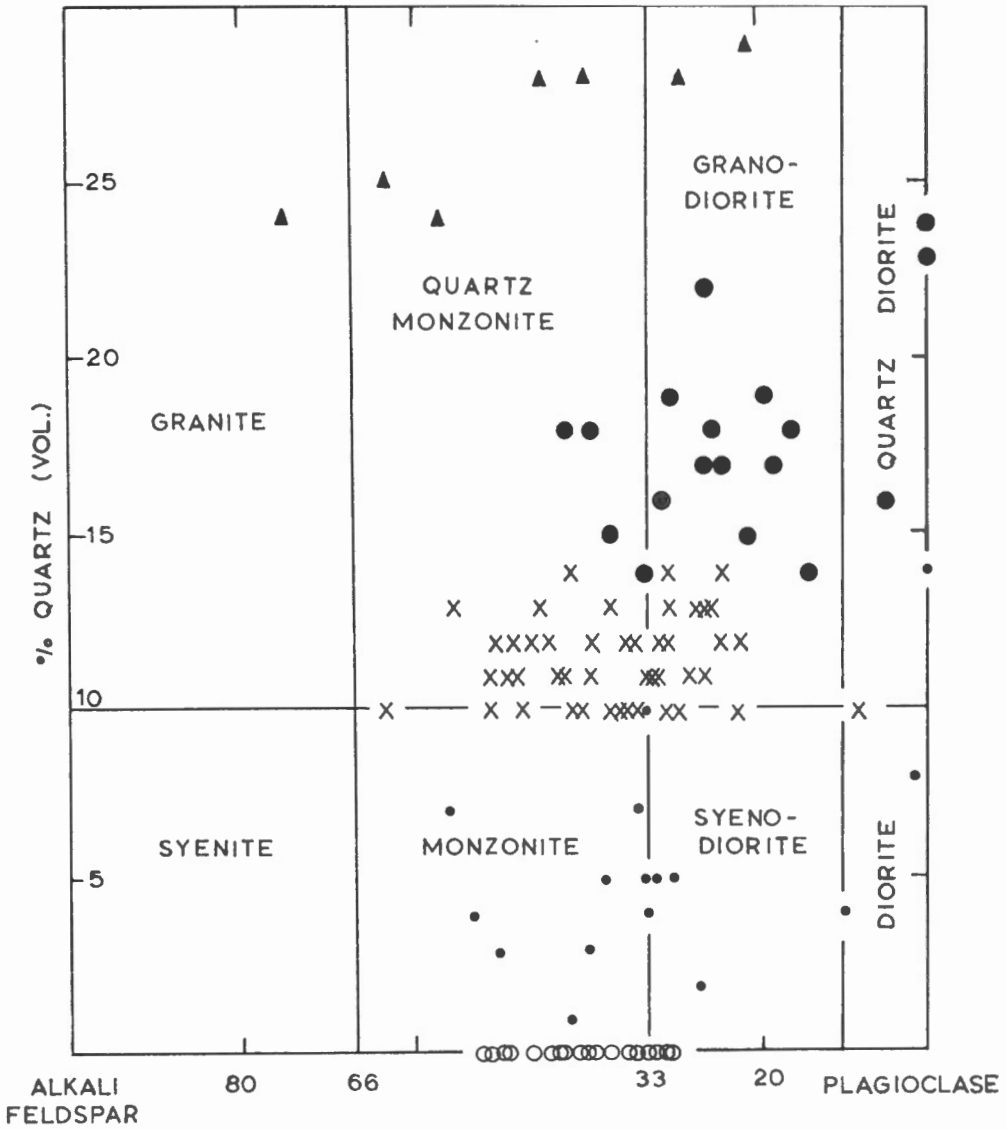

▲ = Pegmatite and aplite
● = Biotite-hornblende granodiorite
× = Hornblende-quartz monzonite
• = Transition zone
○ = Hypersthene-augite monzonite

Figure 12. Modal classification diagram.

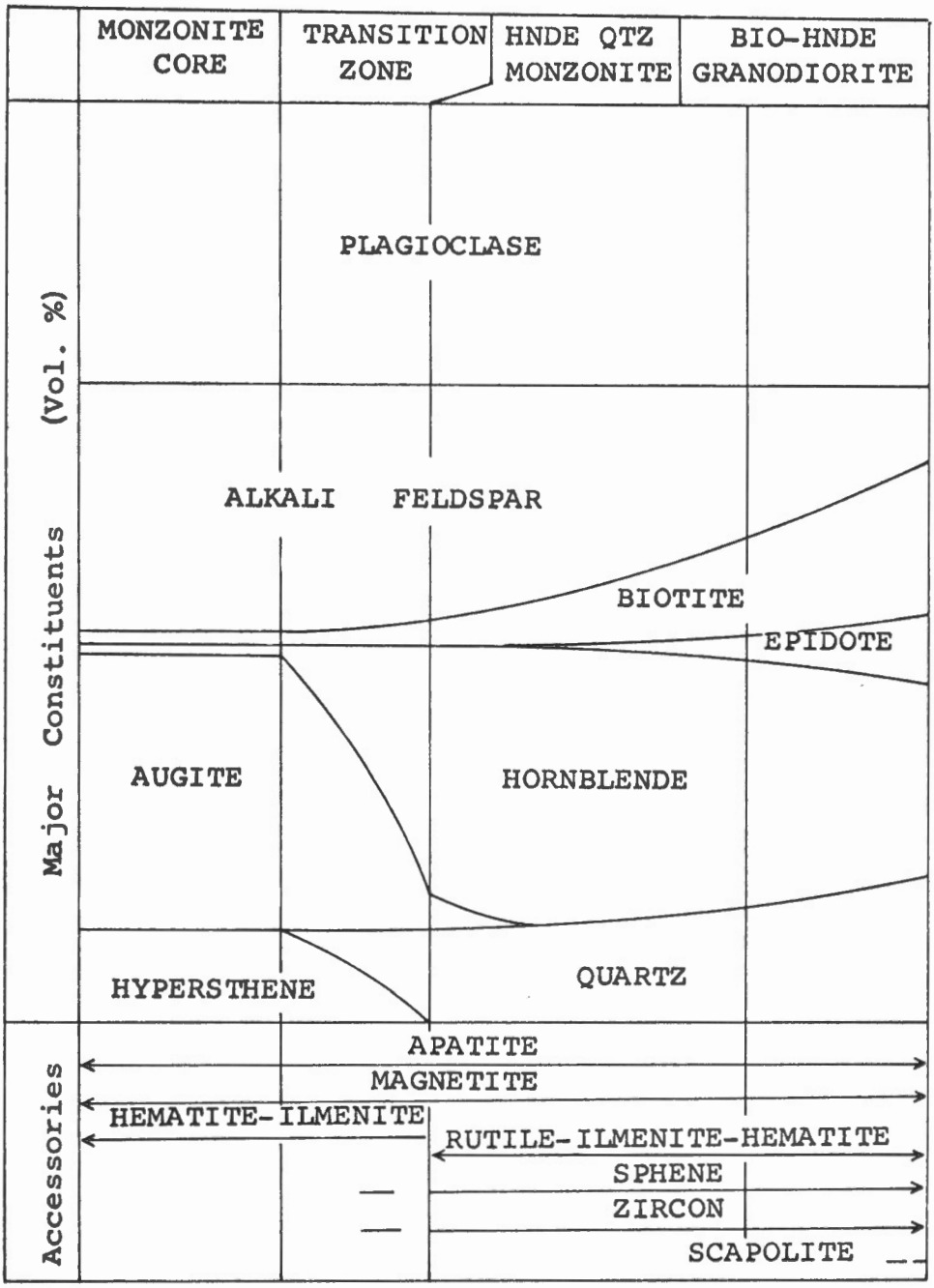

Figure 13. Generalized mineralogical composition and modal variation in different rock units. Diagram shows the general variation from centre to edge (left to right).

Table 1

Average Modal Compositions of the Main Rock Units

	Monzonite	Transition Zone	Quartz Monzonite	Granodiorite
Quartz	+	5	12	18
Plagioclase	34	37	30	31
Alkali feldspar	27	17	17	10
Hornblende	1	15	36	24
Biotite	2	6	4	13
Augite	21	13	+	+
Hypersthene	11	3	-	-
Accessories	4	3	1	4
N	24	17	47	20

+ = present in accessory amounts
- = not found
N = number of analyses

Monzonite (map-unit 3)

(i) Megascopic Description

Hypersthene-augite monzonite makes up the core of the east part of the pluton. It is a dark brown rock weathering to a dark reddish brown. In contrast to the peripheral rocks, inclusions are rare. Apart from a few small indistinct bodies, the only large inclusion is a quartzite block about twenty feet thick exposed on the south face of Black Friar Peak. Sharp-walled pegmatite dykes are common, particularly along the margin of the body. Pegmatites follow joint planes and shear zones, and are bounded by hornblende-rich borders of altered monzonite. The origin of these hornblendic zones has been considered elsewhere by the writer (Fox, 1962).

In hand specimen, monzonite is equigranular, medium grained, 1 to 1.5 mm (Fig. 14). Plagioclase laths are conspicuous and form a planar fabric in the rock. Equant grains of alkali feldspar are also present. Both

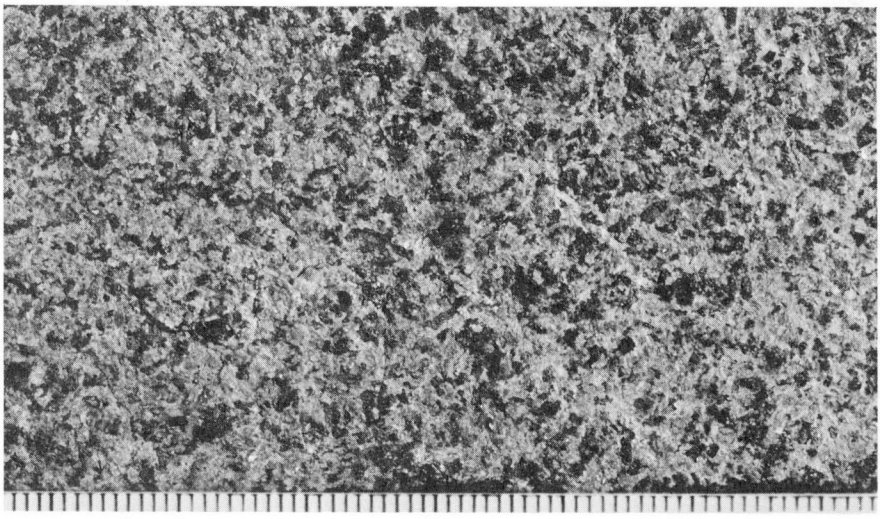

Figure 14. Hand specimen of hypersthene-augite monzonite. Lath-shaped grains are plagioclase crystals, dark stubby mineral is pyroxene. Plate illustrates the equigranular and massive appearance of monzonite. (Scale in millimetres, specimen from south side Mount Adamant.)

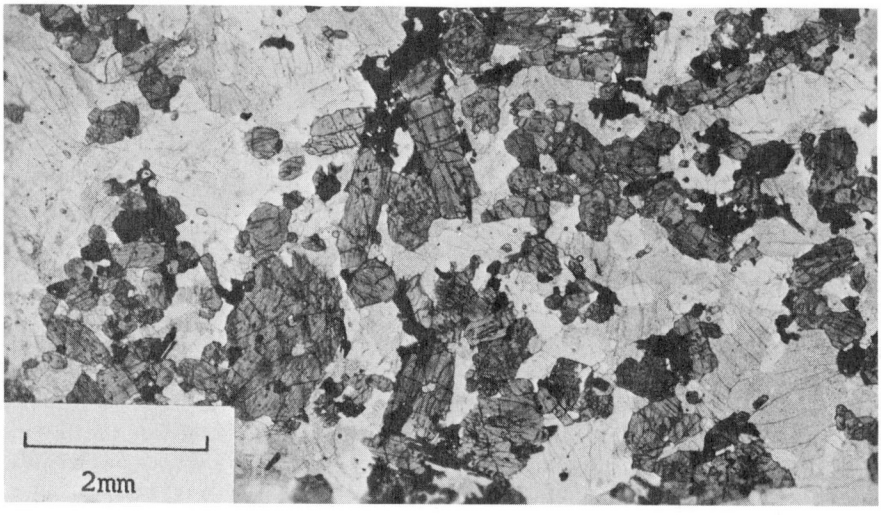

Figure 15. Photomicrograph of monzonite. Subhedral to euhedral pyroxene, locally clumped together, is surrounded by tabular to lath-like plagioclase and alkali feldspar (stained). Hornblende and biotite (opaque) form thin mantles around pyroxene. Plane light.

feldspars have a peculiar brown colour. Stubby crystals of pyroxene, occasionally forming aggregates 2 to 3 mm across, make up the mafic portion of the rock.

(ii) Microscopic Description

In thin section monzonite is typically hypidiomorphic-granular (Fig. 15). Grains range in size from 0.5 to 2 mm, averaging about 1.5 mm. Average composition is shown in Table 1.

Plagioclase occurs as subparallel tablets of andesine, normally and continuously zoned from An_{45} to An_{39}, 1 to 2 mm in length. Many long plagioclase laths are bent and many are broken. Orthoclase microperthite forms equant or tabular anhedral grains 1 to 1.5 mm. Tabular crystals conform to the planar fabric produced by aligned plagioclase laths. Alkali feldspar crystals, although rarely bent and broken, have undulatory and irregular extinction. Grain boundaries between feldspars are smooth and gently curved. Many microperthite grains are crowded with irregular inclusions of twinned plagioclase, many of which have the same optical orientation. More than one oriented group of inclusions may occur within the same alkali feldspar crystal. Plagioclase inclusions are distinguished from albitic lamellae of microperthite by the well-twinned character and calcic composition of the inclusions. Further, the inclusions have the same twinning, composition, and many have the same optical orientation, as nearby plagioclase crystals in the rock, but differ in their minute size and irregular shape. The continuous optical orientation of groups of inclusions suggests that they were once part of a large single plagioclase crystal. Myrmekite is locally abundant and generally occurs between grains of plagioclase and alkali feldspar.

Hypersthene (X = pink, Y = pale pink, Z = pale green) and pale green augite make up about 40 per cent of the rock and form euhedral prisms 1 to 2 mm long. Opaque inclusions are common and frequently occur as trellis patterns, patches, or zonal arrangements within grains of augite. An unknown translucent brown mineral is also found as minute plates in both augite and hypersthene. These plates vary in amount and are frequently absent.

Hornblende and biotite are rarely absent from monzonite but compose only about 5 per cent of the rock. Hornblende forms thin mantles around pyroxene, and radiating clusters of biotite intergrown with minute grains of quartz occur between hypersthene and alkali feldspar.

Accessory minerals in monzonite include magnetite, intergrowths of hematite and ilmenite, apatite, and a few hematite inclusions in biotite.

Transition Zone (map-unit 4)

(i) Megascopic Description

The transition zone forms an envelope around the monzonite core one-half to one-third of a mile thick. A progressive change from monzonite to hornblende quartz monzonite is evident in this zone. It is generally a brown rock much the same as monzonite, but becomes dark grey at its outer boundary. Inclusions are rare, but swarms of sharp-walled pegmatite dykes are locally abundant. As in monzonite the dykes are bordered by hornblende-rich reaction zones. The reaction zones are conspicuous at the inner margin of the transition zone, but are indistinct at the outer boundary where the transition zone grades into hornblende quartz monzonite.

In hand specimen the transition zone is much the same as the monzonite core. It is medium grained, the grain size averaging 2 mm. Aligned plagioclase laths are evident everywhere except at the outer margin where plagioclase, alkali feldspar and small amounts of quartz form an equigranular groundmass around large anhedra of hornblende and biotite. Hornblende and biotite increase in abundance outwards from the monzonite core. Pyroxene, abundant near the monzonite, is elsewhere thickly mantled by hornblende. Large biotite crystals are intergrown with pyroxene, and are notably discordant to the planar fabric produced by plagioclase laths.

(ii) Microscopic Description

Thin sections show the transition zone to vary widely in texture and mineral composition. Texture varies from hypidiomorphic-granular at its inner boundary to xenomorphic-granular where the transition zone grades into the enclosing hornblende quartz monzonite. Grain size is more variable in the transition zone than in the monzonite core, and the smooth outlines of feldspar grains typical in the core rock are absent. Many equant grains 0.02 mm occur between grains up to 2 mm long. Much of the transition zone, particularly near its inner boundary, has a well developed mortar texture. Figure 16a shows fine grained feldspar composing an equigranular matrix and veins that thread their way among much coarser grains of plagioclase, alkali feldspar, and pyroxene.

Quartz is not a common mineral in the transition zone, but increases in abundance and grain size towards the outer margin. It occurs as minute worm-like inclusions in hornblende and biotite at the inner boundary, and where the transition zone passes into hornblende quartz monzonite, it occurs as separate anhedral grains making up 5 to 10 per cent of the rock.

Feldspar has the same tabular habit present in the monzonite core, but grains are commonly bent and fractured, and where the transition zone has a pronounced mortar texture, there is a wide range of grain size. The tabular habit of feldspar grains and associated mortar texture is shown in Figure 16a.

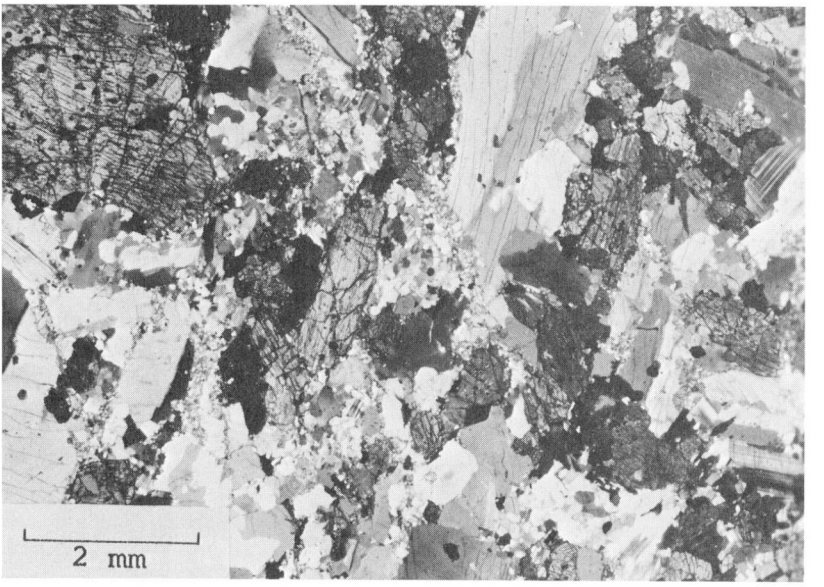

(a)

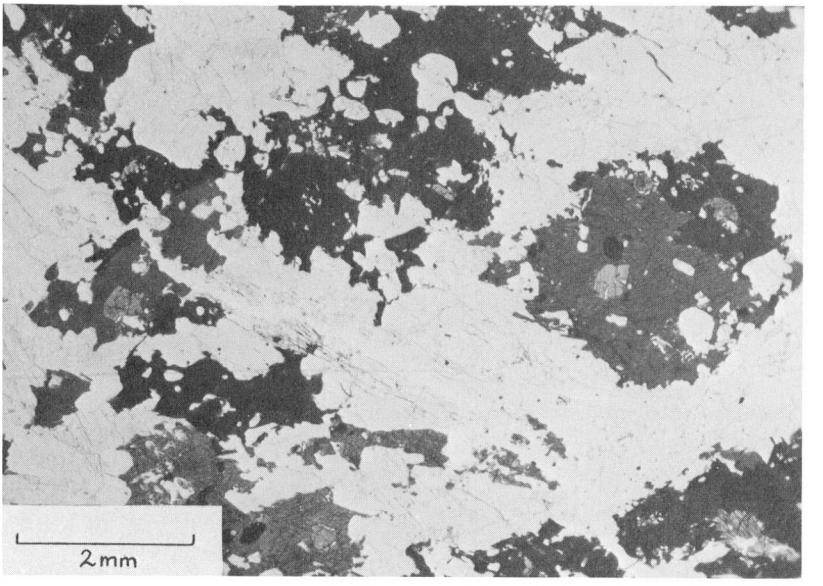

(b)

Figure 16. Photomicrographs of thin sections from the transition zone. See text for explanation. (a) crossed nicols, (b) plane light.

Alkali feldspar is generally orthoclase microperthite in which each grain consists of a single Carlsbad twin. Microcline microperthite occurs in transitional rocks near Remillard Peak. There and elsewhere in the transition zone, grain margins are generally free of exsolved albite lamellae, but the lamellae increase in size towards the centre of the grain. Plagioclase has a wide range in composition, particularly near the outer margin of the transition zone where crystals are zoned from about An_{49} to An_{38}.

Mafic minerals are the most variable constituents of the rock. Thick mantles of hornblende (X = pale brown, Y = dark brownish green, Z = bluish green) about pyroxene are a characteristic feature. Hypersthene and augite are identical optically to that in the monzonite core, but their equant or stubby form is obscured by mantles and complex intergrowths of hornblende and biotite. The typical shape and occurrence of hornblende is shown in Figure 16b. Hornblende (dark) forms large irregular anhedra crowded with inclusions of quartz and feldspar (colourless), and encloses one or two relict pyroxene grains (light coloured mineral with cleavage).

Textural relations among the various mafic minerals are shown in Figure 17. Hornblende (Hn) mantling augite (Px) is shown in Figure 17a. The augite crystal is embayed, almost surrounded by hornblende, and occurs as both large and small irregular grains distributed throughout the hornblende mantle. A single optical orientation and cleavage direction is common to all of the grains suggesting that they are remnants of a much larger augite grain. Figure 17b shows hornblende enclosing remnants of three augite grains. The hornblende is irregular in shape and crowded with inclusions of quartz. Separate hornblende grains near the mantled augite are sponge-like grains charged with quartz inclusions. Hornblende mantles usually consist of one or two grains (Fig. 16a). Biotite mantles, however, consist of complex plumose grains intimately intergrown with quartz and locally with opaque grains. Figure 17c, d show feather-like biotite mantles radiating from hypersthene grains (Px) and embaying microperthite (Or) and plagioclase (P). Hornblende is intergrown with biotite adjacent to the plagioclase grain (Fig. 17c). Replacement of pyroxene, alkali feldspar, and plagioclase by hornblende or biotite is clearly evident from the textural relations shown in Figure 17.

Accessory minerals are apatite, magnetite, and lamellar intergrowths of ilmenite and hematite. Grains of hematite lacking ilmenite lamellae also occur as plates in biotite and as rims and blades in magnetite.

Hornblende Quartz Monzonite and Granodiorite (map-unit 5)

(i) Megascopic Description

Approximately two-thirds of the quartz-bearing rocks of the east part of the pluton are hornblende quartz monzonite or granodiorite. These rocks enclose the transition zone except for a small part of the pluton near

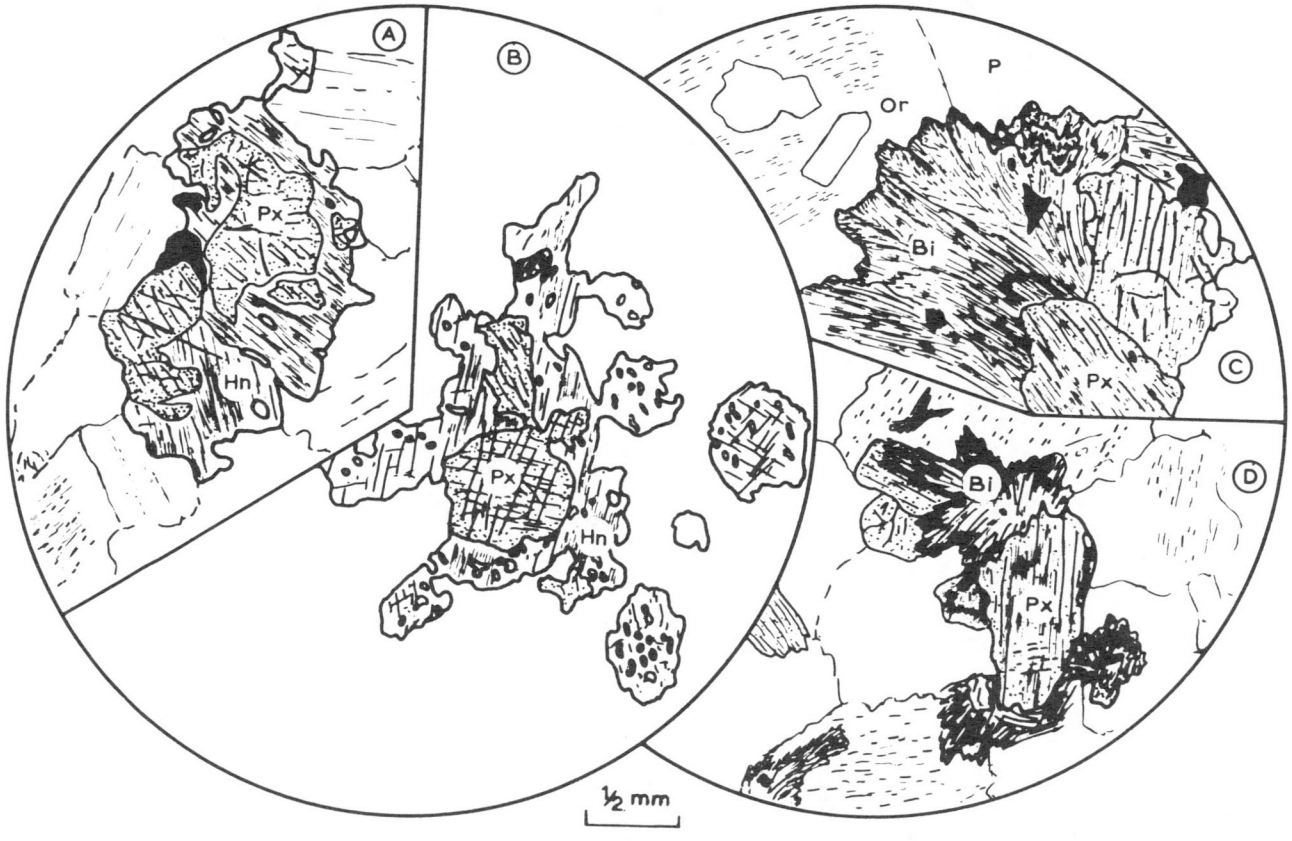

Figure 17. Textural relations among mafic minerals in the transition zone. Hornblende mantling augite is shown in (A) and (B), and the relation between biotite, pyroxene, and feldspar is illustrated in (C) and (D). Hn = hornblende, Px = pyroxene, Bi = biotite, Or = alkali feldspar, P = plagioclase. Diagram drawn from photo micrographs.

Silvertip Glacier where the transition zone lies against the country rock. West of Stitt Creek the pluton is entirely hornblende quartz monzonite except for two pods of transitional rocks at Kates and Remillard Peaks. Quartz monzonite could not be mapped separately from granodiorite in the field and so both are considered together as quartz monzonite.

Pegmatite and aplite dykes are common in quartz monzonite. These bodies form sharp-walled sheets, and near the margin are associated with the migmatitic rocks described earlier. Inclusions in hornblende quartz monzonite are common and many kinds and sizes are present. Those that are found most frequently are country rock xenoliths and mafic-rich disks and rods. Xenoliths consist of quartzite and marble, and range in size from a few inches to a few tens of feet. These are generally confined to the marginal part of the pluton. Marble blocks are invariably rimmed with or partly converted to amphibolite. The mafic-rich inclusions are more widespread than country rock xenoliths. These mafic bodies are generally a few inches long and occur as groups concordant to planar structure in the quartz monzonite. They consist of hornblende and minor amounts of quartz, biotite, and plagioclase.

Other inclusions are rare but wollastonite-diopside-garnet inclusions are locally abundant near Granite Glacier. These pyroxene hornfels bodies are three to six inches in size, equant, and invariably have zones or rings a few millimetres thick at their margin. These consist of an inner garnet-quartz-diopside ring and an outer one of diopside-quartz-plagioclase. These two rings are absent in some inclusions and a single one consisting of quartz-epidote-plagioclase is found instead.

Hornblende quartz monzonite is a dark grey rock weathering to a dark grey, friable surface. Quartz and feldspar form a white matrix around black hornblende and the occasional fleck of reddish brown biotite. In hand specimen (see Fig. 19) the rock is generally equigranular and medium grained. Hornblende is the most abundant and conspicuous mineral in the rock. Quartz and feldspar are equant, and form a granular matrix around the hornblende anhedra. This equigranular matrix, characteristic of all the peripheral rock, is also shown in Figure 21. Biotite is absent or inconspicuous in most hand specimens. Crystals of sphene and epidote are accessory minerals frequently visible.

(ii) Microscopic Description

In thin section, hornblende quartz monzonite is a xenomorphic-granular rock, and has a mean grain size of 1.5 mm. Grains range in size from 0.02 mm to 3 mm. Although the rock is approximately equigranular, quartz and feldspar are somewhat finer grained than associated hornblende. The former are equant and range in size from 0.2 to 1.5 mm, mean size being 1 mm. Hornblende generally forms anhedra 2 to 3 mm in size. Figure 18 shows the modal variability within the unit, and particularly the increasing quantity of biotite and quartz towards the margin of the pluton.

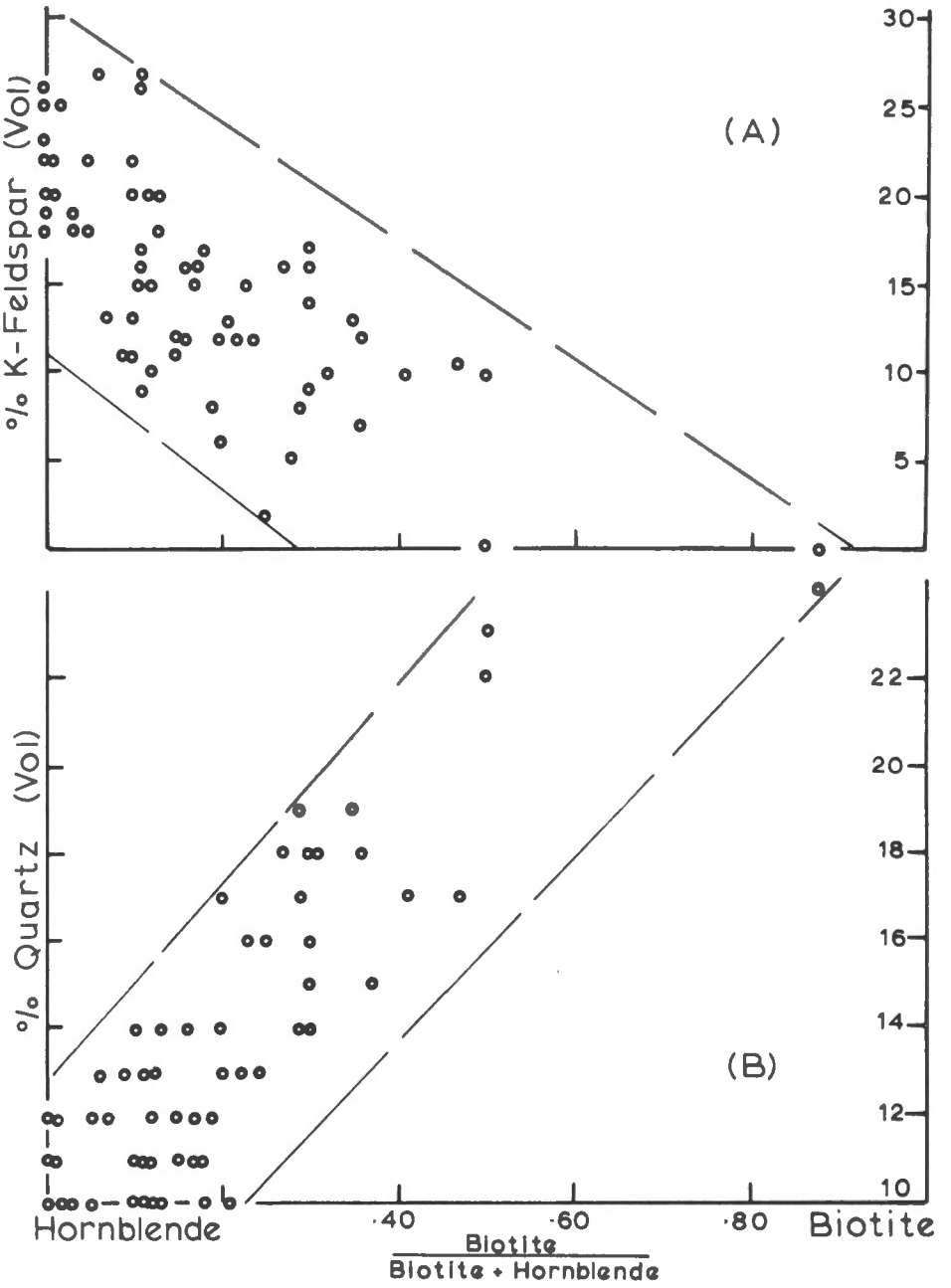

Figure 18. Alkali feldspar (A) and quartz (B) content of hornblende quartz monzonite and biotite-hornblende granodiorite plotted against the ratio of biotite to hornblende + biotite

Quartz occurs as equant anhedral grains. Feldspars are equant and are finer grained than their equivalents in monzonite and in much of the transition zone. Plagioclase is andesine-oligoclase, and is normally and continuously zoned. Alkali feldspar varies from microperthite grains with albite-free margins to nearly optically homogeneous grains that have a few albite lamellae concentrated in the cores. Myrmekite is present but is not as abundant as in monzonite.

Mafic minerals are hornblende and biotite. Hornblende (Fig. 20a) forms large irregular anhedra 2 to 3 mm, commonly crowded with inclusions of quartz and feldspar. Augite grains commonly form cores of the poikilitic hornblende grains throughout this unit. These augite grains, like those in the transition zone appear to represent remnants of augite crystals. A remnant grain of this sort can be seen thickly mantled with hornblende (dark) in the lower right corner of Figure 20a. Biotite is not abundant and is absent from some rocks in the west part of the pluton. Where it occurs biotite forms straight leaves among feldspars and is frequently intergrown with hornblende.

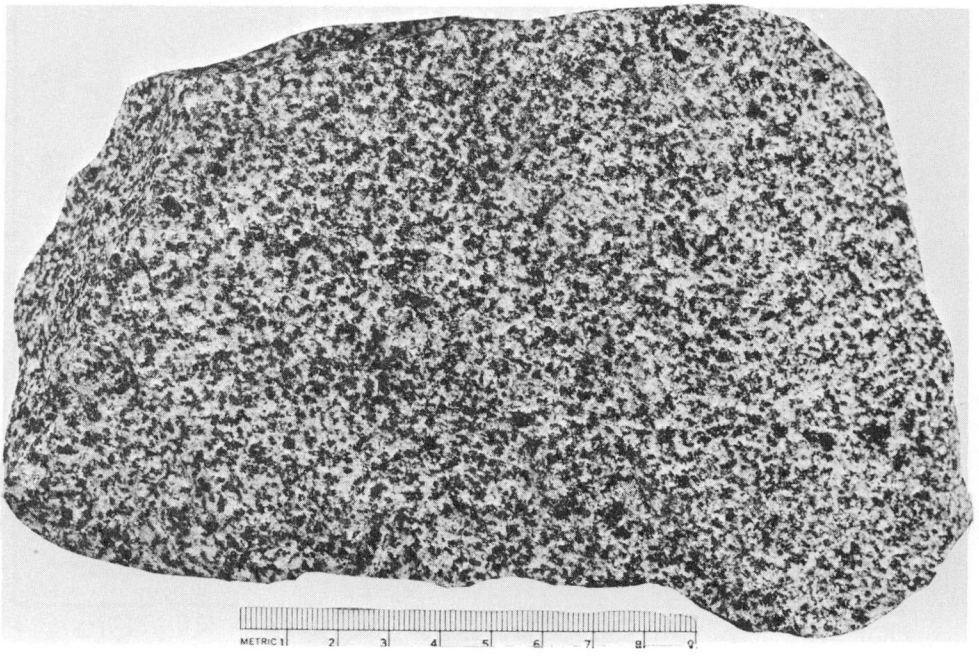

Figure 19. Hand specimen of hornblende quartz monzonite. Hornblende anhedra (dark) are surrounded by a granular matrix of quartz and feldspar (light). (Specimen from Thor Peak)

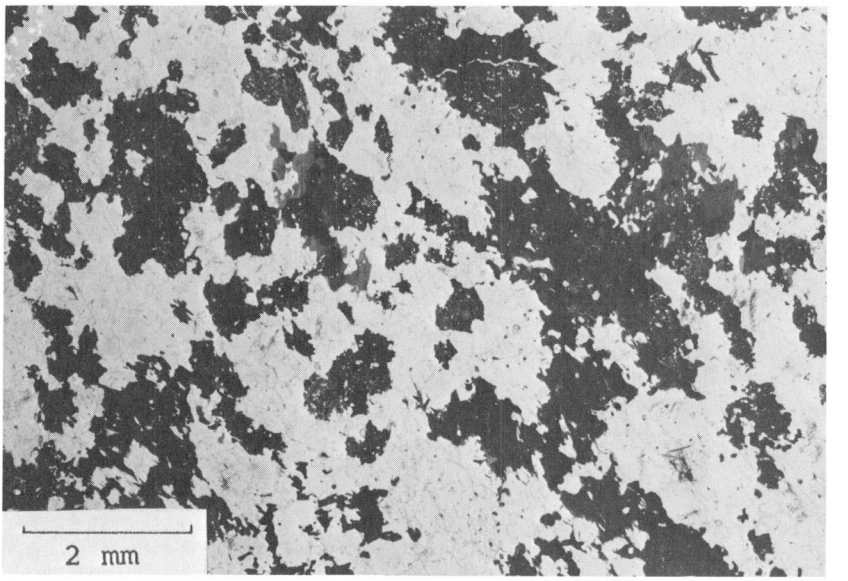

(a)

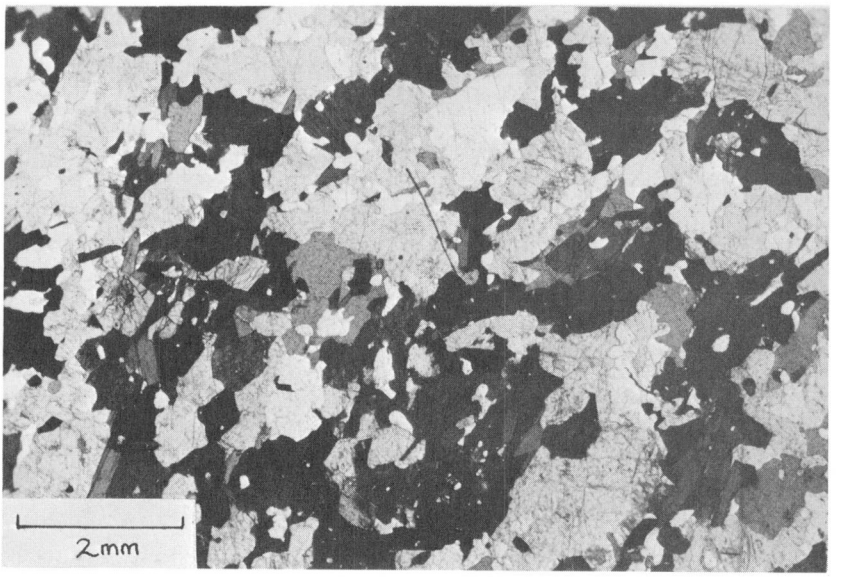

(b)

Figure 20. Photomicrographs of hornblende quartz monzonite (a), and biotite-hornblende granodiorite (b). See text for explanation. Plane light.

Accessory minerals are epidote, apatite, zircon, sphene, magnetite, and hematite grains with lamellae of ilmenite and rutile. Minute plates of hematite free of lamellae occur in biotite. Sericite and chlorite are locally abundant.

Biotite-Hornblende Granodiorite and Quartz Diorite (map-unit 6)

(i) Megascopic Description

Biotite-hornblende granodiorite and quartz diorite form a thin envelope along the margin of the east part of the pluton. This zone is one and one-half miles wide near Mount Stockmer, but thins westward along the south and north flanks. The unit ends at Silvertip Glacier on the south side, and at the headwaters of Windy Creek on the north side of the pluton.

Biotite-hornblende granodiorite is much the same as hornblende quartz monzonite. An increase in biotite content towards the margin of the pluton is evident from data in Appendix A and Figure 13. It was found convenient to assign rocks containing 10 per cent or more biotite to a separate unit. Most of the rocks classed on this basis are granodiorite, a relatively small number are quartz monzonite or quartz diorite (Fig. 12). The same types of inclusions found in hornblende quartz monzonite also occur, but xenoliths of country rock are generally more abundant. Pegmatite dykes are common and form sharp-walled sheets and lenses in migmatitic zones. Weathering features and overall colour of biotite-hornblende granodiorite are the same as hornblende quartz monzonite.

In hand specimen, biotite-hornblende granodiorite is medium grained, the mean size being 1.5 mm. The rock is invariably foliated. The typical appearance of this unit in hand specimen is illustrated in Figure 21. Rocks at the margin of the pluton are rich in biotite and have a pronounced planar fabric (Fig. 22). Quartz and feldspar form an equigranular, sugary matrix around mafic minerals of the rock. Epidote, which is usually visible in hand specimen, is particularly abundant in biotite-rich rocks at the east and southeast margin. Garnet is a notable accessory in quartz diorite that makes up most of the small oval-shaped body south of the contact near the terminus of Adamant Glacier.

(ii) Microscopic Description

Biotite-hornblende granodiorite is typically xenomorphic-granular. The rock is medium grained, averaging 1.5 mm. Its average composition is given in Table 1. Quartz and biotite are more abundant in this unit than in the lithologically similar hornblende quartz monzonite.

Quartz and feldspar are much the same as that in the hornblende quartz monzonite. Alkali feldspar, however, is rarely perthitic and commonly

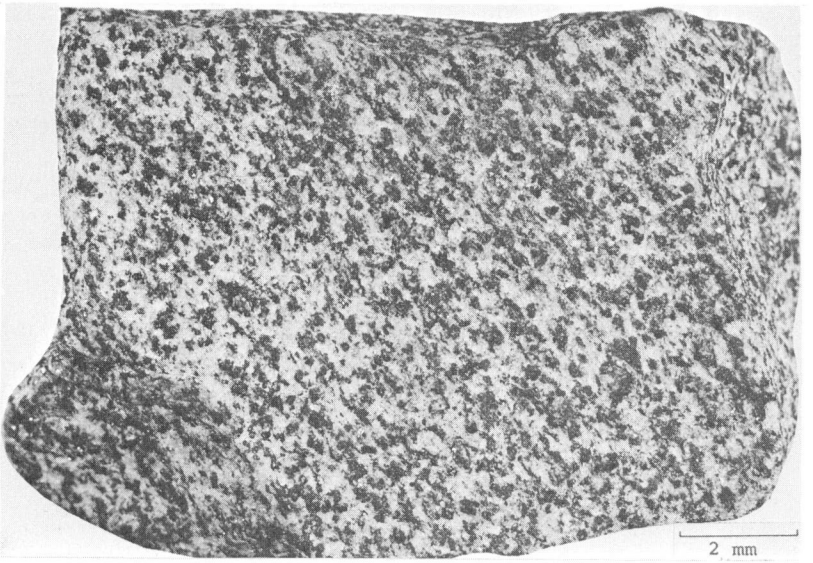

Figure 21. Hand specimen of biotite-hornblende granodiorite.

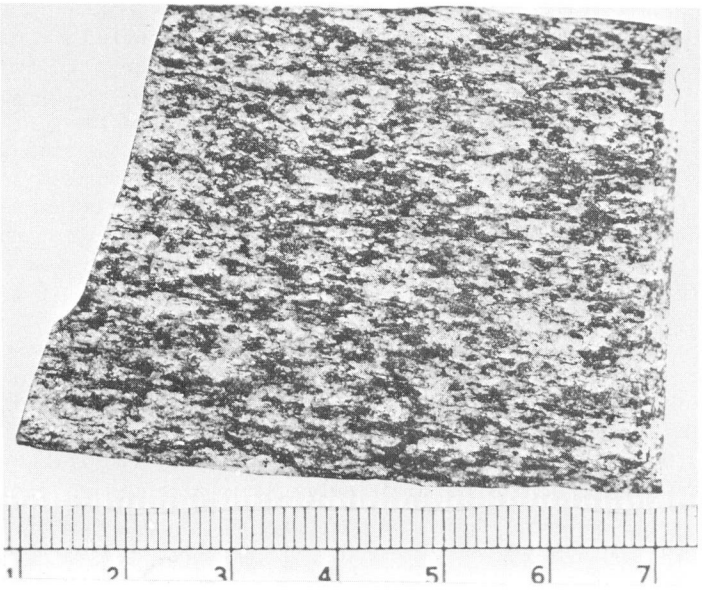

Figure 22. Hand specimen of strongly foliated granodiorite near the east margin of the pluton.

is twinned microcline. Plagioclase is generally oligoclase and occurs as slightly zoned equant grains, locally containing small amounts of sericite in the calcic cores of the crystals. Many grains are intergrown with scapolite.

Figure 20b shows the anhedral to subhedral, irregular form of hornblende in biotite-hornblende granodiorite. The sponge-like appearance typical in the hornblende quartz monzonite is not as pronounced in this unit. Remnant augite grains thickly mantled with hornblende are frequently found in thin section. Biotite is more abundant in this unit than in hornblende granodiorite, and occurs as subhedral plates intergrown with hornblende. Epidote is locally abundant and forms subhedral grains up to 0.5 mm in size.

Accessory minerals are garnet, apatite, sphene, zircon, magnetite, scapolite, sericite, and intergrowths of rutile, ilmenite, and hematite. Minor chlorite occurs along cleavage planes of biotite and along grain boundaries of garnet.

Pegmatite and Aplite

Quartz-plagioclase-microcline bodies are abundant in the pluton and have two modes of occurrence:

(a) Sharp-walled pegmatite and aplite dykes occur in all rocks of the pluton but are particularly abundant in the quartz-bearing rocks. The dykes occur singly, in stockworks, or as flat-lying interconnected swarms. Cross-cutting relations within the dyke swarms are absent, hence all dykes of this type appear to be synchronous. Dykes truncate foliation and frequently incorporate angular inclusions that appear to have been stoped from the walls (Fig. 23). Many of these inclusions can be found in various stages of disintegration to mafic clots that contain hornblende crystals identical in size and appearance to hornblende in the wall-rock. Felsic minerals that usually occur around hornblende grains in quartz monzonite and granodiorite are absent from mafic clots in the pegmatite and their place is taken by coarse grained quartz and feldspar.

(b) Pegmatite and aplite veins less sharply bounded than those just described occur in migmatite zones at the margin of the pluton. These veins are one inch thick or less, and are concordant to and emphasize foliation in granodiorite (Fig. 7). They are invariably contorted, pinch and swell, and frequently form layers, knots, and lenses. Mafic rocks are locally mixed with this pegmatitic material, or occur as selvages bordering the veins.

Pegmatite and aplite dykes vary widely in texture, grain size, structure, and occurrence. Interlayered aplite and pegmatite frequently occur within a single dyke, aplite commonly along the margin. Feldspars vary in size from 0.5 mm to 1 mm in aplite to crystals 6 inches to 1 foot long in pegmatite. Quartz invariably forms anhedral grains and constitutes 25 per cent

of the rock. Plagioclase (An_{22}) and microcline make up most of the pegmatite dykes but the proportion of these two minerals to each other varies from one specimen to another (Fig. 12). Biotite, hornblende, and epidote are accessory minerals. Biotite frequently forms thin plates up to 10 cm in diameter, and thick books 1 centimetre to 2 centimetres across. Hornblende is abundant in pegmatites that occur in monzonite. Here it frequently forms prismatic crystals oriented perpendicular to the walls of the dykes. Other accessory minerals are apatite, sphene, zircon tourmaline, magnetite, and rutile-ilmenite-hematite intergrowths. Chalcopyrite and bornite are locally abundant in quartz-rich segregations within the pegmatite dykes.

Sharp-walled pegmatite and aplite dykes in the pluton differ from those in the country rock. The latter do not have the extreme variation of grain size that is frequently observed in pegmatites in the pluton, nor do they have the same suite of accessory minerals. Hornblende is absent. Biotite occurs in some dykes but is absent from others. Muscovite and garnet are characteristic minerals. Quartz is more abundant than in pegmatites of the pluton. Feldspars have similar optical properties in dykes of both environments. Many pegmatites in the pluton strike towards the contact, but

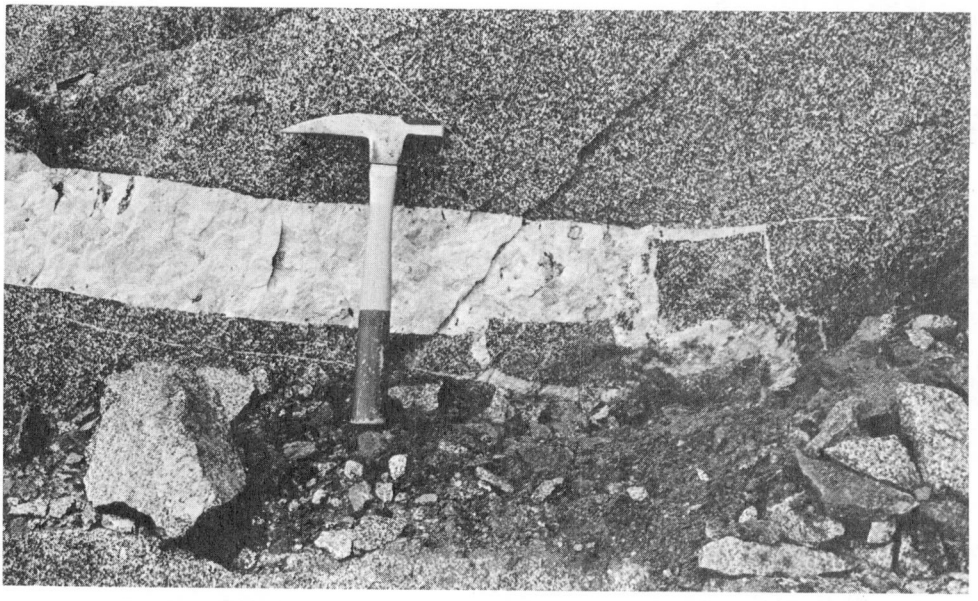

Figure 23. Sharp-walled pegmatite dyke in hornblende quartz monzonite. Blocks of quartz monzonite appear to have been stoped from the walls and floor of the dyke. Inclusions are preserved in various stages of disintegration. Pegmatite consists of quartz and about equal amounts of plagioclase (white) and microcline (grey). (Outcrop near Thor Peak)

invariably terminate within the pluton. A few quartz-feldspar veins occur at the contact but these are concordant and are not the sharp-walled type. It is concluded that sharp-walled quartz-feldspar dykes within the pluton are not equivalent to those in the country rock. Each appears to be confined to its place of origin.

Quartz Veins

Quartz veins are not abundant in the pluton and occur only in the quartz-bearing rocks. These veins frequently occur as quartz-rich segregations in pegmatite dykes. Calcite, scapolite, and epidote are common associates and biotite, specularite, chalcopyrite, bornite and chalcocite are locally abundant. Copper sulphides are particularly abundant in talus blocks at the headwaters of Stitt Creek.

Compositional Variations in the Main Rock Units

(i) Modal Variations

The content of alkali feldspar, quartz, hornblende, and biotite varies in the peripheral rocks of the pluton. Figure 18 shows the variation of alkali feldspar and quartz as a function of biotite and hornblende content (ratio of biotite/biotite + hornblende). Dashed lines in Figure 18 delimit a band of points relating the alkali feldspar and quartz content to the ratio of biotite to hornbelnde. Rocks rich in alkali feldspar are also rich in hornblende but poor in biotite and quartz. Alkali feldspar and hornblende also decrease systematically with an increase of biotite and quartz. In two rocks plotted in the diagram, alkali feldspar is absent.

The scatter of points within the dashed lines reflects the variability of the rock units, and to a lesser extent errors in the modal analyses.

(ii) Plagioclase Composition

Determinations of anorthite content of plagioclase by the Rittmann Zone method are given in Appendix A. Plagioclase grains are usually zoned to some extent, and data in Figure 24 show the range of composition from core to rim of the grains in the four lithologic units. Plagioclase crystals in monzonite show the least variation in composition, and those in the transition zone and hornblende quartz monzonite show the most compositional variation.

Both the rim and core of grains in the transition zone, hornblende quartz monzonite, and biotite-hornblende granodiorite are in general more sodic than the plagioclase in monzonite, although determinations cover a wide range of composition. Thus, in general, plagioclase is more sodic in the peripheral rocks than in the monzonite core.

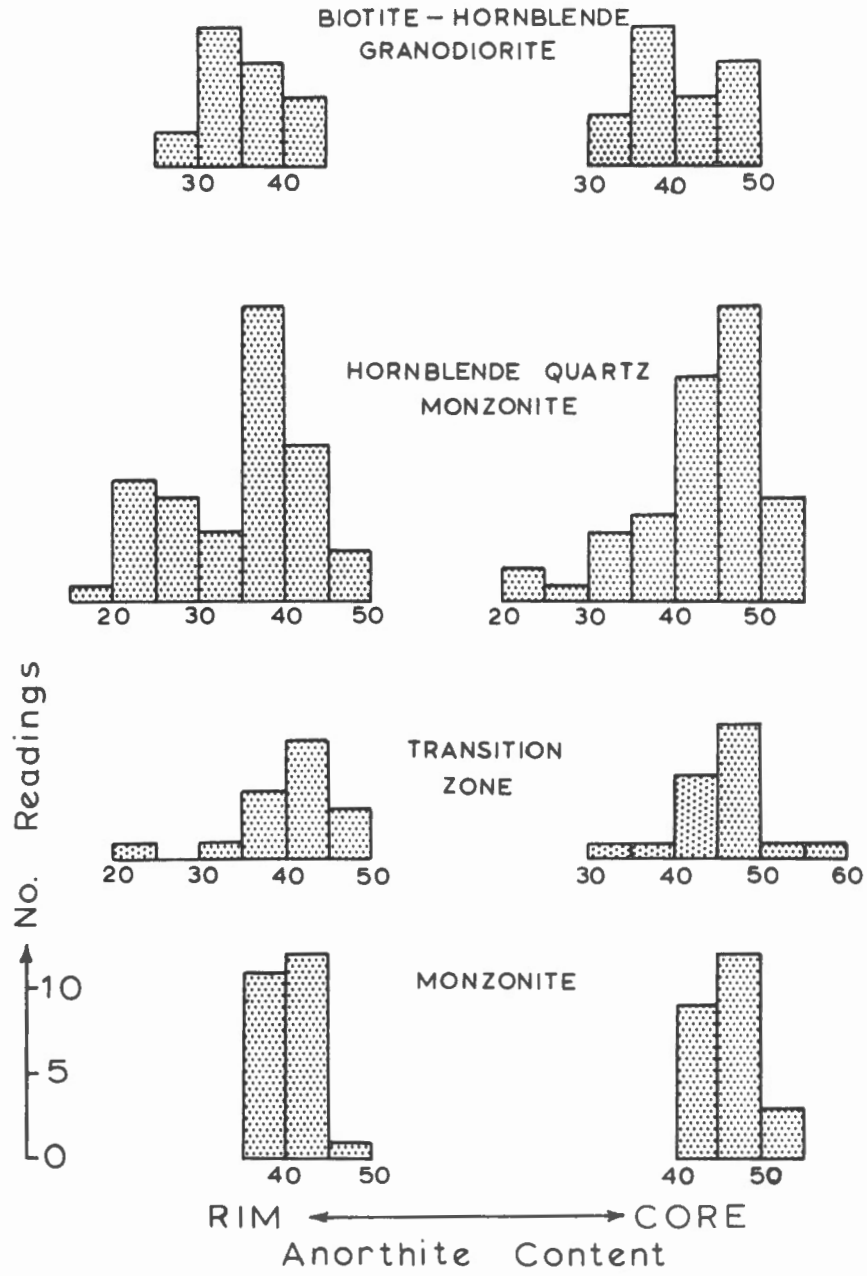

Figure 24. Histograms of plagioclase determinations for the four main rock types. Zoned plagioclase grains are plotted as core and rim compositions; homogeneous crystals plot in both sets of data.

ROCK CHEMISTRY

Chemical analyses of samples from the various rock units are given in Appendix A, and sample localities noted in Figure 3. The concentration of SiO_2, MgO, Fe, and alkalis is plotted against distance from the pluton contact in Figure 25. Table 2 and Figure 25 show that there is only a slight difference of chemical composition between rock units, H_2O, MgO, and SiO_2 being the chief variables. It is important to note that many rocks of identical composition consist of different mineral constituents.

It is concluded that the transition zone and other rock units do not correspond to different bulk chemical compositions, but that there is a general chemical similarity among rocks of different mineral assemblages. Analyses (5) and (6) of Table 2 serve to illustrate this point. Analysis (5) is a hypersthene-augite monzonite from the core near Adamant Mountain, and analysis (6) is a hornblende quartz monzonite four miles to the east near Thor Peak.

The MgO and SiO_2 contents are believed to be original inhomogeneities inherited from the monzonite prior to recrystallization. The effect of these constituents on the new assemblage will be considered in a later section.

SUMMARY AND DISCUSSION

(1) The hypidiomorphic-granular texture of the monzonite body, consisting of lath-like or tabular feldspars and euhedral pyroxenes, and the xenomorphic-granular texture of the hornblende quartz monzonite, composed of irregular, inclusion-charged hornblende anhedra surrounded by an equigranular mosaic of quartz and feldspar, are the predominant textures in the body.

(2) In the transition zone, textures are complex, and mantling and intergrowths of one mineral with another are common. This zone records the textural relation between the two main units of the pluton. Hornblende commonly encloses augite grains, and these mantles, although thin and discontinuous at the inner boundary of the transition zone, increase in thickness at the expense of augite cores until, at the outer boundary, most of the augite is replaced.

(3) Biotite is intergrown with hypersthene and alkali feldspar, and appears on textural evidence to have formed at the expense of these minerals. Plagioclase is less commonly involved in this texture, but where it is, hornblende and biotite are associated. The reactions

$$\text{hypersthene} + \text{K-feldspar} + H_2O = \text{biotite} + \text{quartz}$$
$$\text{hypersthene} + \text{K-feldspar} + \text{plagioclase} + H_2O = \text{biotite} + \text{hornblende} + \text{quartz}$$

are thus indicated by textural relations.

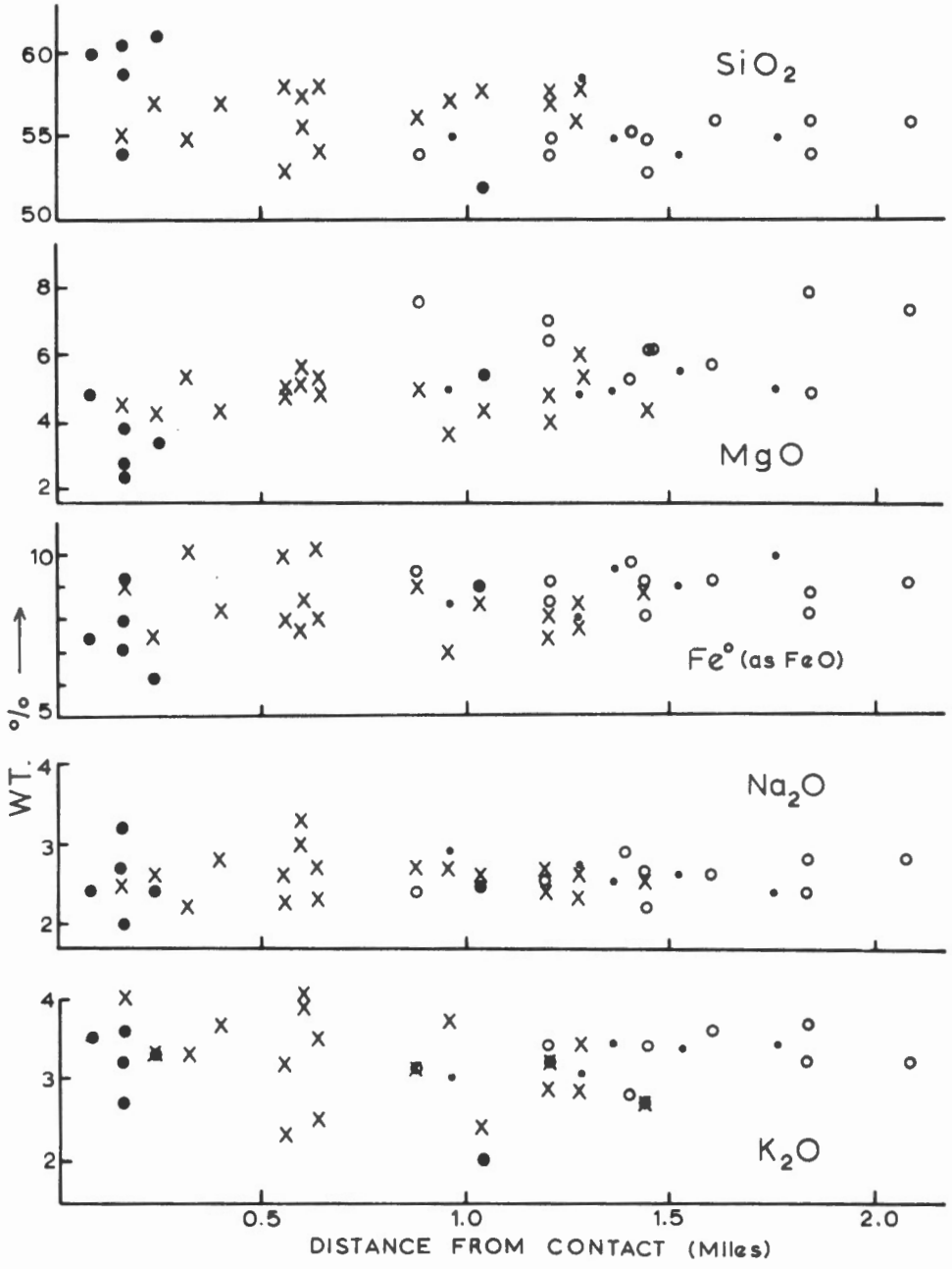

Figure 25. Bulk chemistry shown as a function of distance from the pluton contact (elements in weight per cent). Symbols same as Figure 12.

(4) Feldspars change progressively across the transition zone from tabular or lath-like grains to equant grains. This change is accompanied by cataclastic reworking of feldspar near the inner boundary, and an overall decrease in grain size from two millimetres to one millimetre.

(5) Quartz increases in size and abundance towards the outer boundary of the transition zone. This increase accompanies the progressive breakdown of pyroxenes to hornblende and biotite. The abundance of quartz inclusions in hornblende mantles and intergrown with biotite suggests that quartz is also a product of the breakdown of pyroxene.

(6) The amount of alkali feldspar and hornblende in the peripheral rock decreases systematically with an increase in the biotite and quartz content. Thus rocks rich in biotite and quartz, but poor in hornblende and alkali feldspar are frequently found along the margin.

A number of conclusions can be drawn from the above summary and the data presented in this section. These are listed below.

(1) A progressive mineralogical reconstitution of the pyroxene monzonite to hornblende quartz monzonite is recorded in the transition zone. All minerals of the monzonite are involved in the transformation.

(2) Hornblende, biotite, and quartz have formed at the expense of augite, hypersthene, and alkali feldspar.

(3) Hornblende quartz monzonite has evolved from pre-existing monzonite and is thus younger than the monzonite body.

(4) The two pods of transitional rocks in the interior of the body west of Stitt Creek, and the occurrence of remnant augite grains thickly mantled with hornblende throughout the quartz monzonite and granodiorite suggest that pyroxene monzonite was more extensive than it is now, and that it once occupied much, if not all, of Adamant pluton.

Lithologic and petrographic data in this section are in accord with the relatively young age deduced for the peripheral rocks on structural grounds. The fact that all minerals of the monzonite are recrystallized in the transition zone (conclusion (1) above) implies that the rocks were essentially solid when these changes occurred. This is an important point and must be emphasized. Any fluid or liquid must have been confined to the intergranular space, and because this is small in proportion to the solid phases, the presence of a significant amount of liquid must be ruled out as a means of effecting the recrystallization of the monzonite body. The mineralogical changes observed in the transition zone must be attributed to a metamorphic process, essentially interaction among solids and a vapour phase.

The orientation of mafic minerals in the resulting metamorphic rock in part reflects regional structural patterns. This relation suggests that the peripheral rocks evolved during regional deformation, and that recrystallization of the early monzonite is synchronous with deformation in the region.

MINERALOGY

ALKALI FELDSPAR

Optical Properties

Alkali feldspar in monzonite is orthoclase microperthite in which exsolved albite lamellae form strings and rods. Many grains in the transition zone are identical to perthite in the monzonite, but grain margins are conspicuously free of visible albite. Nearly optically homogeneous feldspar occurs in biotite-hornblende granodiorite and in the outer part of the hornblende quartz monzonite. In general, feldspars in both these rocks, although microperthites (see below), do not have sufficient exsolved albite on a microscopic or submicroscopic scale to be recorded on powder patterns.

Table 2

Chemical Composition of the Main Rock Units

	(1)	(2)	(3)	(4)	(5)	(6)
SiO_2	54.6	55.8	56.4	58.3	53.5	53.5
Al_2O_3	14.0	14.1	14.6	14.6	14.2	13.5
Fe_2O_3	2.5	3.9	3.0	2.6	2.6	3.2
FeO	6.82	5.59	5.64	5.30	7.06	7.44
MgO	6.4	5.0	4.6	4.0	5.3	5.3
CaO	7.7	6.6	6.9	8.6	8.4	8.2
Na_2O	2.6	2.6	2.6	2.5	2.9	2.3
K_2O	3.2	3.4	3.2	2.8	2.8	2.5
TiO_2	0.73	0.80	0.85	0.90	0.91	1.1
MnO	0.13	0.14	0.15	0.11	0.16	0.23
P_2O_5	0.61	0.57	0.51	0.70	0.75	0.94
H_2O	0.46	0.77	0.86	0.79	0.40	1.4
CO_2	0.02	0.01	0.06	0.05	0.00	0.00
	99.8	99.3	99.4	101.2	99.1	99.6
N	11	4	18	6	-	-

Mean composition of monzonite (1), transition zone (2), quartz monzonite (3), granodiorite (4). N = number of analyses. (5) analysis of monzonite # 83, (6) analysis of quartz monzonite # 3.

Extinction character is variable. Alkali feldspars in monzonite, and the odd grain in the transition zone and hornblende quartz monzonite, have sharp extinction. These grains have monoclinic optics, extinction being parallel to (010). Feldspar in much of the transition zone and in parts of the hornblende quartz monzonite has patchy or undulatory extinction. Poor to well developed grid twins are visible in feldspar grains in the marginal parts of the hornblende quartz monzonite and in the biotite-hornblende granodiorite. The distribution of grid twins varies from grain to grain. Some grains have twin lamellae only around inclusions in the crystal, whereas other grains are twinned throughout. There is thus a progressive development of twin lamellae from patchy extinction to typical grid twinning; this is common within a single grain.

Extinction character is plotted on a geological map of the pluton in Figure 26. The diagram shows feldspars that exhibit sharp extinction concentrated in the monzonite core, the prevalence of grains with patchy extinction in the transition zone and in parts of the hornblende quartz monzonite, and the occurrence of twinned microcline in the marginal rocks, particularly along the edge of the body.

Irregular or patchy extinction may be the result of: (1) strain due to external stress in which the grains are deformed without significantly changing the lattice geometry; and (2) structural inversion in which there is a change of lattice parameters. It was observed in rocks that have cataclastic features that, although large alkali feldspar grains have undulatory extinction, the small grains do not. This relation suggested that the formation of small grains from large relieved strain caused by an external stress. Thus small grains were selected for study in rocks that have a wide range of grain size.

Optic angle is probably the most readily obtained optical property, and its relation to structural state of the feldspar polymorphs has long been established although the effects of composition have not been fully evaluated. $2V_x$ determinations are plotted in Figure 27 (data in Appendix C). The mean of at least five 2V determinations per slide, one measurement per grain, is shown for feldspars classed by the extinction type shown in Figure 26. The 2V of grains in a single thin section varies 5° to 10° from grain to grain. Occasionally a single grain was found to vary 15° from core to edge, the high 2V being at the margin. Crystals zoned in this manner, however, are rare. The total mean 2V range is from 40° to 70°. Feldspars with sharp extinction range from 40° to 52°, with patchy extinction 44° to 60°, and with grid twins 52° to 70°. Thus there is a general correlation between 2V and extinction character. This is shown in histogram (v) of Figure 27. Patchy feldspars (histogram, iii) have been omitted assuming that they represent states of partial inversion, or grains in which domain structure (microcline twinning) is not visible. The change from optically monoclinic feldspar with sharp extinction to grid-twinned microcline occurs at 52° 2V. This, of course, is not a

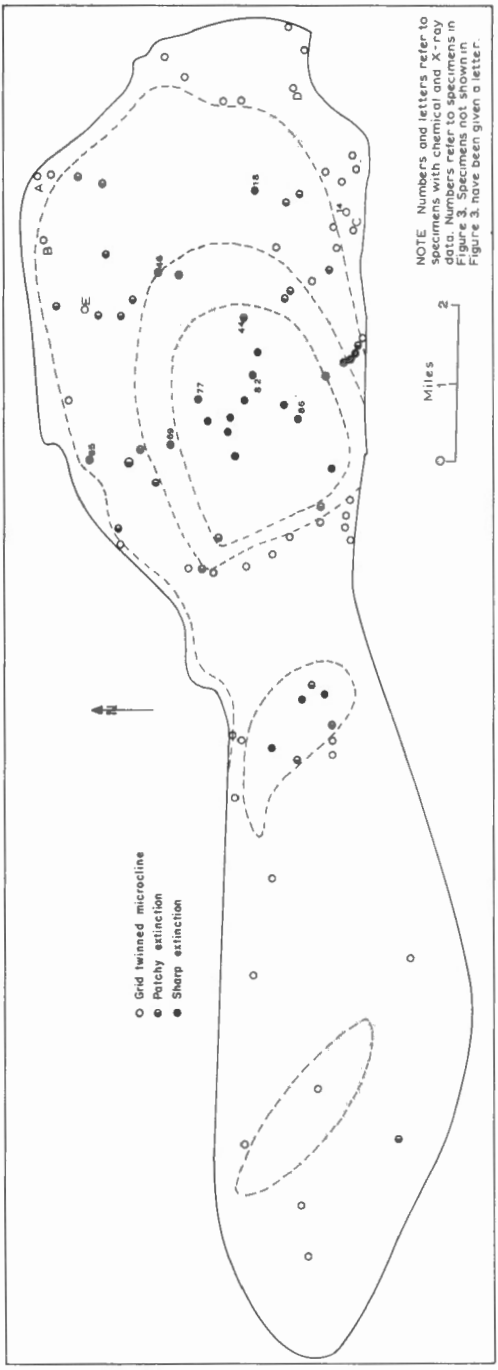

Figure 26. Optical character of alkali feldspar.

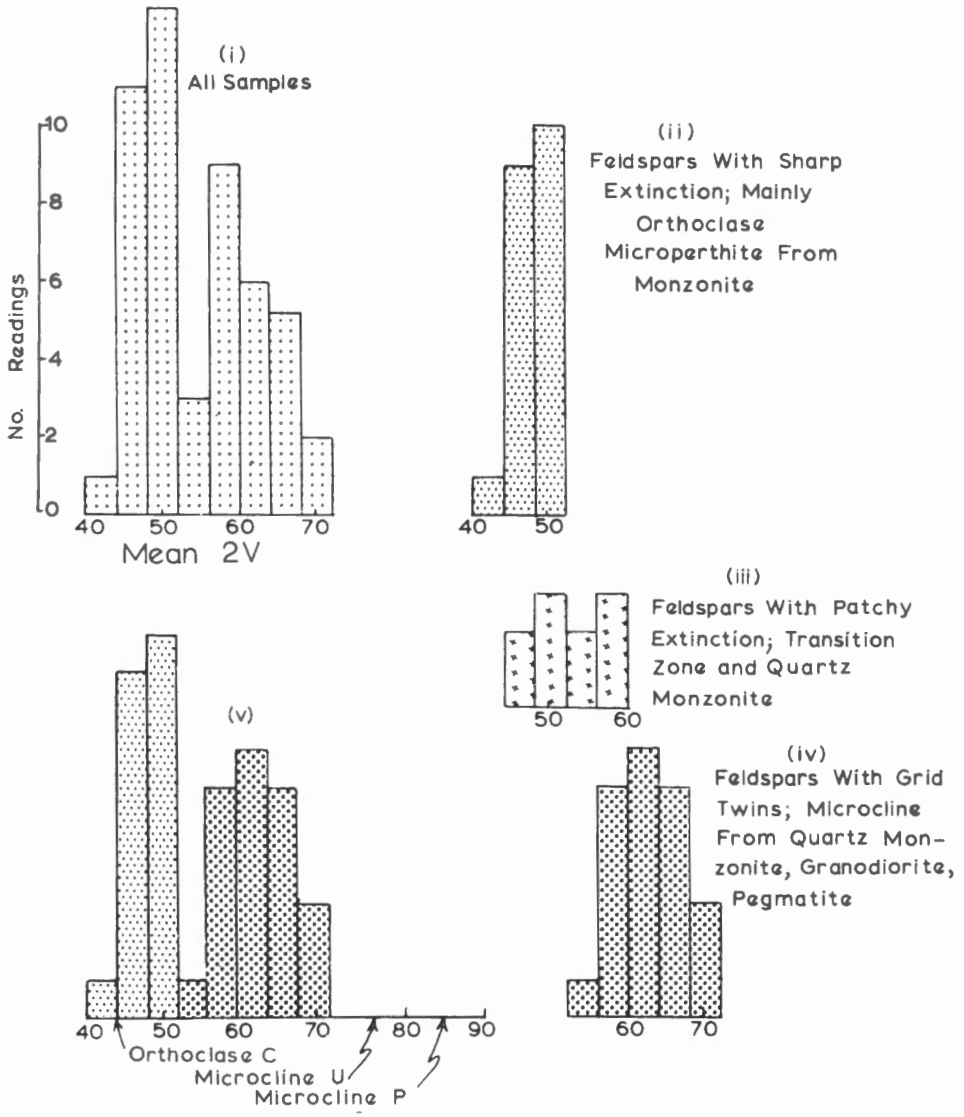

Figure 27. Mean 2V histograms of alkali feldspars. Orthoclase microperthites and microclines are compared with Spencer C orthoclase (orthoclase C, Jones and Taylor, 1961), Spencer U intermediate microcline (microcline U, Bailey and Taylor, 1955), and the Pellotsalo maximum microcline (microcline P, Brown and Bailey, 1964).

sharp transition, as testified by grains with patchy extinction overlapping both fields, and by the variability of 2V within a single grain. Nevertheless, grid twins appear consistently in grains that have 2V near 52°. 2V for Spencer C orthoclase (orthoclase C), Spencer U intermediate microcline (microcline U), and that for the Pellotsalo maximum microcline (microcline P) are also shown in the diagram. Optically, the Adamant feldspars range from orthoclase in the monzonite core to intermediate microcline at the periphery of the body.

Structural State

Powder methods were used for study of structural state. X-ray and optical data are given in Table 3. The degree of triclinicity is indicated by the (131, 130) reflections, and Δ (relative separation of (131) and ($1\bar{3}1$) reflections, see footnote to Table 3). The (131) and (130) reflections are sharp for all except for a broadening of the reflections in C, D, and 65. Microclines from the two pegmatites have broad (131) reflections or a diffuse doublet. For most of the feldspars Δ is thus O, but ranges from an estimated 0.15 to 0.98 for the grid-twinned microclines. Sample 65 is anomalous in that it has a broad (131) reflection, sharp extinction, and a 2V of 49°. These optical observations are inconsistent with those corresponding to a broad (131) reflection shown by samples C and D.

Wright (pers. comm., 1964) has studied the determination of composition and structural state of alkali feldspars from cell dimension data (see Fig. 28). A standard feldspar series was made from natural and synthetic specimens by ion exchange methods, resulting in a maximum microcline-low albite series, orthoclase-intermediate albite series, low sanidine series, and a high sanidine-high albite (or synthetic) series. The a axis dimension is virtually independent of structural state, but b and c are structurally dependent. Cell dimensions are calculated from powder data and then compared with the standard series. Figure 14 represents the potassic end of the standard suite and shows b and c dimensions of the various potassic alkali feldspar polymorphs. Solid circles represent alkali feldspars from Adamant pluton plotted from the data in Table 3. The mean 2V of each specimen is shown in brackets beside the sample number. Spencer C (orthoclase C), Spencer U (microcline U), and the Pellotsalo maximum microcline (microcline P) are also shown on the diagram.

Samples 18, 46, 82, and 86 plot with the orthoclase group, and correspond to Spencer C. A and B are displaced towards maximum microcline, and C, D, and E are close to the end member maximum microcline. All of the Adamant microclines (those having grid twins) are structurally intermediate microclines. There is also a progression from orthoclase in the monzonite, transition zone, and hornblende quartz monzonite to intermediate microcline in the peripheral rocks and pegmatites. Optical data, both 2V and

Table 3

X-ray and Optical Data for Alkali Feldspars

Rock Unit	No.	(131,130)	Δ	Extinction	Mean 2V	a	b	c	α	β	γ
BHG	A	Sharp	0	Grid twins	53°	8.5529	12.9829	7.1981		116°00.729'	
BHG	B	Sharp	0	Grid twins	56°	8.5545	12.9877	7.2005		116°00.316'	
BHG	C	Broad	.15+	Grid twins	60°	8.5636	12.9760	7.2066		116°02.104'	
BHG	D	Broad	.15+	Grid twins	64°	8.5602	12.9709	7.2052		116°00.755'	
HQM	18	Sharp	0	Sharp	48°	8.5516	12.9939	7.1948		116°01.106'	
HQM	65	Broad	.15+	Sharp	49°	-	-	-		-	
TZ	69	Sharp	0	Patchy	44°	-	-	-		-	
TZ	46	Sharp	0	Sharp	45°	8.5580	12.9936	7.1948		116°00.539'	
Monz	44	Sharp	0	Sharp	49°	-	-	-		-	
Monz	77	Sharp	0	Sharp	47°	-	-	-		-	
Monz	82	Sharp	0	Sharp	49°	8.5580	12.9939	7.1934		116°01.029'	
Monz	86	Sharp	0	Sharp	45°	8.5580	12.9957	7.1940		116°00.966'	
Pegm	14	Broad	.25	Grid twins	68°	-	-	-		-	
Pegm	E	Diffuse doublet	.67 .98	Grid twins	70°	8.5644	12.9705	7.2077	90°16.430	116°02.471'	89°06.228'

- = not determined
+ = estimated
Max. error in a,b,c, = 0.006 A°
Max. error in angles = 0.03'
Cell dimensions determined by T.L. Wright and D.B.Stewart, U.S. Geological Survey,
BHG = Biotite-hornblende granodiorite
HQM = Hornblende quartz monzonite

$\Delta = 12.5(d_{131}-d_{\overline{131}})$. Δ is the fractional deviation of α^* and γ^* in terms of maximum microcline for which $\alpha^* \sim 90°25'$, $\gamma^* \sim 92°20'$. Δ Maximum microcline = 1, Δ for monoclinic crystals = 0.
TZ = transition zone
Monz = monzonite
Pegm = pegmatite

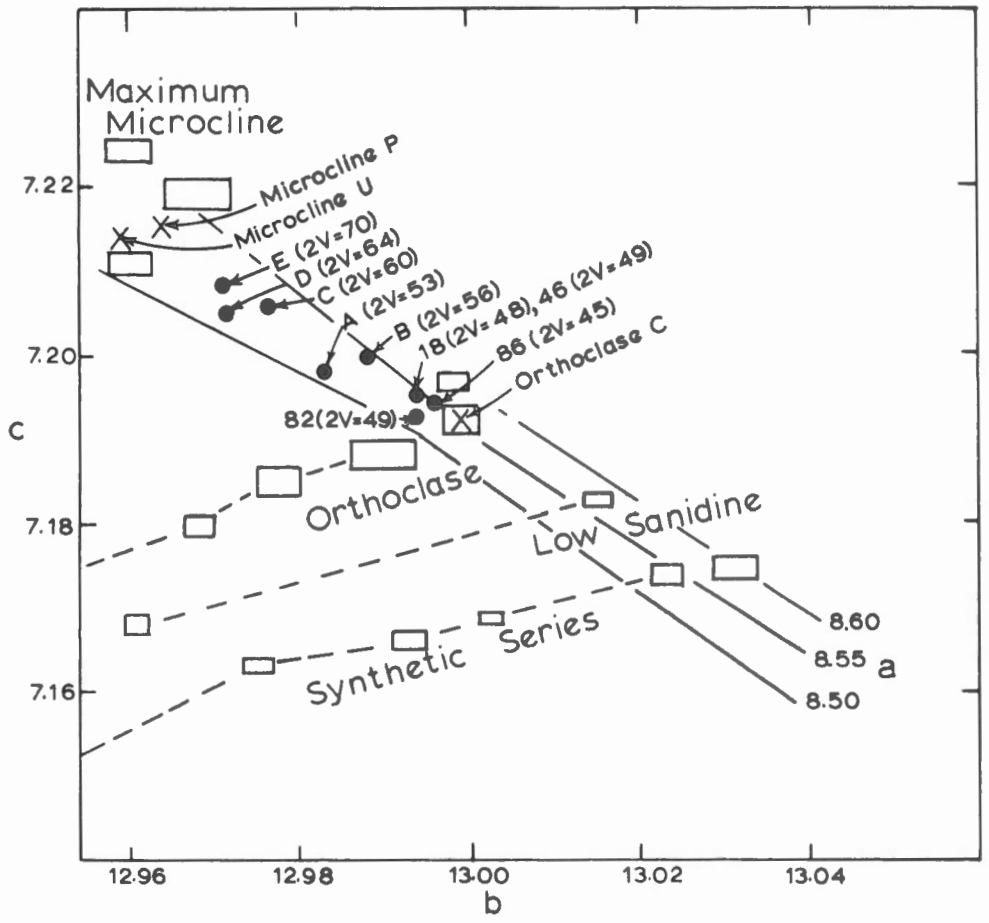

Figure 28. Structural state of alkali feldspars. Standard feldspar data shown as boxes. Samples 82 and 86 from monzonite, 46 from the transition zone, 18, A, B, C, and D from the peripheral rock, and E from a pegmatite dyke. Cell dimension data by T. L. Wright (pers. comm., 1964).

extinction character, confirm the progressive change of structural state. 2V increases as the triclinicity of the specimens, as shown by their proximity to maximum microcline, increases.

Composition

Bulk compositions of the feldspars are listed in Table 4 along with the albite content of the potassic phase determined from data supplied by Wright. The procedure used for determination of albite content is discussed

Table 4

Chemical Composition of Alkali Feldspars

Sample No.	Bulk Composition						Ab in
	K_2O	Na_2O	CaO	Or	Ab	An	S.S.
A	-	-	-	-	-	-	11.0
B	13.5	1.23	0.43	86.4	11.3	2.3	11.0
C	14.0	1.01	0.27	89.4	9.2	1.4	9.5
D	14.0	1.13	0.21	88.7	10.3	1.0	10.0
18	13.0	1.47	0.49	82.4	14.9	2.7	11.0
65	13.3	1.41	0.26	85.6	13.0	1.4	-
69	12.4	1.89	0.62	79.4	17.3	3.3	-
46	12.8	1.67	0.57	81.7	15.2	3.1	10.5
44	12.3	1.97	0.64	78.6	17.9	3.5	-
77	12.1	1.85	0.76	78.6	17.2	4.2	-
82	12.2	1.71	0.98	78.7	15.9	5.4	14.0
86	12.2	1.65	0.89	79.7	15.3	5.0	14.0
14	-	-	-	-	-	-	-
E	13.1	1.65	0.13	84.1	15.2	0.7	8.0

K_2O, Na_2O by flame photometry (P.E.F.), CaO by X-ray fluorescence (G.R.Lachance). Albite in solid solution (right column) by a dimension of unit cell. Or,Ab,An recalculated to 100%.

in Appendix D. Albite content by d_{201} (Orville, 1963) and by d_{400} (Goldsmith and Laves, 1961) are compared with the a axis method and the chemically determined bulk albite content in Table 5. Samples B, C, and D, as noted below, are essentially homogeneous materials and hence are convenient standards to test the reliability of each method. Table 5 lists the albite content determined for the Adamant alkali feldspars. Agreement between the various X-ray methods for samples B, C, and D is not encouraging. The a

axis method is in acceptable agreement with the chemical analyses but compositions by d_{201} and d_{400} are of doubtful value. Although d_{201} compositions agree for B and C, that for sample D is too low. Compositions by d_{400} are in poor agreement with the analyzed homogeneous samples. It would appear that the a axis method is a more reliable means of estimating the amount of albite in solid solution than the other two methods presently available.

Bulk albite content and albite held in solid solution are compared in Figure 29a. All of the samples except for B, C, and D plot in the perthitic feldspar field. Homogeneous feldspars, those for which bulk albite equals solid solution albite, should fall on or near the diagonal line separating the perthite field from the lined area (prohibited field). Such feldspars are represented by B, C, and D. A measure of the amount of albite exsolved from an original homogeneous feldspar is given by the vertical distance of the sample above the diagonal line. In microcline E, all but 8 per cent of its original albite content has evidently exsolved from the crystal, whereas orthoclase 82 and 86 have lost about 1.5 per cent of their solid solution albite.

Table 5

Albite Content of K-Phase

Sample No.	Chemical Bulk Albite	a axis ± 1.5% Ab	d_{201}	d_{400}
A	-	11.0	11.5	13.8
B	11.3	11.0	11.5	13.5
C	9.2	9.5	10.0	9.8
D	10.3	10.0	6.5	8.5
18	14.9	11.0	14.0	13.0
65	13.0	-	11.5	13.5
69	17.3	-	6.5	11.5
46	15.2	14.0	8.5	11.0
44	17.9	-	14.0	13.5
77	17.2	-	10.5	13.5
82	15.9	14.0	11.5	11.5
86	15.3	14.0	11.5	13.5
14	-	-	-	9.5
E	15.2	8.0	-	9.5

- = not determined. B,C, and D are optically and X-ray homogeneous. A and 14 not determined because of plagioclase impurities. Determinative curve for d_{201} in Orville (1963), for d_{400} in Goldsmith and Laves (1961). d_{400} compositions by G. Pouliot using curve midway between microcline-low albite and sanidine-analbite. d_{201} by PEFox.

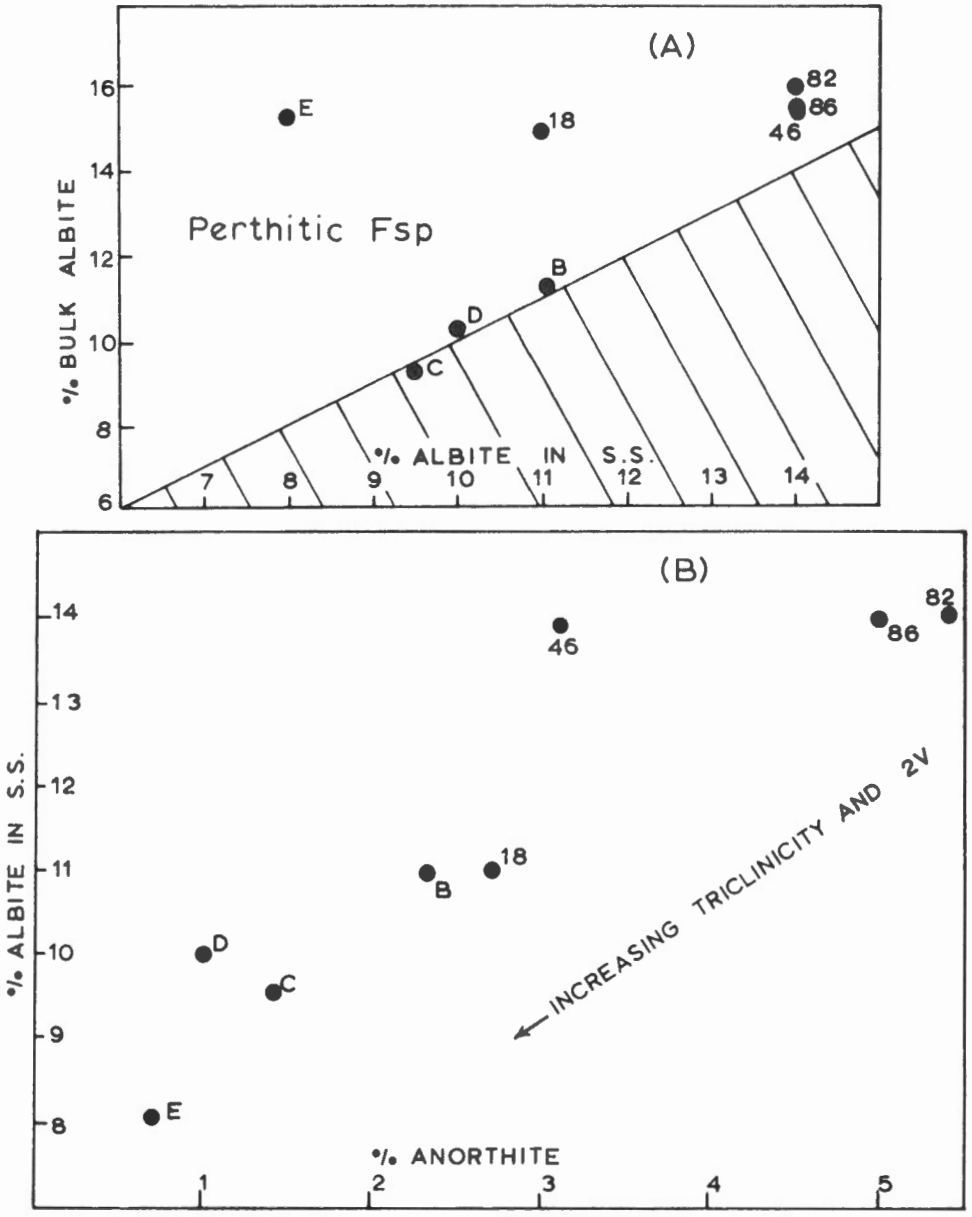

Figure 29. Albite in solid solution related to bulk albite content (A) and bulk anorthite content (B) of the alkali feldspars (weight %).

Figure 29b relates the anorthite content of alkali feldspar to albite in solid solution. Samples B, C, and D reflect the anorthite content of the potassic phase, but the others are bulk compositions. There is a decrease of anorthite content with a decrease of solid solution albite in the feldspars. This decrease of the albite and anorthite content corresponds to increasing 2V and the degree of triclinicity (Fig. 28). Albite retained in the K-phase and 2V of the K-phase are plotted in Figure 30. The solid arrow in the diagram joins samples with increasing triclinicity, and the dashed arrow joins orthoclase microperthite samples that differ only in the amount solid solution albite. Presumably the dashed arrow represents exsolution of albite with no significant change of structural state, and the solid arrow compositional changes attendant on structural adjustment.

The amount of albite and anorthite in solid solution in the feldspars of the peripheral rocks decreases towards the margin of the pluton, and these chemical changes accompany an increase of triclinicity and 2V. Microclines in the pegmatites contain the least amount of albite and anorthite in solid solution, are the most triclinic, and have the highest 2V of the feldspars studied. Thus feldspars in the peripheral rocks and pegmatites are closer to the orthoclase composition ($KAlSi_3O_8$), and at the same time closer to maximum microcline than feldspars in the monzonite core.

Figure 31 shows the approximate phase relations of the Adamant feldspars. The sanidine solvus (Orville, 1963) has been adjusted for structural changes as suggested by Wright (1964). Perthites between X and Y are structurally intermediate between sanidine and maximum microcline (U). Samples plot in the same sequence as that observed for the plot of $\underline{b}$ vs. $\underline{c}$ dimensions (Fig. 28). The solid circle on the Or side of the diagram represents the first order transition temperature between sanidine and microcline. Such an inversion is suggested by the heating experiments of Goldsmith and Laves (1954), and the analogous relations between iron microcline and iron sanidine (Wones and Appleman, 1963). The inversion temperature is not known with certainty, but 500° to 550°C is indicated by the experiments of Goldsmith and Laves. The straight lines joining this point to the solvus are contours of equal Si/Al order (contours could be represented by curved lines as well). Samples A, B, 18 plot at a point that represents the composition (and temperature) at which grid twins become visible, that is, the dividing point between orthoclase and intermediate microcline. Thus feldspars that plot in the dotted area have Si/Al distributions equivalent to that of orthoclase. The positions of the other feldspar polymorphs relative to orthoclase are shown in the diagram.

Wright (1964) observed similar structural and compositional relations among feldspars of the Tatoosh pluton as those shown for the Adamant feldspars in Figure 17. These relations may indicate a series of equilibrium states ranging from orthoclase to microcline governed primarily by the Al/Si distribution (Barth, 1934), or, as suggested by Wright, metastable states

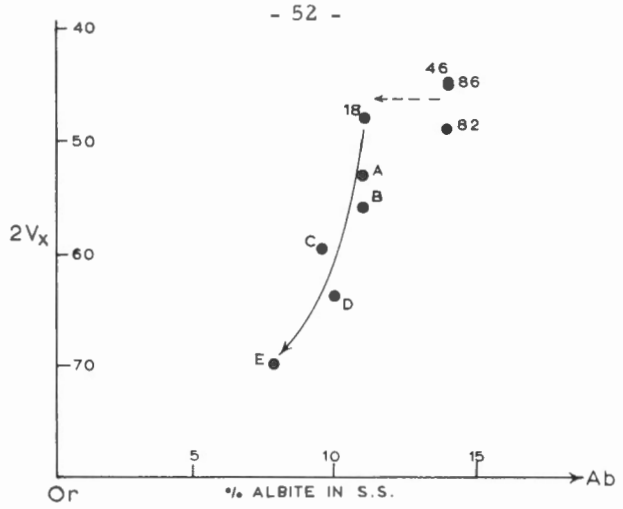

Figure 30. Albite in solid solution (weight %) related to 2V of the potassic phase. Solid arrow represents trend of increasing triclinicity, dashed arrow presumably represents exsolution without change of structural state.

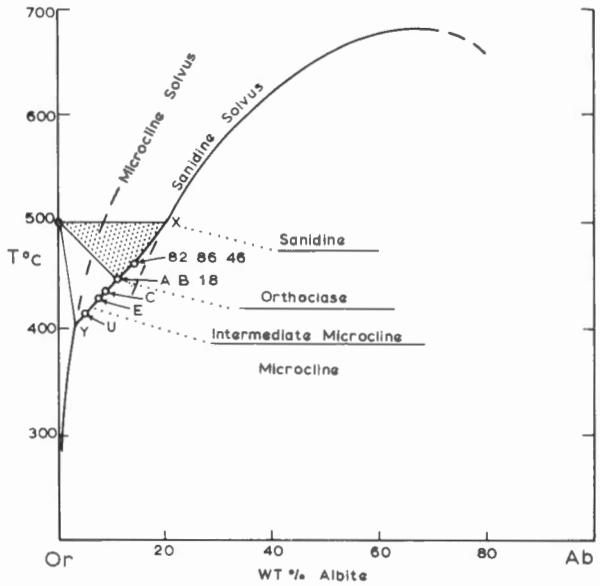

Figure 31. Approximate phase relations for the potassium-rich alkali feldspars. Sanidine solvus has been adjusted for feldspars structurally intermediate between sanidine (X) and microcline (Y). Solid circle represents the presumed first order transition temperature for sanidine and microcline. Feldspars that have Si/Al distributions equal to that of orthoclase plot in the dotted area. Dashed lines are metastable extensions of the solvi (after Wright, 1964).

related to a first order transition on the solvus. Feldspars should show a compositional discontinuity, and intermediate states should not occur if equilibrium was maintained during such an inversion. The observed continuous compositional and structural variation, if metastable, must reflect the kinetics of both exsolution and the Al/Si ordering process. In this view orthoclase and intermediate microcline are metastable minerals relative to sanidine and maximum microcline.

Coexisting Plagioclase

Plagioclase feldspars were not studied in detail but J. E. Mekarski at Carleton University is presently studying coexisting feldspars from the pluton. Compositions determined by optical means are noted in Appendix A.

PYROXENES

Chemical analyses, structural formulae, and optical properties of hypersthene-augite pairs are given in Tables 6 and 7. Differences among the analyses are small, but there are notable variations in the alumina and silica content of augite. Fe^2:Mg ratios vary within precision limits of the determinations, and are represented by a single tie line (sample 44) in Figure 32. Pyroxenes from other rocks are included for comparison. The Adamant pyroxenes coincide with some of those from the charnockitic rocks of Madras, but are conspicuously more calcic than augites from tholeiites (Skaergaard trend).

Bartholomé (1962) studied coexisting calcium-rich and calcium-poor pyroxenes selected from gabbroic and various metamorphic rocks. The distribution of Fe^2 and Mg between pyroxene pairs can be expressed by the relation

$$\frac{Fe^2}{Mg}\ \text{calcium poor} = \frac{Fe^2}{Mg}\ \text{calcium rich} \cdot k_{T,\,P}$$

The distribution coefficient k varies with temperature, but is insensitive to pressure changes. Bartholomé calculated the change of k with temperature, and suggested that k could be used as a geological thermometer. Although not a sensitive measure, k may be used for estimating the formation temperature of the pyroxene pairs. Non-equilibrium conditions between the pyroxenes and errors in the analyses are possible errors effecting the result. Estimated temperatures for the six Adamant pyroxene pairs are listed in Table 8.

Table 6

Chemical Composition and Optical Properties of Augite

Number	44	69	86	82	75	72
SiO_2	50.06	48.74	48.90	47.94	48.44	49.82
Al_2O_3	3.71	6.88	5.22	6.77	6.70	4.76
Fe_2O_3	3.44	2.81	3.08	3.23	2.75	2.97
FeO	8.53	7.71	9.38	9.00	8.05	9.29
MgO	12.16	12.30	12.63	12.53	12.41	12.38
CaO	20.06	19.76	19.30	18.78	19.70	18.72
Na_2O	0.73	0.66	0.63	0.63	0.71	0.75
K_2O	0.15	0.08	0.08	0.08	0.09	0.19
TiO_2	0.44	0.42	0.48	0.58	0.52	0.54
MnO	0.27	0.35	0.30	0.25	0.19	0.28
P_2O_5	0.03	0.06	0.04	0.04	0.04	0.03
F	0.00	0.00	0.00	0.00	0.01	0.01
H_2O	0.04	0.06	0.04	0.08	0.28	0.20
Total	99.62	99.83	100.08	99.91	99.89	99.94
Si	1.82	1.84	1.81	1.80	1.88	1.90
Al	0.18	0.16	0.19	0.20	0.12	0.10
Al	0.13	0.07	0.11	0.09	0.09	0.06
Fe^3	0.08	0.09	0.09	0.08	0.08	0.10
Fe^2	0.24	0.29	0.28	0.25	0.29	0.27
Mg	0.69	0.71	0.71	0.69	0.70	0.69
Ca	0.79	0.78	0.76	0.78	0.76	0.83
Na	0.05	0.05	0.05	0.05	0.04	0.05
K	0.004	0.004	0.004	0.004	0.01	0.01
Ti	0.01	0.01	0.02	0.01	0.02	0.01
Mn	0.01	0.01	0.01	0.01	0.01	0.01
XY	2.00	2.01	2.03	1.96	1.99	2.03
$2V_z$	57°	64°	56°	-	-	-
N_y	1.695	1.692	1.698	1.698	1.696	1.691

Analyses by the Geological Survey of Canada.
Cations adjusted to 6 oxygens. $(XY)_2(SiAl)_2O_6$

Table 7

Chemical Composition and Optical

Properties of Hypersthene

Number	69	86	82	75	72	44
SiO_2	52.4	52.2	52.5	52.4	52.3	52.4
Al_2O_3	1.2	1.3	1.4	1.4	1.2	1.4
Fe_2O_3	2.0	2.9	2.6	2.4	2.5	2.2
FeO	22.48	22.39	22.00	19.90	22.85	22.84
MgO	19.4	19.0	19.1	18.8	18.2	18.6
CaO	1.5	0.9	1.1	3.5	1.2	1.4
Na_2O	0.07	0.06	0.07	0.15	0.07	0.14
K_2O	0.00	0.00	0.00	0.00	0.00	tr
TiO_2	0.16	0.21	0.26	0.29	0.19	0.22
MnO	0.95	0.58	0.65	0.66	0.70	0.80
P_2O_5	0.02	0.02	0.04	0.08	0.02	0.18
Total	100.2	99.6	99.7	99.6	99.2	100.2
Si	1.97	1.98	1.98	1.99	1.99	1.97
Al	0.03	0.02	0.02	0.01	0.01	0.03
Al	0.02	0.04	0.04	0.05	0.05	0.03
Fe3	0.06	0.08	0.07	0.05	0.07	0.06
Fe2	0.71	0.71	0.69	0.63	0.73	0.71
Mg	1.09	1.08	1.08	1.07	1.04	1.05
Ca	0.06	0.04	0.06	0.14	0.05	0.06
Na	0.004	0.002	0.004	0.01	0.002	0.01
Ti	0.004	0.01	0.01	0.01	0.005	0.01
Mn	0.03	0.02	0.02	0.02	0.02	0.03
XY	1.98	1.98	1.97	1.98	1.97	1.96
$2V_x$	64°	64°	66°	64°	61°	60°
N_y	1.702	1.712	1.712	1.707	1.712	1.707

X = pink Y = Pale pink Z = Pale green

Analyses by REFox. Cations adjusted to 6 oxygens.
$(XY)_2(SiAl)_2O_6$

Table 8

Estimated Temperature of Formation of

Adamant Pyroxenes

Number	Fe^2:Mg Hypersthene	Fe^2:Mg Augite	k	T°C
44	0.622	0.384	1.6	870
69	.650	.350	1.8	600
86	.657	.426	1.6	870
82	.645	.392	1.6	870
75	.536	.350	1.7	750
72	.700	.426	1.6	870

$$k = \frac{(Fe^2:Mg)\ \text{Hyp.}}{(Fe^2:Mg)\ \text{Augite}}$$

Temperatures from calculated curve of Bartholomé (1962, p12).

Temperature estimates range from 600° to 870° with four of the six results being 870°. A crystallization temperature of 800° to 900°C seems to be indicated by these results, certainly within possible magmatic temperatures for granitic rocks, or for the highest grade of metamorphism.

HORNBLENDE AND BIOTITE

Analyses, structural formulae, and optical properties of analyzed samples of hornblende and biotite are given in Tables 9 and 10. Fe^2:Mg ratios for coexisting samples are plotted in Figure 33. A progressive increase of Fe^2:Mg from sample 26 to sample 10, and a constant Fe^2:Mg distribution for the mineral pairs are evident in the figure. An inspection of Tables 9 and 10 shows that differences in the magnesium content are small, and that total iron is essentially the same for all samples; only ferric iron and the proportion of ferrous iron to magnesium change.

The relationship between Fe^3:Fe^2 and Mg:Fe^2 ratios of hornblende and biotite is shown in Figure 34. Samples are joined by the appropriate tie lines and plot on two divergent lines (dashed). In each case, hornblende is richer in ferric iron than coexisting biotite, and for each mineral pair, those with high Fe^3:Fe^2 ratios are more magnesian than those with low Fe^3:Fe^2 ratios. The ratio of magnesium to ferrous iron is clearly related to changes in the proportion of ferric to ferrous iron.

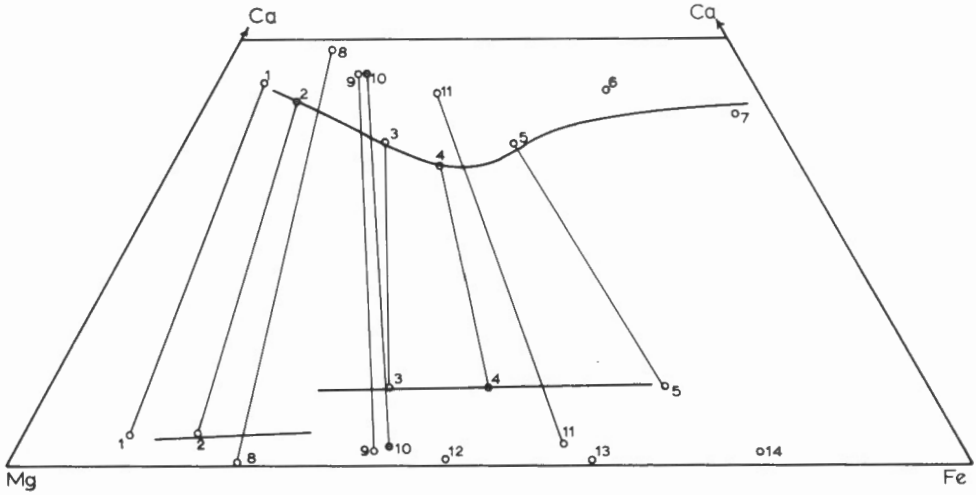

Figure 32. Comparison of Adamant pyroxenes (solid circle) with the Skaergaard crystallization trend (solid line) and pyroxenes from other rock types. Samples 1-5 and 7 are pyroxenes from gabbroic rocks, 6 is from an acid glass, 8-15 are pyroxenes from Adamant pluton (10), the Madras charnockite suite, and from charnockites in Africa (14). Diagram from Subramaniam (1962).

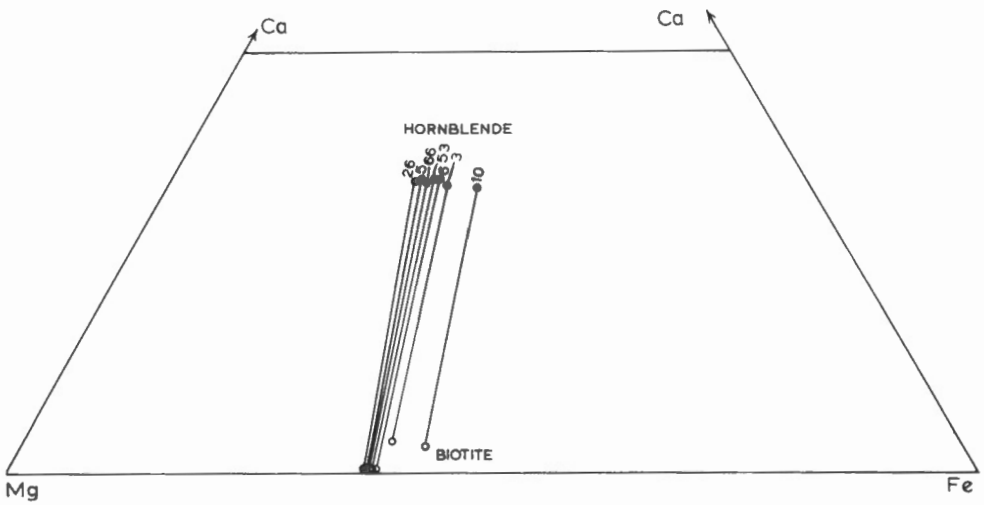

Figure 33. Fe/Mg ratios of coexisting biotite and hornblende in the peripheral rock of Adamant pluton. (Mole %).

Table 9

Chemical Composition and Optical

Properties of Hornblende

No.	5	3	12	26	10	6	53	65	66
SiO_2	39.88	40.61	40.84	41.00	40.76	40.72	40.16	40.74	40.62
Al_2O_3	14.50	13.41	14.60	14.02	14.68	13.69	14.17	13.80	13.69
Fe_2O_3	6.48	5.97	5.32	6.67	5.10+	6.51	6.44	5.56	6.88
FeO	11.12	12.53	12.81	11.00	13.24	11.60	11.69	11.38	11.43
MgO	9.06	8.87	8.67	9.63	8.06	9.08	9.21	9.42	9.36
CaO	11.54	11.60	11.66	11.40	11.32	11.52	11.66	11.70	11.52
Na_2O	1.31	1.43	1.38	1.51	1.49	1.45	1.35	1.44	1.48
K_2O	1.44	1.78	1.65	1.40	1.56	1.79	1.78	1.73	1.77
TiO_2	1.50	1.80	0.94	0.94	0.80	1.29	1.22	1.39	1.29
MnO	0.26	0.27	0.30	0.35	0.40	0.27	0.26	0.26	0.31
P_2O_5	0.05	0.05	0.06	0.04	0.04	0.04	0.08	0.04	0.04
F	0.15	0.15	0.11	0.12	0.13	0.11	0.23	0.15	0.36
H_2O	1.52	1.32	1.68	1.72	1.48	1.54	1.43	1.56	1.57
Total	99.50	99.73	99.97	99.75	99.01	99.56	99.58	100.11	100.17
FeO Total	16.96	17.90	17.59	16.00	17.83	17.46	17.49	16.38	17.63
Si	6.07	6.17	6.18	6.14	6.22	6.15	6.08	6.12	6.09
Al	1.93	1.83	1.82	1.86	1.78	1.85	1.92	1.88	1.91
Al	0.66	0.56	0.77	0.60	0.88	0.58	0.61	0.56	0.50
Fe^3	0.75	0.68	0.60	0.74	0.51	0.74	0.73	0.74	0.77
Fe^2	1.41	1.59	1.61	1.38	1.69	1.47	1.46	1.43	1.43
Mg	2.08	2.03	1.97	2.17	1.84	2.05	2.09	2.13	2.11
Ti	0.18	0.20	0.11	0.11	0.09	0.15	0.14	0.15	0.14
Mn	0.04	0.04	0.04	0.04	0.05	0.04	0.04	0.04	0.04
Ca	1.88	1.89	1.86	1.83	1.85	1.87	1.89	1.89	1.85
Na	0.38	0.42	0.40	0.43	0.44	0.42	0.40	0.42	0.43
K	0.27	0.35	0.31	0.27	0.31	0.34	0.36	0.33	0.34
OH	1.53	1.33	1.69	1.73	1.50	1.56	1.46	1.57	1.48
F	0.07	0.07	0.05	0.05	0.06	0.05	0.11	0.07	0.17
X	2.55	2.66	2.57	2.53	2.60	2.63	2.65	2.64	2.62
Y	5.12	5.10	5.10	5.04	5.06	5.03	5.07	5.04	4.99
OH,F	1.60	1.40	1.74	1.78	1.56	1.61	1.57	1.64	1.65
Ny	-	1.687	1.683	1.683	1.684	1.684	1.686	1.687	1.686
$2V_x$	-	64	70	60	60	60	62	60	-

X = pale brown, Y = dark green, Z = dark green to bluish green

Analyses by the Geological Survey of Canada, + by P.E.Fox Cations adjusted to 24 (0,OH,F), $X_{2-3}Y_5Z_8O_{22}(OH,F)_2$. Totals corrected for fluorine.

Table 10

Chemical Composition and Optical Properties of Biotite

Number	26	6	53	66	5	3	10
SiO_2	37.7	37.6	37.6	38.0	36.7	38.0	37.64
Al_2O_3	15.2	15.2	15.2	15.2	15.5	15.0	16.14
Fe_2O_3	4.6	4.3	4.3	4.16	4.8	4.2	3.98
FeO	12.53	12.82	13.07	12.56	12.91	13.09	15.12
MgO	12.8	12.3	12.2	11.8	12.1	11.2	11.11
CaO	0.68	0.18	0.26	0.36	0.09	1.16	0.94
Na_2O	0.15	0.04	0.05	0.17	0.01	0.17	0.32
K_2O	8.60	9.12	9.12	8.81	9.42	8.15	8.59
TiO_2	2.2	3.0	4.3	3.8	4.1	4.4	2.10
MnO	0.31	0.27	0.32	0.29	0.26	0.27	0.44
H_2O+	4.32	3.85	3.48	3.76	3.34	3.78	3.24
F	-	-	-	-	-	-	0.63
Total	99.1	98.7	99.9	99.4	99.2	99.4	100.19+
Total FeO	16.7	16.7	16.9	16.7	17.1	16.9	18.7
Si	5.60	5.63	5.63	5.67	5.64	5.68	5.55
Al	2.40	2.37	2.37	2.33	2.36	2.32	2.45
Al	0.44	0.33	0.33	0.34	0.44	0.35	0.34
Fe^3	0.50	0.44	0.43	0.52	0.50	0.41	0.45
Fe^2	1.66	1.62	1.63	1.66	1.66	1.63	1.87
Mg	2.78	2.79	2.74	2.64	2.78	2.51	2.48
Ti	0.47	0.45	0.49	0.43	0.47	0.50	0.23
Mn	0.04	0.04	0.04	0.04	0.04	0.04	0.05
Ca	0.02	0.03	0.05	0.05	0.02	0.19	0.15
Na	0.02	0.01	0.01	0.05	0.02	0.05	0.09
K	1.84	1.76	1.74	1.68	1.84	1.56	1.62
OH	3.42	3.89	3.36	3.74	3.42	3.78	3.21
F	-	-	-	-	-	-	0.07
X	1.88	1.80	1.80	1.78	1.88	1.80	1.86
Y	5.89	5.67	5.66	5.53	5.89	5.44	5.42
OH,F	3.42	3.89	3.36	3.74	3.42	3.78	3.28
Ny	1.630	1.636	1.642	1.638	1.644	1.646	1.633

X = straw yellow, Y,Z = reddish brown

Sample 10, alkalis, H_2O+, F by the Geological Survey of Canada, other elements by REFox.+ includes 0.16 BaO and 0.03 P_2O_5, totals corrected for fluorine. Cations adjusted to 24 (O,OH,F), $X_2Y_6Z_8O_{20}(OH,F)_4$.

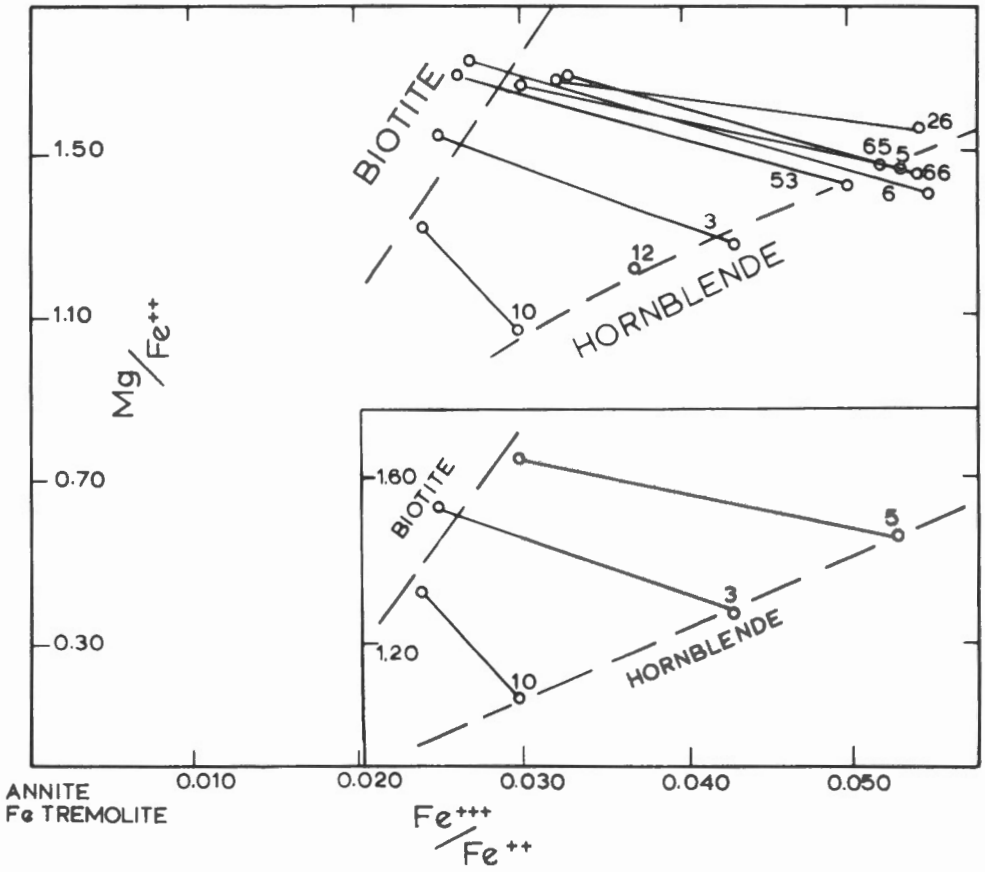

Figure 34. Relationship between Mg: Fe++ ratio Fe+++: Fe++ ratio of hornblende and biotite (moles). Insert shows the general case in which sample 5 was taken as representative of samples 53, 6, 66, 5, and 26. Theoretical compositions of annite and ferrotremolite occur at the origin. 12 and 65 are hornblende samples only

Both $Mg:Fe^2$ and $Fe^3:Fe^2$ ratios of the hornblende samples cover a wider range of values than those of the coexisting biotite. This relation is reflected by the change of tie line orientation for different values of $Fe^3:Fe^2$. Thus a change in proportion of ferric to ferrous iron in the rock, that is a change of oxidation state or oxygen content, affects the $Mg:Fe^2$ ratios of the minerals. This is shown in Figure 35. The oxidation ratio of the rock (Chinner, 1960) is plotted against the $Fe^2:Mg$ ratio of hornblende (a), biotite (b), and rock (c). In each graph, rocks with relatively high oxidation ratios contain magnesian hornblende and biotite, and the rocks are also magnesium-rich relative to Fe^2. The correlation of rock $Fe^2:Mg$ ratios with oxidation ratio is due to the absence of large amounts of iron oxides in the rock; hence oxidation ratios reflect the $Fe^3:Fe^2$ ratios of hornblende and biotite. Graph (c) also shows that there is no correlation between rock type and oxidation ratio or $Fe^2:Mg$ ratio. Rocks differ only in the proportions of the minerals present. The fact that biotite-rich rocks occur at the margin of the pluton must clearly be due to some factor other than, or in addition to, the oxidation ratio (or bulk oxygen content of the rock).

OXIDE MINERALS

Oxide minerals, although not abundant, are distinctive of the rocks in which they occur. The associated silicate assemblages are listed in the following section. In the pyroxene monzonite, oxide grains consist of magnetite and ilmenite-hematite intergrowths. Hematite makes up less than 20 per cent of the assemblage, generally about 10 per cent. In the inner part of the hornblende quartz monzonite and recrystallized parts of the transition zone, ilmenite and hematite are present in about equal amounts. Rutile lamellae, which intersect the laths of ilmenite and hematite, are intergrown with magnetite in which most of the hematite is concentrated as discontinuous mantles at the grain margins. A few lamellae, apparently on the (111) plane, occur in the centre of the magnetite grains. Rocks at the margin of the pluton invariably contain hematite with conspicuous laths of rutile. A few ilmenite lamellae are generally present but make up less than 10 per cent of the assemblage. Magnetite is not as abundant in the marginal rocks as elsewhere, and is absent in the garnet-bearing rock.

Estimates of the relative amounts of the various oxide minerals were made from polished sections, X-ray patterns, and magnetic versus non-magnetic oxides. Samples from the monzonite core have the lowest oxidation ratios in the pluton, and contain almost constant amounts of magnetite, ilmenite, and hematite. In the peripheral rock, however, proportions vary. Hematite and rutile are more abundant in rocks of low oxidation ratio than in those of high, and the opposite is true for magnetite and ilmenite. Thus relatively oxidized iron and titanium oxides occur with relatively reduced silicate phases in the biotite and hornblende-rich rocks. This relation is notably different to that found by Chinner (1960) and Hounslow (1965) in amphibolite

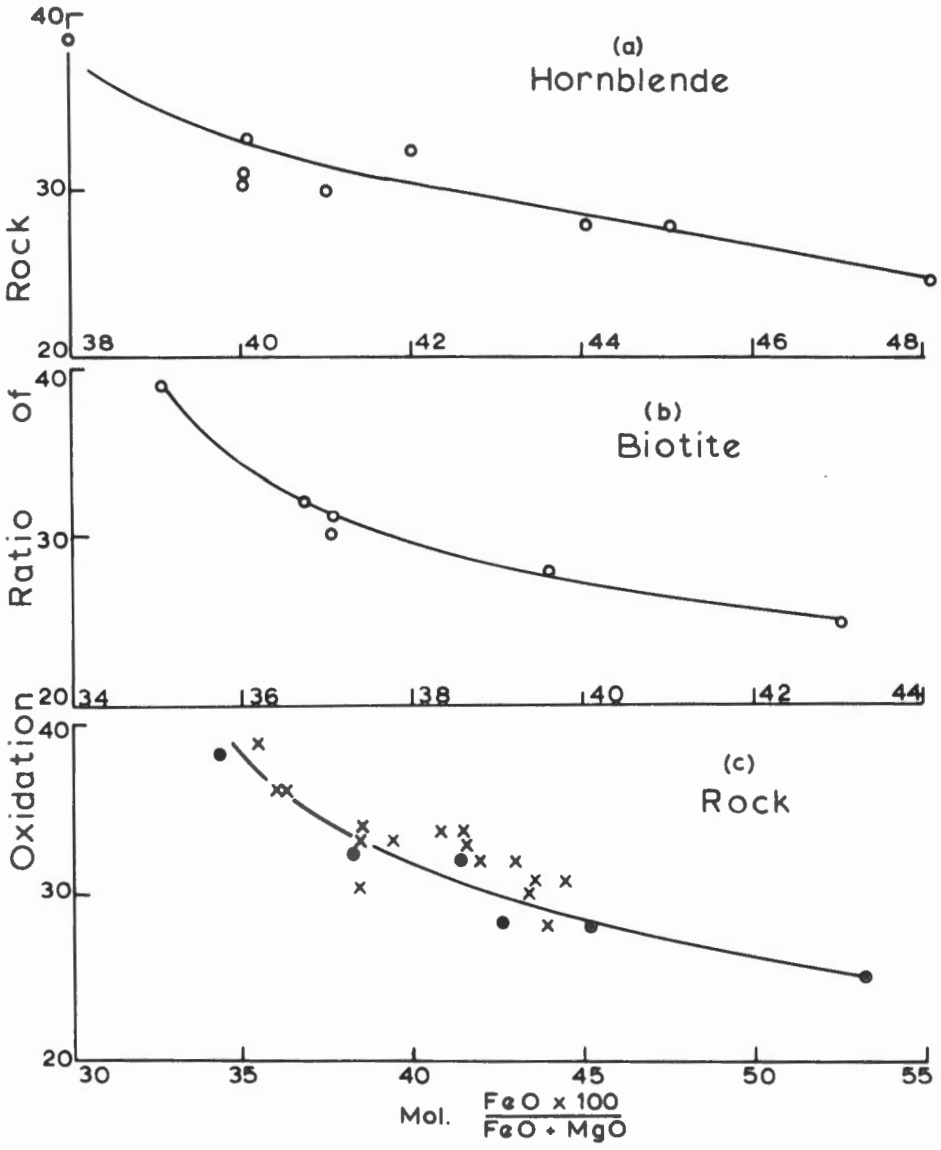

Figure 35. FeO:MgO ratios of hornblende (a), biotite (b), and rock (c) plotted against the oxidation ratio (mol $2Fe_2O_3/2Fe_2O_3 + FeO$). In (c), solid circles represent biotite-hornblende granodiorite, and X hornblende quartz monzonite.

facies metamorphic rocks. Here, hematite, and occasionally rutile occur in rocks of highest oxidation ratio rather than in the lowest. Clearly, this difference is fundamental to the interpretation of the Adamant peripheral rocks as distinct from the metamorphosed pelites studied by Chinner and Hounslow.

Three observations can be made about the oxide minerals:

(1) The proportion of ilmenite to hematite varies progressively from ilmenite grains with minor hematite lamellae in the monzonite to hematite grains with a few lamellae of ilmenite and rutile in the peripheral rock. The rutile lamellae appear at the 1:1 ratio of ilmenite to hematite and increase in abundance as ilmenite decreases.

(2) The amount of magnetite decreases from centre to edge of the pluton. Textural relations in the hornblende quartz monzonite suggest oxidation of magnetite to hematite.

(3) Oxidized iron and titanium minerals in the peripheral rock are associated with relatively reduced silicates (Fe^2-rich). This relationship is opposite to that observed in metamorphosed pelites studied by Chinner (1960) and Hounslow (1965).

INTERPRETATION AND SIGNIFICANCE

Alkali Feldspar

Alkali feldspars show a progressive change from monoclinic to triclinic forms. These structural changes accompany textural and other mineralogical changes evident in the peripheral rock. Generally there is a close relationship between structural state, chemical composition, and lithology. Structural state can be related to 2V and chemical composition; the most triclinic feldspar has the highest 2V and contains the least amount of albite and anorthite in solid solution. It is not evident from the available data whether these observations represent stable or metastable states. In either case the change of the potassium-rich feldspars to triclinic forms and to compositions near the pure $KAlSi_3O_8$ end-member is probably temperature controlled. This implies that the margin of the pluton reached equilibrium at lower temperatures than the core rock, but there is another possibility. The catalytic effect of water vapour on exsolution, structural inversion, and on reactions involving feldspar is well known from experimental work. Thus P_{H_2O} is an important but a difficult variable to evaluate in rocks. High P_{H_2O} could extend the interval in which structural and chemical adjustment occurs to lower temperatures than in rocks with low P_{H_2O}. Temperatures determined from the structural state and composition of the feldspars would then reflect an apparent thermal gradient from areas of high to areas of low P_{H_2O}.

Moreover, if the structural and chemical data reflect the kinetics of exsolution and Si/Al ordering, in other words, are functions of reaction rates, the indicated temperatures have no useful meaning. The feldspars are thus not reliable thermometers because thermal data derived from their structural or chemical states may depend on factors other than temperature alone.

It may be concluded that (1) the recrystallization of the monzonite body was a penetrative one. Not only was the rock fabric reorganized but the K, Na, and Ca contents and the Si/Al distribution of the feldspars changed as well. (2) There may have been a temperature gradient within the peripheral rock from centre to edge, but this is not a reliable conclusion based on the feldspar data alone. Not enough is known about the structural inversion, reaction kinetics, and the exsolution process at present to justify the use of feldspar as a geothermometer. This is a promising field of study but more information is needed.

Pyroxenes

Hypersthene and augite have a constant $Mg:Fe^2$ ratio throughout the monzonite body. This constant ratio implies that there were no pronounced thermal gradients or differences in bulk chemical composition within the mass when these minerals formed. Thus the monzonite does not reflect any differentiation trends within its mass. The formation temperature of 800° to 900°C indicated by the pyroxene pairs is discussed later.

Hornblende and Biotite

(1) Hornblende and biotite have variable $Mg:Fe^2$ and $Fe^3:Fe^2$ ratios. These ratios reflect the effects of oxidation and reduction on the peripheral rock.

(2) The hornblende:biotite ratio is unrelated to oxidation ratio (Fig. 35).

(3) Hornblende is more Fe^3-rich than coexisting biotite, and thus its stability field should extend to higher partial pressures of oxygen than biotite.

The problem of oxidation of Fe^2-bearing silicates has been discussed by Eugster and Wones (1958, 1963), Eugster (1959), Chinner (1960), Hounslow (1965). The effect of oxidation is to change the $Mg:Fe^2$ ratio of minerals that belong to a solid solution series. In such a series in which Fe^2 is replaced by a divalent ion (generally Mg^2 and Mn^2), formation of the Fe^2-bearing member is inhibited by an increase in oxygen content (Chinner, 1960). Biotite-garnet (Chinner, 1960), biotite-garnet-staurolite (Hounslow, 1965), and biotite-hornblende associations (this study) have been shown to obey this principle. According to Chinner (1960), oxygen contents are inherited from

the parent material, and oxidation ratio does not change significantly during metamorphism. The oxidation ratio (mol. $2Fe_2O_3/2Fe_2O_3 + FeO$) gives the proportion of ferric to total iron atoms in the rock, and hence the relative oxygen contents. In the regionally metamorphosed pelites studied by Chinner and Hounslow, temperature was considered not to vary significantly over the area studied. This assumption cannot be justified for Adamant pluton. It is thus instructive to examine oxidation ratio in terms of a few simple phase diagrams in which oxidation of iron is important.

Oxidation Ratio

Part of the Fe-Si-O system is shown in Figure 36 in which the oxidation ratio (OR) is shown for the various fields. Point X represents a magnetite + quartz + vapour assemblage at 700°C. Four paths are shown that trace the oxidation of magnetite. At constant T and with increasing oxygen content of the vapour, point X shifts to point a on the univariant magnetite-hematite reaction curve. Here, magnetite is oxidized to hematite at constant T and P_{O_2}, and the oxidation ratio of the solid assemblage increases from 66 to 100, at which point hematite + quartz + vapour is the stable assemblage. This situation corresponds to the one visualized for regional metamorphism by Chinner (1960) and Hounslow (1965). Path 2 traces the univariant relations between a and b. Oxidation ratio increase from 66 at a to 100 at b. Here, both T and P_{O_2} increase with increasing oxidation ratio. Path 3 represents constant P_{O_2} conditions but decreasing T. Point c is an invariant point at which magnetite is oxidized to hematite, again oxidation ratio changing progressively from 66 to 100. Path 4 shows that the increase of oxidation ratio due to the increasing amount of Fe_2O_3 between c and d occurs with decreasing T and P_{O_2}.

Figure 36 shows that for the simple oxide system oxidation ratio reflects the oxygen content of the solid phases, and is not directly related to P_{O_2}. Oxidation of magnetite to hematite can occur with decreasing temperature and P_{O_2} (between c and d), and conversely, reduction can occur with increasing temperature and P_{O_2}. At constant temperature and P_{O_2}, changes in the oxygen content of the solids is reflected by a change in the oxidation ratio.

Titanium can be added to the system to account for rutile and ilmenite: the phase relations will not change significantly. Reactions at a and c or between a and b, and c and d, can be represented by

$$Fe_3O_4 + FeTiO_3 + O \rightarrow 2Fe_2O_3 + TiO_2.$$

A more complicated system represented by the annite-phlogopite join (Eugster and Wones, 1958) is shown in Figure 36b. The diagram represents constant total pressure ($P_{H_2O} + P_{H_2}$) conditions and shows the stability

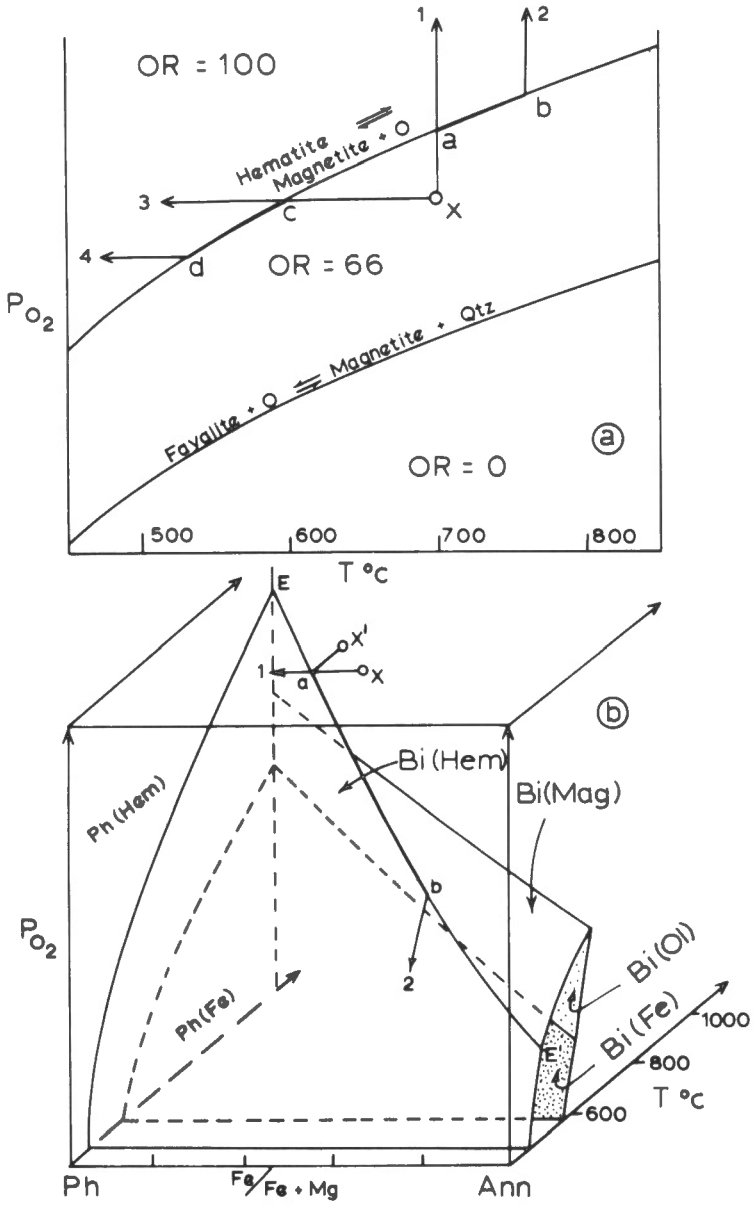

Figure 36. (a) Part of the Fe-Si-O system at constant total pressure showing the relation between oxidation ratio, T, and P_{O_2} for various oxidation paths of a system represented by X. (b) Part of the phlogopite (Ph)-annite (Ann) join showing various iron and magnesium phases in equilibrium with biotite (Bi). Ol = olivine, Mag = magnetite, Hem = hematite.

relations of biotite in P_{O_2} - T - composition space. The relations shown are only slightly affected by changes in total pressure. The various surfaces bounding the biotite volume are labelled in Figure 36b (only Fe and Mg phases are noted). At constant total iron content, oxidation ratio reflects the relative amounts of hematite, magnetite, olivine, and biotite. Rocks containing magnesium biotite will have higher oxidation ratios than those containing ferrous biotite, thus oxidation ratio increases from right to left in the diagram for assemblages in equilibrium with biotite.

Point X represents an assemblage consisting of K feldspar + magnetite + vapour. At constant temperature and increasing oxygen content of the vapour, biotite forms at point a on the univariant curve EE' by the reaction

$$\text{K feldspar} + \text{magnetite} + H_2O \rightarrow \text{biotite} + \text{hematite}.$$

Point a is invariant for constant T, P_{total}, P_{O_2} conditions. In rocks having variable $Mg:Fe^2$ ratios, hematite and magnetite in equilibrium, and for which the above variables are fixed, oxygen content defines the $Mg:Fe^2$ ratio. An increase in oxygen content of the rock will change this ratio by the reaction

$$Bio_{Fe} + mag + O_2 \rightarrow Bio_{Mg} + K\ fsp + hem + H_2O.$$

If hornblende is present,

$$Hnde_{Fe} + mag + O2 \rightarrow Hnde_{Mg} + \text{Plagioclase (or epidote)} + hem + H_2O.$$

In each reaction, the high oxidation ratio assemblage is on the right. For such reactions there should be a correlation between oxidation ratio and the volume per cent of the minerals involved in the reactions. Such a relation was found by Chinner (1960) in which the biotite, garnet, muscovite, and oxide content of pelitic gneisses varies systematically with oxidation ratio. No such relation was found in the peripheral rock of Adamant pluton.

Path 2, leading from point X' in the K feldspar + magnetite field, traces the oxidation path when neither T nor P_{O_2} is presumed constant. Biotite forms at point a on the univariant curve EE' and with decreasing T, the system moves along EE' to b. Between points a and b, oxidation ratio decreases progressively as biotite becomes Fe^2-rich. At the same time magnetite is oxidized to hematite as T and P_{O_2} decreases. The final assemblage is either $biotite_{Fe}$ + K feldspar + hematite or K feldspar + hematite, iron oxides being consumed in reactions along EE'.

The reactions along EE' are equivalent to those occurring between points c and d on the hematite-magnetite reaction curve in Figure 36a. In both a decrease of T results in the oxidation of magnetite to hematite with decreasing P_{O_2}. If small amounts of oxide grains are present relatively

reduced silicates (Fe^2-rich) occur with oxidized iron oxides. This is different from the constant temperature case in which an increase in oxidation ratio (path 1) produces both oxidized silicates and oxides together.

A more general relationship between T and oxidation ratio can be suggested in addition to that observed along the univariant curve EE'. This is the well known relation that high T favours the Mg-rich end-member of a solid solution series. A change of the Mg:Fe^2 ratio in minerals that also contain Fe^3 will cause the Fe^3:Fe^2 ratio to change, hence the oxidation ratio of the rock, provided iron oxides are only minor constituents. In general, an increase of T will cause an increase of the oxidation ratio of the rock. This is, of course, implied in the relations described along EE', but hematite and magnetite are not essential constituents. This effect of T on oxidation ratio is limited because a large change of T often produces a new mineral assemblage. This leads to a final observation about Figure 36b, and concerns the relation of T and the oxidation ratio of different mineral assemblages. The high T assemblages in this system are biotite + olivine + leucite + kalsilite, and biotite + olivine + Fe° + K-feldspar. Low T assemblages are biotite + magnetite + K-feldspar and biotite + hematite + K-feldspar. Clearly the high oxidation ratio assemblages are found at low T and those observed at high T have low oxidation ratios. High T also favours anhydrous assemblages, and so one finds that in general high T mineral assemblages are anhydrous, low oxidation ratio rocks, and low T assemblages are hydrous, high oxidation ratio rocks. It is concluded that:

(1) Oxidation ratio changes during progressive metamorphism in response to T but that this change is probably insufficient to mask original differences of O_2 content. Indeed, it is probable that inherited differences persist during metamorphism, and that only the absolute values of the oxidation ratio change. In general, a marked increase of T results in the formation of assemblages of low oxidation ratio.

(2) For a limited range of T, the oxidation ratio of rocks that have similar original O_2 contents will increase with an increase of T. Such a T change will result in relatively reduced silicates coexisting with oxidized iron oxides.

The above conclusions are important in the interpretation of the oxidation ratio distribution in Adamant pluton. First, Appendix A and Figure 38 show that the oxidation ratio of the monzonite core is generally less than that in the peripheral rocks. This is not an unexpected observation if the metamorphic history proposed on p. 16 is correct. The monzonite core represents an anhydrous, high temperature magmatic rock with inherited low oxidation ratio, whereas its recrystallized periphery consists of hydrous rocks of high oxidation ratio, which have formed at lower temperatures than the core.

Secondly, the oxidation ratio in the peripheral rocks, shown in Figures 37 and 38, decreases systematically away from the core. There are two possibilities to account for this distribution: (1) metamorphism of the monzonite under constant temperature conditions in which the systematic change of oxidation ratio is due to an inward increase of O_2 content inherited from the parent monzonite; (2) a gradual decrease of temperature away from the core which controls the $Mg:Fe^2$ ratio of hornblende and biotite, and hence the oxidation ratio of the rock. This hypothesis assumes that there were no large differences in the original O_2 content of the monzonite.

Which of the two possibilities is chosen depends on the interpretation of the iron oxide minerals. If they are considered to be in equilibrium with the silicates during metamorphism then process (2) must be selected because a variable temperature appears to be the only way to produce oxidized iron oxides in equilibrium with reduced silicates. Process (1) will produce both oxidized silicates and oxides together. If the iron oxides are due to cooling after recrystallization, then no choice can be made, both explanations being possible. However, it was observed that textural changes in the iron oxides accompany textural and chemical changes in the associated silicates, hence there is no reason to suppose that the iron oxides are not equilibrium products in the mineral assemblage. On this basis process (2) is thought to be the most likely explanation. Diapiric intrusion to a higher, cooler level during recrystallization of the body would be expected to result in a thermal gradient from the unrecrystallized core to the margin.

Bulk Composition

It was noted in an earlier section that apart from differences in SiO_2 and MgO contents, the rocks of the pluton have essentially the same chemical composition. The composition of the periphery is believed to be inherited from the parent pyroxene monzonite, allowing for some addition of water to the rocks during recrystallization. The small variations of SiO_2 and MgO probably originate from minor differentiation of the original monzonite magma. The effect of these constituents on the nature of the recrystallized periphery is considered below.

(i) SiO_2

Changes in silica affect only the quartz content because the peripheral rocks all contain quartz, and hence are saturated with silica. The data given in Appendix A show that an increase in silica is usually reflected by an increase in the amount of quartz, hence this factor need not be considered further.

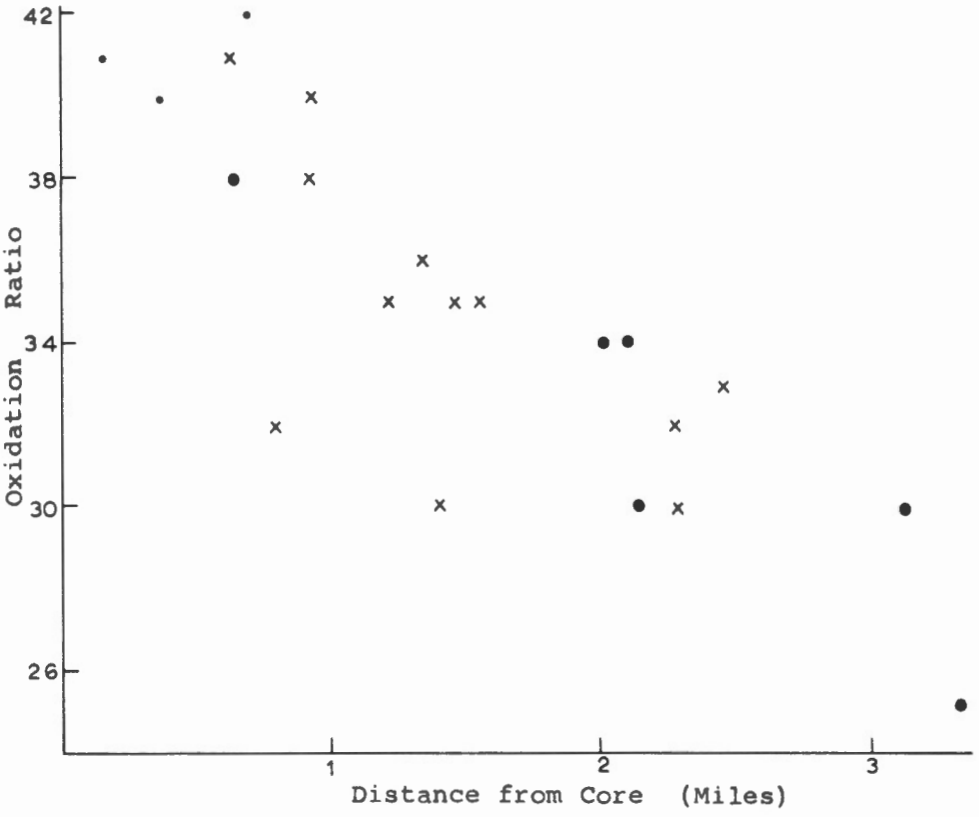

Figure 37. Oxidation ratio plotted against distance from the core. Diagram shows a systematic decrease of oxidation ratio away from the core (Symbols same as Figure 12).

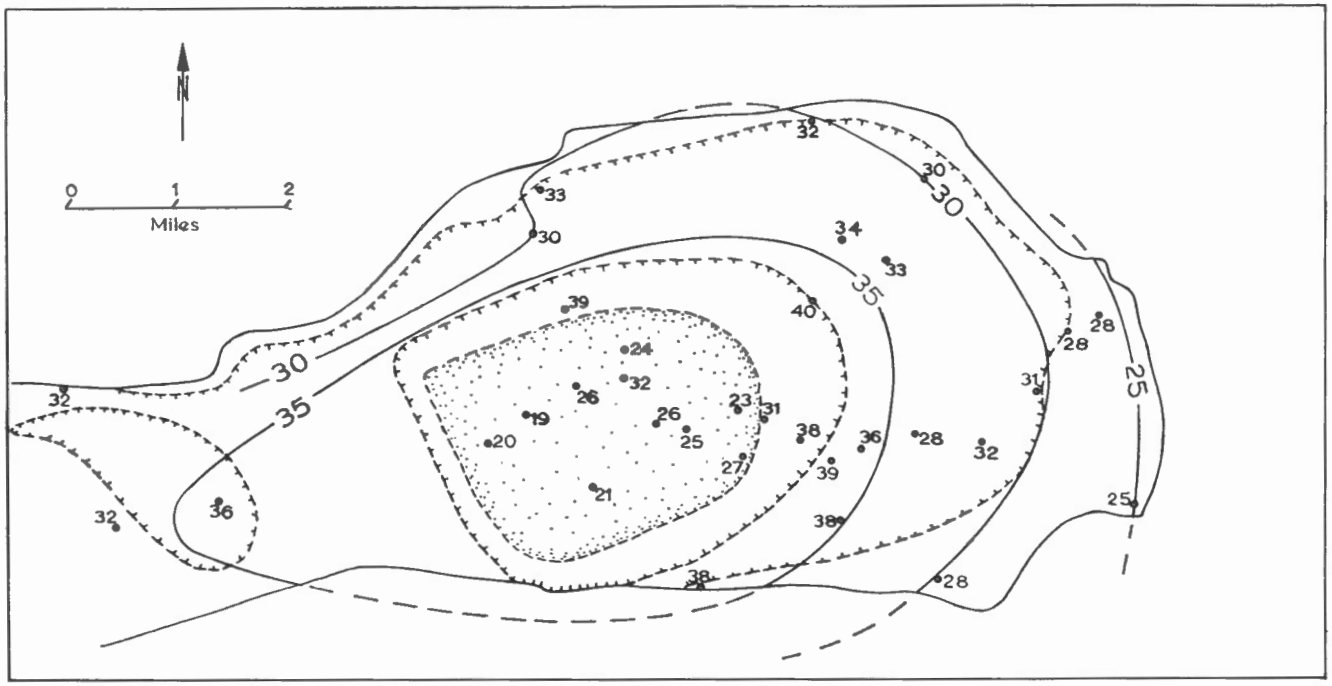

Figure 38. Oxidation ratio plotted on a map of the east part of Adamant pluton. Dark lines are oxidation ratio contours, which are believed to be isotherms. The hachured lines represent lithologic contacts and are believed to be H_2O isobars. The stippled area is the monzonite core showing the inherited low oxidation ratios of the original monzonite batholith.

(ii) MgO

Variation of the MgO:FeO ratio of the original monzonite body affects only the total mafic content of the recrystallized periphery. The hornblende: biotite ratio is unaffected because hornblende and biotite have similar MgO: FeO ratios. Thus bulk MgO does not control which of the two mafic minerals will predominate but rather the sum of the mafic constituents of the rock.

Ratio of Biotite:Hornblende

The ratio of biotite to hornblende may depend on the chemical potential of water (μH_2O) in the system because biotite is more hydrous than hornblende. Assuming that the surrounding country rocks were a source of water during metamorphism (Thompson, 1957), then the movement of water into the pluton would have been affected by a marked chemical gradient between the country rock and the dry monzonite batholith, and a temperature gradient decreasing outward from the core of the pluton. The net effect would have been that water slowly diffused into the pluton against a thermal gradient. The effect of a temperature gradient on chemical potential can be assessed from the well known Gibbs-Duhem equation for a pure substance:

$$SdT - VdP + d\mu = O.$$

Assuming that the vapour phase diffusing into the pluton was essentially H_2O in composition, then

$$\left(\frac{\partial \mu H_2O}{\partial T}\right)_P = -S.$$

Thus, in general, μH_2O will be lower in the high temperature interior than in the relatively cool margin of the stock. Water will distribute itself according to the value of its chemical potential and it follows that the concentration of water and the biotite:hornblende ratio will be higher at the margin of the pluton than in the interior. However, μH_2O will not be totally dependent on T because the enclosing country rock acts as a reservoir for water and thus controls the amount of water supplied to the system. This factor has the same effect on μH_2O as a decrease of T at the pluton margin.

Figure 39 is a generalized form of Figure 34 showing a suggested relation between μH_2O, oxidation state or temperature, and the composition of biotite and hornblende. The diagram illustrates the conclusion reached earlier that the biotite:hornblende ratio is independent of oxidation ratio.

In a general way, lines of constant oxidation ratio in the pluton correspond to isotherms, and the contacts between rock units to H_2O isobars. Oxidation ratio contours are shown as dark lines in Figure 38, and lithologic

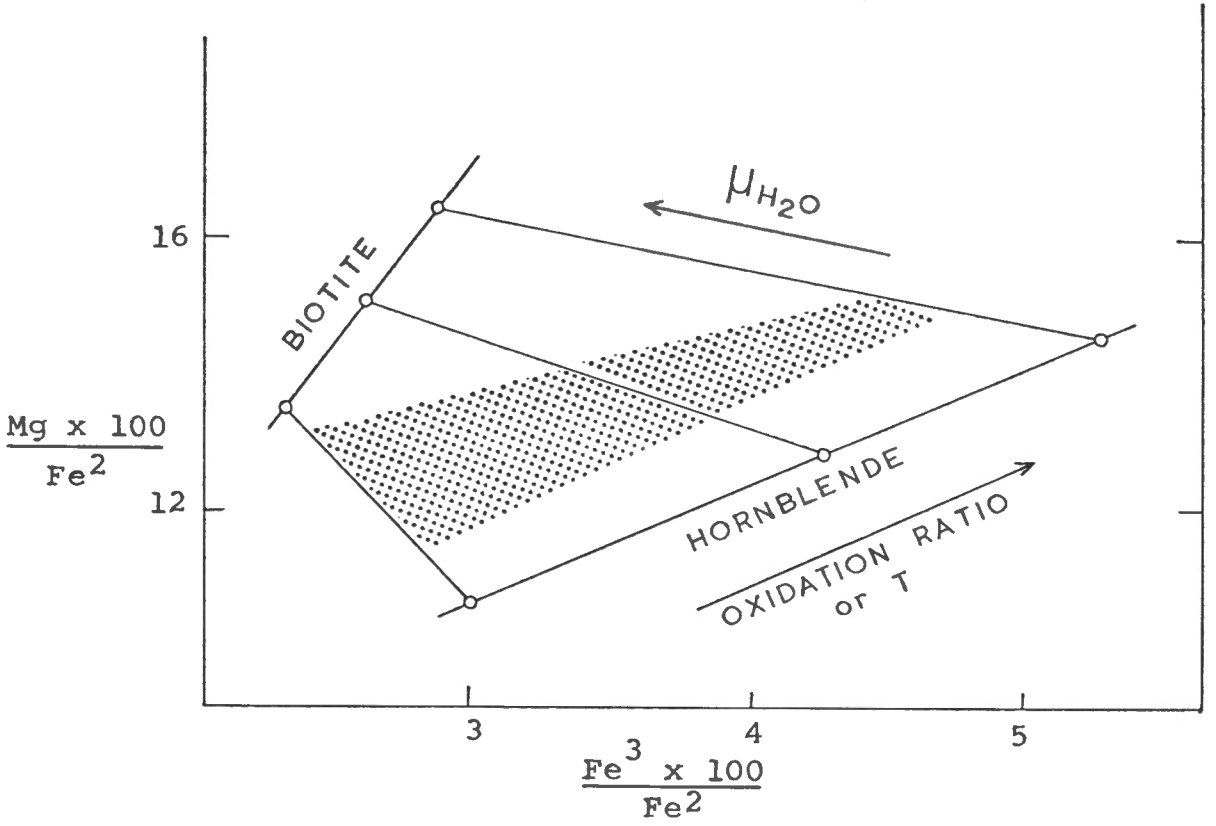

Figure 39. Generalized data taken from Figure 34 showing the effect of oxidation ratio and μH_2O on biotite and hornblende. An increase of oxidation ratio or temperature of the rock shifts tie lines from left to right and μH_2O governs the biotite:hornblende ratio. Stippled area represents biotite:hornblende ratios found in the biotite–hornblende granodiorite.

contacts are shown as hachured lines. Because of the irregular shape of the pluton, which may have been considerably modified during intrusion, the two sets of contours are not strictly parallel, and the composition of biotite and hornblende is not correlative with their ratio. The stippled area in Figure 38 is the monzonite core, which represents a discontinuity in the trend of inward-increasing oxidation ratio (or temperature) and μH_2O. The decrease in the oxidation ratio within the transition zone represents partial recrystallization, the inherited low oxidation ratio of the original body becoming dominant as the core is approached. The "isotherms" and "isobars" drawn in Figure 38 are consistent with, and bear out, the intrusive and metamorphic history proposed on page 16.

PETROGENESIS AND EMPLACEMENT HISTORY

ORIGIN OF THE MONZONITE

The origin of the monzonite body is not directly evident from the available petrologic and structural information. The texture is typical of igneous fabrics in which planar structures are attributed to magma flowage. Planar fabrics are more typical of metamorphic than igneous rocks but such features rarely consist of aligned laths of plagioclase. Considering the euhedral nature of the pyroxene and associated plagioclase feldspar, the rock fabric suggests an igneous origin.

Pyroxenes have the same Fe:Mg ratio throughout the body and appear as a single tie line on a CFM diagram. Coexisting pairs indicate a temperature of 800° to 900°C. Figure 40 shows the minimum melting curves of hydrous granite, syenite (minimum in the Ab-Or-H_2O system), and tholeiitic and alkali basalts. The temperature interval between the basalt curves is the solid + liquid field. The melting curve for Adamant monzonite in a hydrous system would occur between curves (1) and (4), probably close to (3). If the required water is present in the magma (approximately 4 to 6 per cent, Tuttle and Bowen, 1958, p. 58), then the estimated 800° to 900°C temperature is reasonable for water pressures near 1,000 to 2,000 bars. However, if the rocks represented in Figure 40 are anhydrous, the minimum melting curves will have a gentle positive slope, and the 800° to 900° range would then be below the anhydrous melting curves of granite, hence in a field of "dry" metamorphism.

The problem of "dry" versus "wet" systems cannot be resolved with certainty; only the two extremes can be treated. The fact that the mineral assemblage is anhydrous does not necessarily mean that a parent magma was also "dry", much of its original water content may have been expelled during crystallization, and at high temperatures, such as the 800° to 900° range, an anhydrous assemblage would not be unexpected.

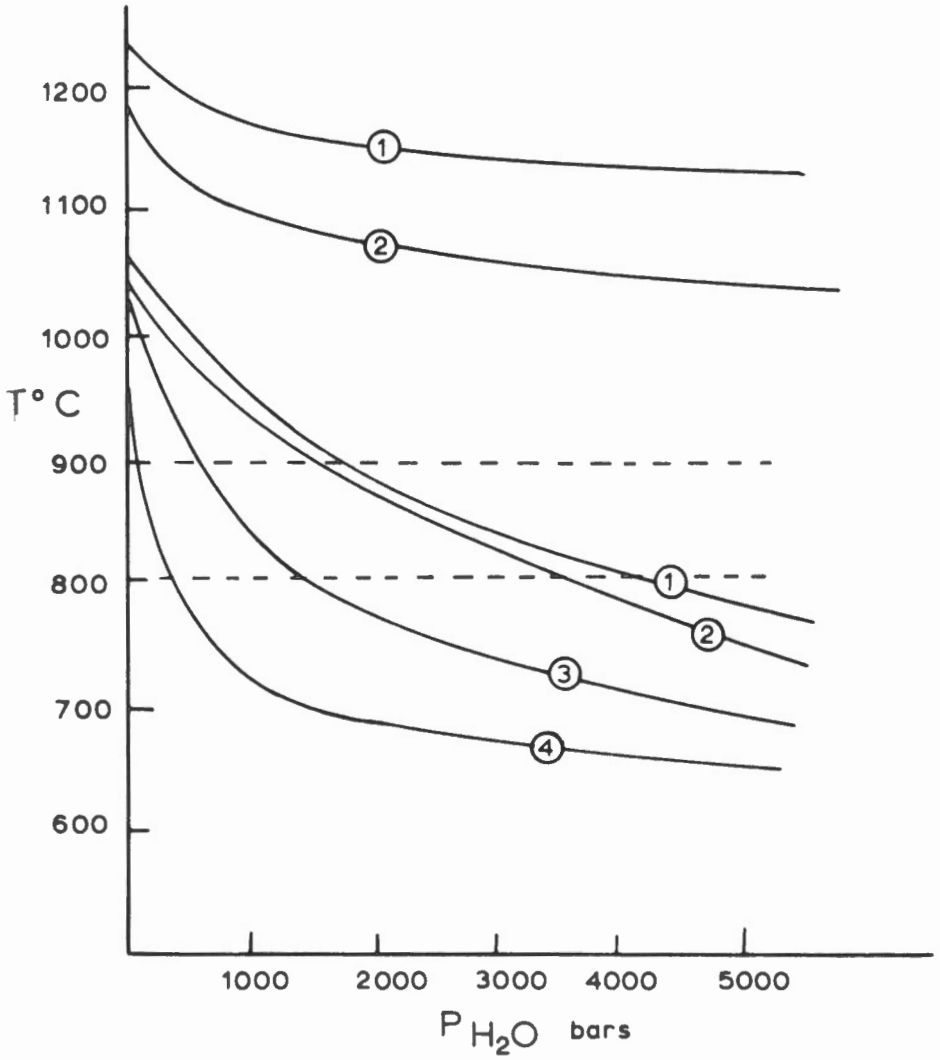

Figure 40. Temperature - water vapour pressure diagram showing the minimum melting curves for (1) olivine tholeiite, (2) alkali basalt, (3) "syenite" (minimum in the Or-Ab-H_2O system), (4) granite (Tuttle and Bowen, 1958). Liquidus and solidus curves shown for tholeiite and alkali basalt. Curves assume load pressure = water vapour pressure, for anhydrous systems melting curves will have positive slopes. Dashed lines denote estimated crystallization temperature of Adamant monzonite. Diagram after Yoder and Tilley (1962, p. 463).

In view of the typical "igneous" rock fabric and the reasonable estimated temperature of formation, the Adamant monzonite is best considered a product of early magmatic activity, probably associated with contemporaneous formation of the easterly trending structures in the region.

ORIGIN OF THE PERIPHERAL ROCKS

Observations bearing on the origin of the peripheral rock are considered in detail in previous sections. These are summarized and listed below.

(1) The peripheral rock is younger than the monzonite core.

(2) There is an imprint of the latest and most pronounced period of regional deformation on the recrystallized periphery of the pluton.

(3) Evidence of progressive recrystallization of the monzonite is preserved in the transition zone. All minerals of the rock are involved in the reconstitution, hence significant amounts of molten rock were not present. Monzonite appears to have occupied all of the pluton during an early period in its history. The rock subsequently recrystallized to the quartz-bearing peripheral rocks. Texturally, minerals composing the peripheral rock are of a single generation.

(4) Lithologic zoning in the peripheral rock can be explained by solid-solid reactions (also involving a vapour phase) which are controlled by temperature and μH_2O changes of these variables produced the different rock units.

The only explanation congruent with these observations is that of a single intrusion of an essentially crystalline body which underwent metamorphism during the latest period of metamorphism and deformation in the northern Selkirks. Single or multiple intrusion of magma cannot account for the gradational contacts, structural discontinuities, and the regional imprint on the body. These relations are readily accounted for by intrusion of a crystalline diapir.

COMPOSITION AND ORIGIN OF THE VAPOUR PHASE

Reactions described in the previous section require equilibrium with a vapour phase, and the addition of water to the monzonite is the main factor in the mineralogical reconstitution of the body. Water content, as reflected by the mineralogy of the rocks and by the chemical analyses in Appendix A, is the chief chemical difference between monzonite and the periphery. Other constituents remain essentially constant. Oxidation and reduction of the

hydrous minerals implies that there was an exchange of O_2 as well as H_2O between the vapour and solids. The vapour phase was thus an aqueous phase containing other dissolved volatiles, most important of which are oxygen and hydrogen. The relatively oxidized nature of the recrystallized periphery of the pluton implies a net gain of oxygen by the hydrous rocks. Figures 37 and 38 indicate that the largest addition has been to the outer boundary of the transition zone. This effect is consistent with the interpretation proposed above in which the most reduced silicates are formed in the coolest part of the recrystallized body. The core, on the other hand, has inherited a low oxidation ratio imposed during magmatic crystallization.

Possible sources for this vapour phase are limited. The monzonite itself is devoid of water, and thus should have acted as a local "sponge" for volatiles during metamorphism. A probable source is the enclosing country rock. Recrystallization started at the margin and continued inward as the aqueous front advanced.

DISCUSSION

Adamant pluton has features characteristic of both mesozonal and catazonal plutons of Buddington (1959). The composite character and complex emplacement relations, the well developed planar structure along the margin of the mass, structural disruption of the country rock, and the discordant internal structures are typical of many mesozonal plutons. A thin, discontinuous migmatite zone in the mantling country rock is also characteristic. The structural position of Adamant pluton in the region is identical to mesozonal plutons farther to the south, for example, White Creek batholith (Reesor, 1958). However, the country rocks enclosing Adamant pluton are amphibolite facies rocks typical of catazonal environments. The absence of a thermal metamorphic aureole, and the impression of regional structure on the pluton are in accord with catazonal granites. Adamant pluton is thus transitional between these two classes of granitic rock, but the structural position of Adamant pluton in the fold belt, and the absence of a marked migmatite zone typical of catazonal rocks, suggests that Adamant pluton properly belongs to the mesozone.

Mesozonal plutons are generally post-tectonic features by virtue of their independence of regional structure. Many such plutons have internal structures and lithology consistent with emplacement of crystallizing magmas. Nonetheless, plutons frequently bear imprints of regional structure, for example Colville batholith (Water and Krauskopf, 1941) and Rattlesnake pluton (McColl, 1964), indicating at least some regional control of the pluton. No less than two structural episodes in the Selkirk fold belt can be related to internal structures of Adamant pluton. This feature suggests that granitic bodies formed early in the evolution of a fold belt can later be re-emplaced during succeeding orogenic pulses.

Judging from the recent review of granites by Buddington (1959), the concept of emplacement of mesozonal granitic rocks as solid bodies is not popular among North American geologists. Emplacement of magma with a suspended crystal load has been appealed to by most authors. Local replacement and granitization of country rock are often inferred but are considered to be subsidiary effects of magma intrusion. Solid emplacement and intrusion of magma[1] are end-members of a complicated emplacement process. The prevalence of internal structure in accord with intrusion of partly crystalline bodies implies that the conditions of emplacement of granites studied to date lie between the two extremes. How much of the mass is solid, how much liquid? There have been few estimates of this, presumably because the proposed magmas are crystallizing during their emplacement. Buddington (1959, p. 734) estimates that much of the rock material that yielded mesozonal plutons was "predominantly liquid". Turner and Verhoogen (1960, p. 388) refer to "largely liquid" rock materials. Read (1957, p. 160) suggests that many plutons are a "mash of crystals, lubricated with a rather small amount of fluid...". Read (1957, pp. 160, 365-366) and others consider that granitic rocks in general (Read's parautochthonous granites) intrude as entirely solid bodies or diapirs. Read appeals to fluid materials to effect the mobilization and granitization of deep-seated rocks. Fluids and regional deformation are relied upon by Read to mobilize the autochthonous granites and to drive resulting granitic materials into upper crustal levels. Once moving, the fluid lubricates the intruding mass and allows rocks to recrystallize. Ramberg (1952, pp. 240-248, 260-261) considers that most plutons rise from plutonic regions by crystalline flow. Orogeny is the driving force, and fluids catalyze chemical reactions permitting mechanical emplacement.

How far solid bodies of the Adamant type can move is open to question (the same can be asked of magmatic bodies). Orogeny is probably the driving force behind emplacement of solid plutons. The ability of Adamant pluton to deform its wall rock suggests that crystalline bodies intrude country rock in much the same manner as magmas, and can be considered to be true diapirs.

Emplacement of solid plutonic bodies is frequently appealed to as an emplacement mechanism of alpine peridotites and serpentinites. Intrusion of these rocks as crystalline or largely crystalline bodies has been suggested by

[1] In recent years the term "magma" has received a different meaning than the original term used by petrologists early in the study of granitic rocks (Tyrrell, Johannsen, Tilley, Holmes, Grout, Rosenbusch, and others). Magma as defined by Turner and Verhoogen (1960) and apparently by many North American geologists, includes all liquid rock matter and solid phases that have crystallized from it, and incorporated foreign matter. Magma on this basis describes rock bodies that vary from almost solid to entirely liquid materials. The writer prefers the definition of early workers -molten rock material. Magma in this view is synonymous to the liquid phase of rock matter. Solids may or may not be present.

many authors (Bowen, 1928; Taliaferro, 1943; Smith and MacGregor, 1960; Mackenzie, 1960; and others). Green (1964) described a peridotite intrusion in Cornwall in which a high temperature and high pressure peridotite (similar to peridotite nodules in basalts) has been mineralogically and structurally reconstituted along the margin of the body during its emplacement as a crystalline mass. Green considers that the peridotite body first crystallized at depth under conditions equivalent to the development of peridotite nodules. The mass was then mobilized and moved vertically as a crystalline diapir within a cataclastic and foliated shell into upper crustal levels. Mobilization of the crystalline mass was due to regional deformation. Recrystallization of the early phase of the pluton during later deformation and reintrusion is the same process postulated for Adamant pluton. Remnants of the original rock can still be found in the interior of both plutons.

EMPLACEMENT HISTORY

The formation of pyroxene monzonite and northeast-oriented structures are the earliest recorded events in the northern part of the Selkirk fold belt. A syntectonic igneous pluton of pyroxene monzonite probably intruded these early structures. A hot, deep-seated environment is indicated by the coarse grained, anhydrous mineral assemblage of the monzonite. The east-west orientation and general shape of the pluton were fixed at this time. Further evolution of the fold belt produced the prominent northwest trending structures evident in the region. Regional deformation caused the upward emplacement of the mass as a crystalline diapir pushing aside country rocks along its roof and flanks. Metamorphism of pyroxene monzonite is related to this structural displacement of the mass.

The effects from a petrologic point of view, of an aqueous phase permeating into the anhydrous monzonite have been noted above. Structurally, such a phase would have affected the mechanical properties of the rock in such a way that resistance to flow was reduced. The absorption of an aqueous phase at the margin of the mass during regional metamorphism resulted in the upward movement of a crystalline core within a shell of rock being deformed by plastic flow. Lineation and foliation in the interior rocks are thus due to recrystallization in a regional stress pattern transmitted through the walls of the pluton.

The marginal rock of the pluton acted as a lubricant between the crystalline core and the country rock, and thickened at the expense of the interior rock as water diffused inward, and to compensate for "frictional drag" between the moving pluton and enclosing country rock. A system of this sort would not be effective in transporting the entire pluton to higher levels in the crust. Splinters of the pluton would undoubtedly shear from the flanks of the mass and remain behind. The eccentricity of the monzonite core can be accounted for in this manner. Part of the south flank near Silvertip

Glacier split off from the main part of the pluton, and continued emplacement left the detached block below the present surface. Pronounced cataclastic textures in rocks in this vicinity are probably due to the loss of the lubricating effect of the marginal rock. Recrystallization of the monzonite here is consequently not as advanced as elsewhere in the pluton.

Heat and energy supplied by orogenic forces were probably limiting conditions to emplacement. Loss of heat to the surroundings decreased the ability of rocks to recrystallize and flow. Marginal flowage and structural adjustment of the country rock became increasingly difficult with decreasing temperature. As a result, the lubricating effect of marginal flow decreased, and the country rock at high crustal levels offered increasing resistance to further emplacement.

The structural and petrologic evolution stopped as the pluton ascended to cool crustal levels. Continued upward movement during a transition from plastic to brittle behaviour produced joints and inward dipping shears along the margin of the mass. Volatile-rich fluids that formed during the mobilization period migrated into the developing joints and shears and produced dykes of pegmatite and aplite.

REFERENCES

Bailey, S.W., and Taylor, W.H.
1955: The structure of a triclinic potassium feldspar; Acta Cryst., vol. 14, pp. 612-632.

Barth, T.F.W.
1934: Polymorphic phenomena and crystal structures; Am. J. Sci., vol. 27, pp. 273-286.

Bartholomé, P.
1962: Iron-magnesium ratio in associated pyroxenes and olivines; Petrologic studies in Buddington volume pp. 1-20, publ. by Geol. Soc. Am.

Bowen, N.L.
1928: The evolution of the igneous rocks; Reprinted 1956; Dover Publications.

Buddington, A.F.
1959: Granite emplacement with special reference to North America; Bull. Geol. Soc. Am., vol. 70, pp. 671-747.

Brown, B.E., and Bailey, S.W.
1964: The structure of maximum microcline; Acta Cryst., vol. 17, pp. 1391-1399.

Chinner, G.A.
1960: Pelitic gneisses with varying ferrous/ferric ratios from Glen Clova, Angus, Scotland; J. Petrol., vol. 1, pp. 178-217.

Emmons, R.C.
1943: The universal stage; Geol. Soc. Am., Mem. 8.

Eugster, H.P.
1959: Reduction and oxidation in metamorphism; Researches in Geochemistry, Abelson, ed., John Wiley & Sons New York; pp. 397-426.

Eugster, H.P., and Wones, D.R.
1958: Annual report of the Director, Geophysical Laboratory, 1957-58; Yearbook Carnegie Inst. Wash., vol. 57, pp. 193-95.

1963: Stability relations of the ferruginous biotite, annite; J. Petrol., vol. 3, pp. 82-125.

Fox, P.E.
1962: Reaction zones in the Adamant Range batholith, British Columbia; unpubl. M.Sc. thesis, Queen's Univ.

Goldsmith, J.R., and Laves, F.
1954: The microcline-sanidine stability relations; Geochim. Cosmochim. Acta, vol. 5, pp. 1-19.

1961: The sodium content of microclines and the microcline-albite series; Cursillos Conferencias del Instituto "Lucas Mallada"; vol. 8, pp. 81-96.

Green, D.H.
1964: The petrogenesis of the high temperature peridotite intrusion in the Lizard area, Cornwall; J. Petrol., vol. 5, pp. 134-88.

Hounslow, A.W.
1965: Chemical petrology of some Grenville schists near Fernleigh, Ontario; unpubl. M.Sc. thesis, Carleton Univ.

Jones, J.B., and Taylor, W.H.
1961: The structure of orthoclase; Acta Cryst., vol. 14, pp. 443-55.

Maccoll, R.S.
1964: Geochemical and structural studies in batholithic rocks of southern California; Part 1, structural geology of Rattlesnake Mountain pluton; Bull. Geol. Soc. Am., vol. 75, pp. 805-22.

Mackenzie, D.B.
1960: High temperature alpine-type peridotite from Venezuela; Bull. Geol. Soc. Am., vol. 71, pp. 303-18.

Orville, P.M.
1963: Alkali ion exchange between vapor and feldspar phases; Am. J. Sci., vol. 261, pp. 201-37.

Ramberg, H.
1952: The origin of metamorphic and metasomatic rocks; Univ. Chicago Press.

Read, H.H.
1957: The granite controversy; Murby, London.

Reesor, J.E.
1958: Dewar Creek map-area; Geol. Surv. Can., Mem. 292.

Smith, C.H., and MacGregor, I.D.
1960: Ultrabasic intrusive conditions illustrated by the Mount Albert ultrabasic pluton, Gaspé, Québec; Abst. in Bull. Geol. Soc. Am., vol. 71, p. 1978.

Stevens, R.E., and others
1960: Second report on a cooperative investigation of the composition of two silicate rocks; U.S. Geol. Surv., Bull. 1113.

Subramanian, A.P.
1962: Pyroxenes and garnets from charnockites and associated granulites; Petrologic studies, in Buddington volume pp. 21-36, publ. by Geol. Soc. Am.

Taliaferro, N.L.
1943: The Franciscan-Knoxville problem; Bull. Am. Assoc. Petrol. Geol., vol. 27, pp. 109-219.

Thompson, J.B. Jr.
1957: The graphical analysis of mineral assemblages in pelitic schists; Am. Mineralogist, vol. 42, pp. 842-58.

Turner, F.J., and Verhoogen, J.
1960: Igneous and metamorphic petrology; McGraw Hill, New York.

Tuttle, O.F., and Bowen, N.L.
1958: Origin of granite in the light of experimental studies; Geol. Soc. Am., Mem. 74.

Waters, A.C., and Krauskopf, K.
1941: Protoclastic border of the Colville batholith; Bull. Geol. Soc. Am., vol. 52, pp. 1355-1418.

Wheeler, J.O.
1963: Rogers Pass map-area; Geol. Surv. Can., Paper 62-32.

1965: Big Bend map-area; Geol. Surv. Can., Paper 64-32.

Wones, D.R., and Appleman, D.E.
1963: Properties of synthetic triclinic $KFeSi_3O_8$, iron-microcline, with some observations on the iron-microcline-iron-sanidine transition; J. Petrol., vol. 4, pp. 131-37.

Wright, T.L.
1964: The alkali feldspars of the Tatoosh pluton in Mount Rainier National Park; Am. Mineralogist, vol. 49, pp. 715-735.

Yoder, H.S., and Tilley, C.E.
1962: Origin of basalt magma types: an experimental study of natural and synthetic rock systems; J. Petrol., vol. 3, pp. 342-532.

APPENDICES

Hypersthene-augite monzonite

Number	83	44	86	82	75	80	72	73	43	41	77
SiO_2	53.5	56.2	53.7	52.9	53.8	55.7	54.9	55.2	54.9	54.2	56.2
Al_2O_3	14.2	12.9	14.2	13.8	14.2	15.5	13.9	14.6	13.6	13.0	13.9
Fe_2O_3	2.6[X]	2.3	2.2	3.1	2.3	2.8	1.9	1.8	3.1	3.8	2.3
FeO	7.06[X]	7.21	7.33	8.08	6.69	5.45	6.78	6.72	6.19	6.64	6.86
MgO	5.3	5.7	7.7	6.3	7.7	4.8	6.5	6.3	5.6	7.2	7.4
CaO	8.4	7.4	7.6	9.8	8.1	6.4	7.4	6.4	8.8	8.2	6.0
Na_2O	2.9	2.6	2.4	2.2	2.4	2.8	2.5	2.6	2.6	2.6	2.8
K_2O	2.8	3.6	3.1	2.7	3.2	3.7	3.2	3.4	3.3	3.0	3.3
TiO_2	0.91	0.84	0.68	0.72	0.66	0.67	0.57	0.57	0.80	0.93	0.70
MnO	0.16	0.18	0.08	0.13	0.07	0.13	0.07	0.13	0.20	0.14	0.16
P_2O_5	0.75	0.63	0.37	0.38	0.37	0.43	0.43	0.51	0.45	0.45	0.47
H_2O	0.40	0.62	0.31	0.30	0.33	0.48	0.80	0.80	0.40	0.30	0.32
CO_2	0.00	0.04	0.00	0.04	0.00	0.06	0.08	0.03	0.00	0.01	0.00
Total	99.1	100.2	99.7	100.5	99.8	98.9	99.0	99.1	99.0	99.9	100.4
O.R.	25	23	21	26	26	32	20	19	31	27	24

* See symbol legend at end of Appendix A

Hypersthene-augite monzonite

Number	83	44	86	82	75	80	72	73	43	41	77
Qtz		+	+			+	+	+			
Plag	39	31	32	36	30	38	31	33	36	32	35
Kfsp	17	22	28	23	24	36	23	26	23	25	36
Hnde	+	2	+	+	4	4	4	3	1	+	+
Biot	3	8	1	+	1	1	7	3	2	4	+
Aug	25	22	23	26	25	12	23	19	23	26	20
Hyp	12	12	13	12	13	6	10	14	12	12	6
Epid											
Sph											
Ap	+	+	+	+	+	+	+	+	+	+	+
Zir											
Scap											
Op	+	+	+	+	+	+	+	+	+	+	+
An	52	45			44	50	44	44	45	46	44
	42	40			39	44	38	38	40	40	

	Biotite-hornblende Granodiorite						Hornblende Quartz Monzonite					
Number	12	10	2	6	28	60	18	5	3	15	25	26
SiO_2	60.8	59.3	57.7	52.4	59.6	60.5	56.2	57.7	53.5	55.7	56.3	58.4
Al_2O_3	15.5	15.3	14.9	14.4	14.7	14.3	14.3	14.0	13.5	15.5	14.9	14.4
Fe_2O_3	2.0[x]	2.2	2.5	3.1	3.2[x]	2.6	2.8	2.7	3.2	3.2	3.4	3.3
FeO	4.52[x]	5.85	5.66	6.09	4.84[x]	4.86	6.37	6.11	7.44	5.53	5.45	4.65
MgO	3.4	2.8	3.8	5.5	4.8	3.7	4.4	4.4	5.3	4.9	5.3	4.7
CaO	5.0	7.8	7.7	9.1	5.0	7.4	7.3	7.6	8.2	6.4	6.5	5.9
Na_2O	2.4	3.2	2.4	2.5	2.4	2.0	2.5	2.6	2.3	2.5	2.3	2.6
K_2O	3.3	1.4	3.0	2.0	3.5	3.6	2.7	2.4	2.5	3.1	2.8	3.4
TiO_2	0.79	1.0	0.80	1.3	0.74	0.75	0.93	1.0	1.1	0.89	0.85	0.76
MnO	0.11	0.08	0.05	0.06	0.23	0.13	0.18	0.15	0.23	0.15	0.14	0.13
P_2O_5	0.27	1.0	1.0	1.2	0.32	0.38	0.71	0.58	0.94	0.38	0.36	0.38
H_2O	0.68	0.90	0.66	0.76	0.78	0.94	0.84	0.74	1.4	0.67	0.60	0.86
CO_2	0.03	0.00	0.01	0.18	0.00	0.00	0.02	0.05	0.00	0.04	0.00	0.11
Total	98.9	100.9	100.2	98.6	100.1	100.8	99.3	100.0	99.6	99.0	98.6	99.6
O.R.	28	25	28	32	38	32	28	31	28	33	36	39

	Biotite-hornblende Granodiorite						Hornblende Quartz Monzonite					
Number	12	10	2	6	28	60	18	5	3	15	25	26
Qtz	17	24	19	17	14	15	13	13	13	12	14	11
Plag	29	29	34	26	28	46	33	26	33	29	27	32
Kfsp			8	8	14	2	12	12	20	18	16	22
Hnde	23	4	27	32	30	17	33	29	36	38	35	31
Biot	16	28	11	13	13	10	8	9	5	2	7	3
Aug												+
HypEpid	+	13	+	+	+			+			+	
Sph	+	+	+	+	+		+	+			+	
Ap	+	+	+	+	+,	+		+	+	+	+	+
Zir	+	+	+	+		+		+	+	+	+	+
Scap	+		+	+								
Op	+	+	+				+	+	+	+	+	+
An	33	35	47	40	45	35	45	42	44	41	45	45
	31		40	33	33	28	38		35	35	35	32

Hornblende Quartz Monzonite

Number	22	51	53	65	66	100	50	105	103	107	110	111
SiO_2	57.8	56.6	52.5	57.1	58.2	57.4	57.4	56.6	55.2	55.2	57.6	55.6
Al_2O_3	14.1	15.1	14.3	15.4	16.7	16.6	15.4	14.2	13.7	11.7	14.8	14.8
Fe_2O_3	3.2	2.8	3.2[x]	2.8[x]	2.6[x]	2.4	3.1	2.9	3.3	3.6	2.9	3.2
FeO	4.78	5.02	6.12[x]	5.06[x]	5.42[x]	4.70	5.40	5.73	6.20	6.76	5.1	5.6
MgO	5.1	3.9	4.9	4.3	4.8	3.6	4.8	4.3	4.6	5.3	4.1[x]	4.4[x]
CaO	6.2	7.7	9.3	6.3	4.6	5.9	6.0	6.8	7.5	8.2	6.4[x]	7.2[x]
Na_2O	2.6	2.7	2.3	2.6	2.7	2.7	2.4	2.8	2.5	2.3	3.0	3.3
K_2O	3.2	2.8	2.3	3.3	3.5	3.7	3.2	3.7	4.0	3.3	3.9	4.0
TiO_2	0.73	0.74	1.3	0.72	0.72	0.59	0.81	0.90	0.93	1.0	0.70	0.60
MnO	0.15	0.13	0.19	0.13	0.10	0.05	0.14	0.15	0.16	0.18	0.10	0.20
P_2O_5	0.35	0.72	1.4	0.37	0.39	0.22	0.37	0.39	0.43	0.48	0.30	0.40
H_2O	0.74	0.66	0.80	0.78	1.00	1.1	1.1	0.83	0.90	1.0	0.70	0.80
CO_2	0.00	0.05	0.11	0.02	0.03	0.00	0.00	0.05	0.18	0.11	0.10	0.30
Total	99.0	98.9	99.3	98.9	99.9	99.0	100.1	99.4	99.6	99.1	99.7	100.4
O.R.	38	33	30	33	30	32	34	31	32	32	34	34

Hornblende Quartz Monzonite

Number	22	51	53	65	66	100	50 **	105	103	107	110	111
Qtz	10	14	12	14	14	10		10	12	10	12	10
Plag	41	38	27	30	29	23		25	20	13	28	28
Kfsp	20	12	12	13	20	22		22	20	22	22	19
Hnde	37	28	40	34	32	42		41	45	43	36	36
Biot	4	7	7	4	5	2			+	+	+	3
Aug										9		3
Hyp												
Epid											+	
Sph			+	+		+			+	+	+	+
Ap	+	+	+	+	+	+		+	+	+	+	+
Zir	+	+	+	+				+	+	+	+	+
Scap												
Op	+	+	+	+	+	+		+	+	+	+	+
An	40	50	50	42	45	36		34	22	23	32	31
		40	40	36	39	25		21	15		21	21

** mode not available

	Transition Zone				Pegmatite and Aplite				
Number	69	46	98	42	56	6	75	99	101
SiO_2	55.1	55.2	54.8	58.2	69.3	72.0	71.8	71.4	70.9
Al_2O_3	13.1	13.0	15.3	14.8	17.7	17.1	18.0	16.9	16.5
Fe_2O_3	4.2	4.4	3.4	3.4	0.41	0.49	0.40	0.20	0.23
FeO	5.83	5.92	5.50	5.11	0.30	0.32	0.31	0.21	0.40
MgO	5.0	5.1	5.0	4.8	1.6	0.18	0.86	0.47	1.0
CaO	7.6	7.1	6.9	5.4	2.2	3.1	1.5	1.3	0.90
Na_2O	2.5	2.4	2.9	2.7	3.4	3.9	4.2	4.4	3.7
K_2O	3.4	3.4	3.7	3.0	5.0	3.2	2.8	4.7	5.7
TiO_2	0.84	0.92	0.65	0.79	0.04	0.08	0.10	0.05	0.03
MnO	0.12	0.17	0.11	0.15	0.00	0.00	0.02	0.02	0.00
P_2O_5	0.78	0.71	0.39	0.40	0.00	0.02	0.02	0.00	0.00
H_2O	0.48	0.60	1.1	0.90	0.31	0.10	0.14	0.58	0.58
CO_2	0.04	0.03	0.00	0.00	0.18	0.08	0.00	0.00	0.00
Total	99.0	99.0	99.8	99.7	100.4	100.6	100.2	100.2	99.9
O.R.	39	40	36	38	55	57	53	47	35

	Transition Zone				Pegmatite and Aplite				
Number	69	46	98	42	56	6	75	99	101 **
Qtz	4	5	3	5	24	28	29	24	
Plag	27	34	32	46	35	38	55	19	
Kfsp	30	21	13	21	39	31	15	56	
Hnde	17	31	17	10	+		1	+	
Biot	+	1	12	6	+	2	+	+	
Aug	15	6	22	10					
Hyp	4	1		2					
Epid					+	+	+		
Sph							+	+	
Ap	+	+	+	+			+	+	
Zir							+	+	
Op	+	+	+	+		+	+	+	
An	41	44	48	45					
		39	40	40		26	22		

** mode not available

	Biotite-hornblende Granodiorite														Hornblende Quartz Monzonite								
Number	8	29	20	21	4	13	11	9	1	54	67	14	61	59	30	27	35	36	37	7	23	19	24
Qtz	15	18	14	16	23	18	19	18	16	17	22	18	16	17	13	12	10	10	10	12	10	13	12
Plag	29	25	31	23	42	30	31	22	37	27	28	37	33	35	36	26	31	34	34	30	35	31	31
Kfsp	17	16	5	14	--	10	13	16	2	6	10	7	15	11	12	23	17	17	18	8	18	11	13
Hnde	25	28	32	33	17	27	22	30	32	39	18	21	33	16	29	38	33	33	35	39	37	40	40
Biot	10	12	13	10	17	12	12	11	b11	10	18	12	10	14	8	+	7	4	1	9	2	4	3
Aug	2																+	+	+		+		
Hyp																							
Epid	+	1	3	2	+	1	2	+	+	+	+	3	1	2	+					2		+	
Sph		+	+	+	+	+	+	+	+	+	+	+	+	+	+	+				+	+	+	
Ap	+	+	+	+	+	+	+	+	+	+	+	+	+	+	+	+	+	+	+	+	+	+	+
Zir			+	+		+	+	+	+	+	+	+		+		+	+			+	+	+	+
Op	+	+	+	+	+	+	+	+	+	+	+	+	+	+	+	+	+	+	+	+	+	+	+
An	36	35	38	33	47	40	38	32	46	44	45	40	48	37	38	44	45	50	40	42	42	44	45
	34	27			43	30	35		38		40	30	38		28	30	38	38		38	32	36	36

	Hornblende Quartz Monzonite																						
Number	17	16	55	49	52	58	47	56	48	62	63	64	34	93	97	96	95	68	104	109	109	87	91
Qtz	10	11	11	10	12	12	11	10	12	11	11	13	10	13	11	10	11	11	11	12	11		
Plag	29	31	31	36	32	28	26	32	30	31	28	36	32	22	32	26	25	26	26	30	27	30	28
Kfsp	11	11	12	10	9	18	19	13	16	15	18	15	18	27	15	27	26	20	25	26	25	30	28
Hnde	44	39	36	38	42	38	41	34	34	37	42	31	34	33	34	32	32	42	36	26	31	4	+
Biot	5	7	8	5	5	+		9	7	5	+	4	5	2	7	4	4	+		+	2	3	3
Aug				+		+					+			3		+	+			+		22	19
Hyp																						8	9
Epid			+					+		+		+					+				5	3	
Sph			+					+		+	+			+	+	+	+					+	
Ap	+	+	+	+	+	+	+	+	+	+	+	+	+	+	+	+	+	+	+	+	+	+	+
Zir	+	+	+	+	+	+	+	+	+	+	+	+	+	+	+	+	+	+	+	+	+		
Op	+	+	+	+	+	+	+	+	+	+	+	+	+	+	+	+	+	+	+	+	+	+	+
An	45	45	45	45	50	49	45	40	45	45	45	49	40	36	30	52	40	50	27	38	38	46	42
	40	39			38	35	28		42	39		38		28	25	28	25	39	20	21	21	40	38

	Hypersthene-augite Monzonite										Transition Zone												
Number	85	90	84	81	74	79	78	76	70	71	31	32	33	38	39	40	57	45	89	88	102	106	108
Quartz										+	3	1	4	4	10	2	5	7	8	14	5	3	7
Plag	38	36	30	33	28	40	35	37	36	27	37	35	31	46	34	48	34	30	49	45	41	31	21
Kfsp	23	29	33	33	26	30	31	30	27	29	24	25	15	8	17	18	16	17	1		18	31	27
Hnde	+	2	+	1	+	+	1	2	+	+	3	8	8	8	21	2	24	27	6	15	3	18	37
Biot	1	3	+	2	+	2	1	1	+	4	6	3	5	9	4	3	5	4	14	16	8	3	2
Aug	23	19	23	21	29	18	19	18	23	23	17	17	22	16	9	15	12	12	15	3	17	12	4
Hyp	12	8	12	9	15	8	11	9	13	16	9	7	9	1	3	10	1	1	3	4	6	+	
Epid																							
Sph																							
Ap	+	+	+	+	+	+	+	+	+	+	+	+	+	+	+	+	+	+	+	+	+	+	+
Zir																							
Op	+	+	+	+	+	+	+	+	+	+	+	+	+	+	+	+	+	+	+	+	+	+	+
An	40	46 39	45 39	46 38	49 38	40	47 48	52 40	45	45 38	38 30	45 40	48 38	59 40	47	43	45	45 40	44 39	50	45	42 33	32 20

Symbols

x	Determined by PEF	Hnde	Hornblende	Ap	Apatite
O.R.	Oxidation ratio, mol. $2Fe_2O_3/2Fe_2O_3+FeO$	Biot	Biotite	Zir	Zircon
		Aug	Augite	Op	Opaque grains
Qtz	Quartz	Hyp	Hypersthene	An	Anorthite content of plagioclase. Core and rim compositions are shown.
Plag	Plagioclase	Epid	Epidote		
Kfsp	Alkali feldspar	Sph	Sphene		

Analyses of biotite and hypersthene included in this report were done at Carleton University. A discussion of the methods used is given by Hounslow (1965), and a brief summary of the procedures employed is shown in Figure 41. Standard materials were included to provide an internal check on the results. Analyses of granite G-1, diabase W-1, and biotite 10 is given in Table 11.

Table 11

Analyses of G-1, W-1, and Biotite 10

	G-1		W-1		Bio-10	
	PEF	1113	PEF	1113	PEF	GSC
SiO_2	72.0	72.35	52.3	52.40	36.9	37.64
Al2O3	14.3	14.32	15.2	15.11	16.1	16.14
Fe_2O_3	1.2	0.95	1.8	1.62	3.6	3.98
FeO	0.82	0.99	8.22	8.63	15.24	15.12
MgO	0.48	0.40	6.6	6.58	10.8	11.11
CaO	1.3	1.40	10.6	10.97	1.0	0.94
Na_2O	3.29	3.31	2.19	2.07	nd	
K_2O	5.21	5.42	0.65	0.67	nd	
TiO_2	0.23	0.26	1.1	1.07	2.0	2.10
P_2O_5	0.05	0.10	0.10	0.15	nd	

G-1 and W-1 analyses from Stevens (1960), Geological Survey of Canada (GSC) analyses by G. Bender.

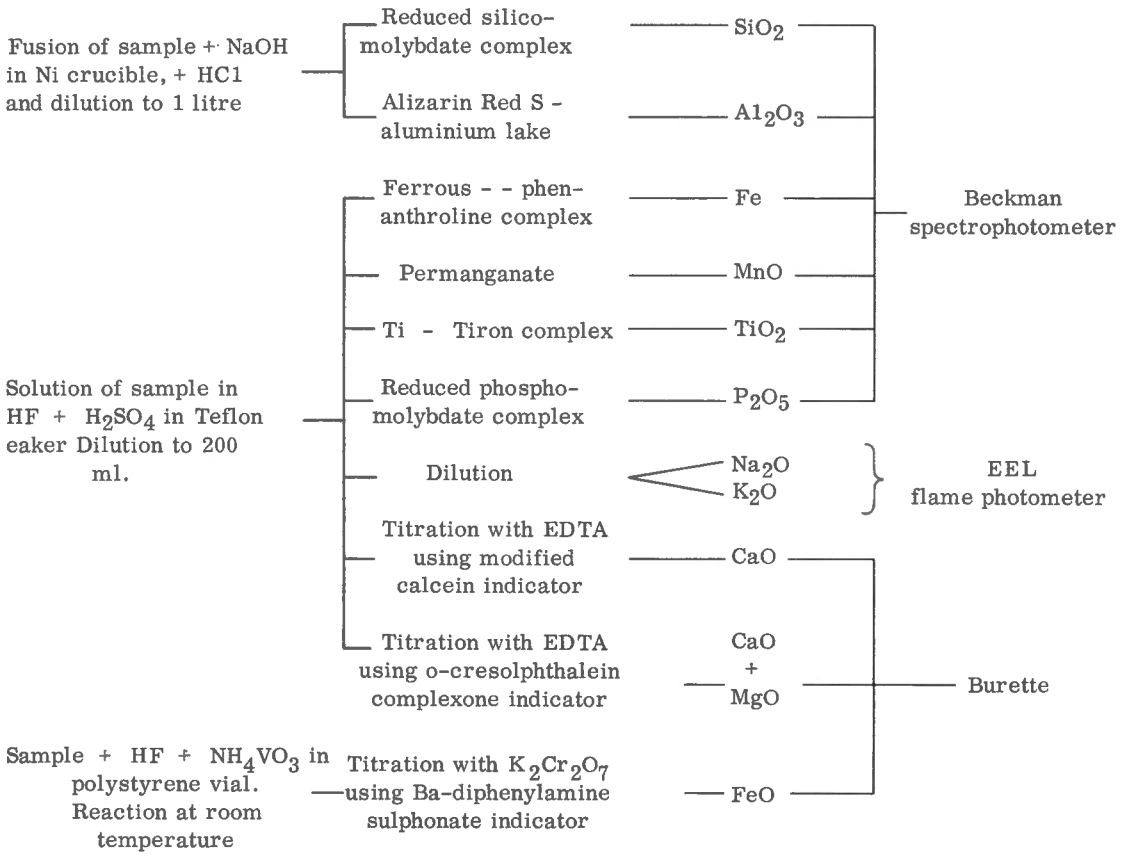

Figure 41. Analytical scheme for analysis of biotite and hypersthene (after Hounslow, 1965).

APPENDIX B

Field and Map Numbers

Map No.	Field No. +	Map No.	Field No. +	Map No.	Field No. +
1	9FK41	38	3F79	75	24FK51(C18)
2	9FK31(C7)	39	3F7-10		24FK53(C19)
3	5F72(5FK)	40	3F7-11	76	25FK41
4	5F61	41	3F88(3FK88)	77	F8-1(FK3-3)
5	5F52(5FK52)	42	F7-6(FK3-2)	78	25FK31
6	10FK21,10FK22 (C8,C9)	43	F75-3(FK3-8)	79	25FK21
		44	4F22(4FK21)	80	25FK11,25FK12(C_2O)
7	5F41	45	14FK81	81	24FK31
8	1F	46	15FK41(C13)	82	24FK21(C17)
9	8FK51	47	14FK71	83	4F33(4FK33)
10	FKC6(C6)	48	15FK21	84	24FK11
11	8FK43	49	13FK21	85	21FK31
12	1FK31(C1)	50	F71-2(FK5-7)	86	21FK41(C16)
13	1FK41	51	13FK41(C11)	87	18FK91
14	2F51	52	13FK61	88	23FK52
15	FKC2(C2)	53	13FK81(C12)	89	23FK51
16	5FK51	54	13FK91	90	21FK51
17	5FK41	55	13FK11	91	21FK11
18	2F31(2FK32)	56	15FK11,15FK12 (C15)	92	23FK10-2
19	4FK11			93	22FK31
20	3F11	57	14FK43	94	29FK42
21	3F31	58	14FK21	95	28FK81
22	2FK41(C5)	59	F6-7	96	28FK71
23	3FK21	60	F6-1(FK5-16)	97	28FK61
24	4FK32	61	FKA3(FKA3)	98	32FK21(C24)
25	FKC3(C3)	62	16FK11	99	32FK63(C25)
26	3FK41(C4)	63	17FK11	100	32FK71(C26)
27	3F41	64	17FK32	101	FKC27(C27)x
28	F11-4(FK5-4)	65	17FK41(C14)	102	32FK10-2
29	1F11	66	30FK72(C23)	103	35FK21(C29)
30	1F51	67	31FK21	104	35FK41
31	1F71	68	30FK61	105	35FK11(C28)
32	1F81	69	11FK31(C10)	106	34FK21
33	1F91	70	27FK32	107	33FK71(C30)
34	18FK52	71	28FK12	108	36FK31
35	3F71	72	29FK11(C21)	109	36FK51(C31)
36	3F72	73	29FK31(C22)	110	40FK11(C32)
37	3F73	74	24FK61	111	40FK51(C33)

Symbols + Field numbers represent modal analyses, numbers in brackets are chemical analysis field numbers.

x Sample taken from talus

APPENDIX C

Optic Angle Determinations on Alkali Feldspar

(i) Feldspars with sharp extinction

No.	31	32	33	1F101	18	44	83	65	46	86	82	21FK21	85	81
Rock type	TZ	TZ	TZ	M	QM	M	M	QM	TZ	M	M	M	M	M
Mean 2V	46	44	41	47	48	49	45	49	45	45	49	48	45	49

No.	24FK41	75	74	76	3F77	45
Rock Type	M	M	M	M	TZ	TZ
Mean 2V	50	47	49	48	44	46

(ii) Feldspars with patchy extinction

No.	29	30	27	111	69	15	52	1F61	30FK21	30FK81
Rock Type	QM	QM	QM	QM	QM	TZ	QM	QM	QM	QM
Mean 2V	57	54	53	57	44	52	50	50	48	45

(iii) Grid-twinned microcline

No.	3F61	A	B	C	D	14	E	110	109	108	107	106
Rock type	QM	BHG	BHG	BHG	BHG	Peg	Peg	QM	QM	QM	QM	QM
Mean 2V	58	53	56	60	64	68	70	63	66	64	62	68

No.	105	104	103	14	2F41	20	21	13
Rock Type	QM	QM	QM	BHG	BHG	BHG	BHG	BHG
Mean 2V	62	67	64	57	60	60	57	56

Mean 2V = average 2V of at least five suitable grains per slide. Range of 2V per slide varies from 5° to 10°. M = monzonite, TZ = transition zone, QM = quartz monzonite, BHG = biotite hornblende granodiorite, Peg = pegmatite.

APPENDIX D

Determination of Albite in Solid Solution in Alkali Feldspar

The determinative curves used for Ab content of alkali feldspar is given below. The data from which these curves were plotted were kindly supplied by T. L. Wright (pers. comm., 1964). Wright has found that the a axis is composition sensitive, and is almost, but not entirely, unaffected by structural state. If the structural state of a feldspar is known, then the amount of albite in solid solution can be determined. To use the curves (Fig. 42), structural state must be estimated first. At present the most satisfactory powder method is to plot b vs. c, and to compare sample data with that for Wright's standard series made up by alkali ion exchange (see Fig. 28 in text). With this information, the appropriate curve, orthoclase-intermediate albite or maximum microcline-low albite, is used.

Albite determinations are adversely affected by uncertainties in structural state, intermediate structural states, and the "distortion" of the a axis (that is when observed a deviated from theoretical a; see a axis contours in Fig. 28). Adamant feldspars were considered by Wright to be either slightly distorted or not at all. Figure 28 was used to estimate structural state; samples A, B, C, D, E were determined from the maximum microcline-low albite curve, samples 18, 46, 82, and 86 from the orthoclase-intermediate albite curve. The success of this method is discussed in the text. Maximum error for the Adamant feldspars judged from cell dimension error is $\pm$ 1.5 per cent albite.

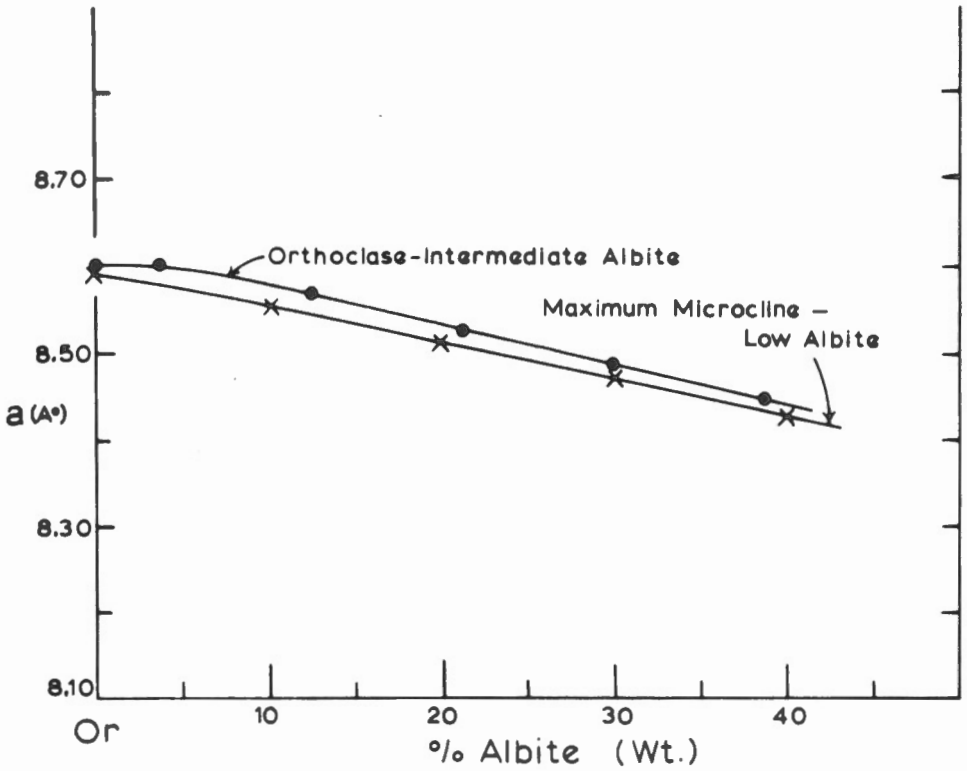

Figure 42. Determinative curves for albite in solid solution in potassic feldspar. Curves plotted from data supplied by T. L. Wright (pers. comm., 1964).